Maastrichtian-Rupelian paleoclimates in the southwest Pacific – a critical re-evaluation of biomarker paleothermometry and dinoflagellate cyst paleoecology at Ocean Drilling Program Site 1172

Peter K. Bijl[1]*, Joost Frieling[1,2], Margot J. Cramwinckel[1,3], Christine Boschman[1], Appy Sluijs[1], Francien Peterse[1]

[1]Department of Earth Sciences, Utrecht University, Utrecht, the Netherlands.
[2]now at: Department of earth Sciences, University of Oxford, South Parks Road OX1 3AN, UK
[3]now at: School of Ocean and Earth Science, National Oceanography Centre Southampton, University of Southampton, Southampton, UK

* corresponding author. email: p.k.bijl@uu.nl

Abstract

Sea surface temperature (SST) reconstructions based on isoprenoid glycerol dialkyl glycerol tetraether (isoGDGT) distributions from the Eocene southwest (SW) Pacific Ocean are unequivocally warmer than can be reconciled with state-of-the-art fully coupled climate models. However, the SST signal preserved in sedimentary archives can be affected by contributions of additional isoGDGT sources. Methods now exist to identify and possibly correct for overprinting effects on the isoGDGT distribution in marine sediments. We here use the current proxy insights to (re-)assess the reliability of the isoGDGT-based SST signal in 69 newly analysed and 242 re-analysed sediments ODP Site 1172 (East Tasman Plateau, Australia) following state-of-the-art chromatographic techniques. We compare our results with paleo-environmental and paleoclimatologic reconstructions based on dinoflagellate cysts. The resulting ~130 kyr-resolution Maastrichtian-Oligocene TEX_{86}-based SST record confirms previous conclusions of anomalous warmth in the early Eocene sw Pacific and remarkably cool conditions during the mid-Paleocene. Dinocyst diversity and assemblages show a strong response to the local SST evolution, supporting the robustness of the TEX_{86} record. Soil-derived branched GDGTs stored in the same sediments are used to

Deleted: SW

Deleted: ,

Deleted: in context of

Deleted: ¶

reconstruct mean annual air temperature (MAAT) of the nearby land using the MBT'$_{5me}$ proxy. MAAT is consistently lower than SST during the early Eocene, independent of the calibration chosen. General trends in SST and MAAT are similar, except for 1) an enigmatic absence of MAAT rise during the Paleocene-Eocene Thermal Maximum and Middle Eocene Climatic Optimum, and 2) a subdued middle–late Eocene MAAT cooling relative to SST. Both dinocysts and GDGT signals suggest a mid-shelf depositional environment with strong river-runoff during the Paleocene-early Eocene, progressively becoming more marine thereafter. This trend reflects gradual subsidence and more pronounced wet/dry seasons in the northward drifting Australian hinterland, which may also explain the subdued middle Eocene MAAT cooling relative to that of SST. The overall correlation between dinocyst assemblages, marine biodiversity and SST changes suggests that temperature exerted a strong influence on the surface-water ecosystem. Finally, we find support for a potential temperature control on compositional changes of branched glycerol monoalkyl glycerol tetraethers (brGMGTs) in marine sediments. It is encouraging that a critical evaluation of the GDGT signals confirms that most of the generated data is reliable. However, this also implies that the high TEX$_{86}$-based SSTs for the Eocene SW Pacific, and the systematic offset between absolute TEX$_{86}$-based SST and MBT'$_{5me}$-based MAAT estimates remain without definitive explanation.

Deleted: except for:

Deleted: drying

Deleted: , probably in part through sea level changes caused by steric effects

Deleted: the vast majority

Deleted: sw

Deleted: remain unexplained

Deleted: s

1. Introduction

1.1 The Paleogene Southwest Pacific Ocean

Reconstructions of deep-sea (Westerhold et al., 2020) and sea surface temperature (Bijl et al., 2009; 2013a; Hollis et al., 2012; 2019; Frieling et al., 2014; Inglis et al., 2015; O'Brien et al., 2017; Evans et al., 2018; Cramwinckel et al., 2018; O'Connor et al., 2019; Sluijs et al., 2020) have revealed overall cool climate in the Maastrichtian and Paleocene, long-term warming towards the early Eocene Climatic Optimum (EECO; 53.4 – 49.2 Ma), and subsequent cooling during the middle and late Eocene (48.6 – 33.6 Ma). The EECO stands out as particularly warm, with ice-free polar regions (Hollis et al., 2009; 2012; Pross et al., 2012; Bijl et al., 2013a; Frieling et al., 2014; Hines et al., 2017). Certain southern high-latitude regions retain warm-temperate conditions into the late Eocene (Bijl et al., 2009; Liu et al., 2009; Houben et al., 2019) and, despite ample evidence for pronounced Antarctic glacial expansion across the Eocene-Oligocene transition (Salamy and Zachos, 1999; Bohaty et al., 2012), even into the early Oligocene (Passchier et al., 2013; 2017; Hartman et al., 2018; O'Brien et al., 2020). Variations in atmospheric CO_2 concentrations (Anagnostou et al., 2016; 2020; Foster et al., 2017) are likely the primary driver of these multi-million-year climatic trends (Cramwinckel et al., 2018). While equatorial proxy-based sea surface temperatures (SSTs) and deep-sea temperatures, assumed to reflect high-latitude SSTs, show good correspondence with numerical model simulations under Eocene boundary conditions and with varying CO_2 forcing (Cramwinckel et al., 2018), proxy-based SST reconstructions of the southwest (SW) Pacific remain warmer than those from model simulations (Bijl et al., 2009; Cramwinckel et al., 2018; Hollis et al., 2019; Crouch et al., 2020; Lunt et al., 2021), despite proposed zonal heterogeneity (Douglas et al., 2014). Specifically, numerical climate models are currently unable to simulate a paleoclimate in which the annual SST difference between the equatorial Atlantic Ocean (Cramwinckel et al. 2018) and the sw Pacific Ocean (Hollis et al., 2012; Bijl et al., 2013a) is as small as the proxy data suggest. Mechanisms explaining this mismatch might be found in the geographic boundary conditions and spatial resolution of the numerical models, and the limitations of the proxies to reflect absolute temperatures. The absolute SST estimates for the SW Pacific are closer to those from the equatorial regions than they

Moved (insertion) [1]

Deleted: Frieling et al., 2014; Hollis et al., 2014; 2019; Inglis et al., 2015; 2020;

Moved up [1]: O'Brien et al., 2017; Evans et al., 2018;

Deleted: Bijl et al., 2013a; Hines et al., 2017;

Formatted: Not Highlight

Deleted: Passchier et al., 2013; 2017;

Deleted: Beerling and Royer, 2011;

Deleted: sw

Deleted: 2012

Deleted: numerical

Deleted: ; Hollis et al., 2012

Deleted: s

Deleted: can be sought

Deleted: sw

Deleted: Atlantic

are to the deep-sea (Cramwinckel et al., 2018), which is implausible given that the South Pacific is inferred to have been the dominant region of deep-water formation during the Eocene (Huber and Thomas, 2010; Thomas et al., 2003; 2014). Without this model-data mismatch resolved, it remains unclear to what extent climate models properly simulate polar amplification or, alternatively, if the current proxies properly reflect high-latitude temperatures under greenhouse conditions (Lunt et al., 2012).

Proxy evidence for warmth in the Eocene derives from a suite of organic and calcite-based proxies for marine or terrestrial temperature. SST reconstructions of the SW Pacific Ocean have primarily relied on organic geochemical proxies, mainly TEX_{86} (Sluijs et al., 2011; Hollis et al., 2009; 2012; Bijl et al., 2009; 2013a; Cramwinckel et al., 2020; Crouch et al., 2020). Although absolute temperatures have significant uncertainties, they have been broadly confirmed by robust oxygen isotope ratios ($\delta^{18}O$) and trace element ratios (Mg/Ca) from well-preserved planktonic foraminifera from Eocene sections in New Zealand (Hollis et al., 2009; 2012; Creech et al., 2010; Hines et al., 2017; Crouch et al., 2020). These proxies require assumptions regarding seawater chemistry (Mg/Ca, $\delta^{18}O$ seawater, pH) that also carry significant uncertainty (e.g., Evans et al. 2018; Kozdon et al., 2020) and these uncertainties may affect trends in multi-million year carbonate-based reconstructions. The application of clumped isotope paleothermometry can reduce some of the uncertainties surrounding carbonate-based proxies and provide additional SST constraints (Evans et al., 2018), as has been demonstrated in work on Seymour Island (Douglas et al., 2014).

Pollen-based vegetation reconstructions from New Zealand, Tasmania and Wilkes Land (Carpenter et al., 2012; Pross et al., 2012; Contreras et al., 2013; 2014; Huurdeman et al., 2020), present mean annual air temperature (MAAT) reconstructions which confirm the warm conditions from SST proxies. Here, uncertainties on absolute temperatures are dependent on the diversity of the pollen assemblage, and the temperature tolerances of nearest living relatives (NLRs). Uncertainties increase when evolutionary distances to NLRs are large. In general, vegetation-based reconstructions arguably deliver the best constraints on winter temperatures. This is because of fundamental physiological restrictions in individual tolerances of plants (e.g., Reichgelt et al., 2018), whereas MAAT exerts much less

Deleted: numerical

Deleted: of Paleogene climates and

Deleted:

Deleted: sw Pacific region

Deleted:

Deleted: southwest

Deleted: 2006; 2009;

Deleted: 2018

Deleted: always carried

Deleted: In terms of the latter, o

Deleted: indicate warm temperatures

Deleted: Hollis et al., 2009; 2012

Deleted: , Evans et al. 2018

Deleted: . On reconstructions covering multi-million years, trends may also be affected by these uncertainties.

Deleted: has great potential to

Deleted: partially alleviate such concerns

Deleted: as evident from

Deleted: the Tasman region

Deleted: ; Pross et al., 2012

Deleted: absolute

Deleted: broadly

Deleted: however,

Deleted:

Deleted: ,

Deleted: and

Deleted: their

Deleted: mean annual air temperature (

Deleted:)

Deleted: reconstructions from pollen assemblages are complicated because MAAT

control on the standing vegetation than seasonal temperature and (seasonal) hydrological extremes. Absolute air temperature reconstructions from soil-derived lipid biomarkers (e.g., using brGDGT-based paleothermometry; e.g., Weijers et al., 2007a; De Jonge et al., 2014a) have also yielded MAAT reconstructions for the Eocene (Pancost et al., 2013; Bijl et al., 2013a; Huurdeman et al., 2020; Lauretano et al., 2021). The resulting MAAT records are more in line with numerical model simulations (Lunt et al., 2021), but considerably colder than the SSTs from the same sections. This is difficult to reconcile in a coastal climate setting, where SST and adjacent air temperature should be broadly consistent.

These uncertainties in lipid-based absolute temperature reconstructions have been put forward as underlying reason for the data-model mismatch in past climate reconstructions. This sparked major research efforts to improve understanding of proxy functioning and potential confounding factors, ultimately to improve the accuracy of biomarker-derived temperature estimates, and to resolve the mismatch between model simulations and proxy data.

1.2 Advances in GDGT paleothermometry

TEX_{86} utilizes the correspondence of proportionally higher numbers of cyclopentane rings in sedimentary archaeal membrane lipids, the isoprenoid glycerol dialkyl glycerol tetraethers (isoGDGTs), with higher SST (Schouten et al., 2002). This relationship is attributed to a viscoelastic adaptation of the membrane of pelagic Thaumarcheota, the dominant source organisms of isoGDGTs, to temperature (Schouten et al., 2002; 2013). For some periods in geological deep time, including the Paleocene and Eocene, TEX_{86} calibrations based on GDGTs in core top sediments need to be extrapolated above the modern SST range (~30°C) to estimate SST. It remains unclear if the relationship between SST and TEX_{86} is linear or exponential beyond the high-end of the core-top calibration (e.g., Cramwinckel et al., 2018; Hollis et al., 2019). It is therefore recommended that both linear and exponential calibrations are presented, which typically lead to higher and lower SST estimates, respectively (Hollis et al., 2019). Yet, as the absolute TEX_{86} values of many Eocene sediments exceed those observed for modern core-tops, even the most conservative calibrations yield SSTs >30°C in the warmest intervals. Increasingly, such temperatures are

Deleted: Reconstructions of the warm Eocene primarily relied on organic geochemical proxies, notably TEX_{86} (Bijl et al., 2009; 2013a; Cramwinckel et al., 2018; 2020; Crouch et al., 2020; Hollis et al., 2009; 2012; Sluijs et al., 2006; 2009; 2011). These absolute SST estimates for the sw Pacific are closer to those from the equatorial Atlantic as they are to the deep-sea (Cramwinckel et al., 2018), which is surprising given that the South Pacific was presumably the dominant region of deep-water formation during the Eocene (Huber and Thomas, 2010; Thomas et al., 2003; 2014).

Formatted: English (US)

Deleted: MBT, or associated approaches

Formatted: English (US)

Moved down [3]: Pancost et al., 2013; Bijl et al., 2013a; Huurdeman et al., 2020)

Deleted: absolute

Formatted: English (US)

Formatted: English (US)

Moved (insertion) [3]

Deleted: air temperature reconstructions, albeit with considerably large uncertainties

Deleted: reconstructions

Deleted: consistently colder than the SSTs from t… [1]

Deleted: , thus

Deleted: .

Deleted: The ubiquitous applicability of the organ… [2]

Deleted: and potential biases

Deleted: the

Deleted: derived from these proxies led to

Deleted: mplicati

Deleted: confidence in

Deleted: these

Deleted: proxies

Formatted: English (US)

Deleted: abundances

Deleted: termed

Deleted: of the overlying surface water

Deleted: The

Deleted: nlinearity ature of

Formatted: Subscript

Deleted: at and

Deleted: is poorly knownconstrained

Deleted: ,

Deleted: leading to very highinflated uncertainty i… [3]

Deleted: The available information leaves ambigu… [4]

Deleted: However

corroborated by estimates from other SST proxies (e.g., Bijl et al., 2010; Douglas et al., 2014; Hines et al., 2017; Crouch et al., 2020).

Along with calibration uncertainties, a number of confounding factors have been identified since the first publication of the isoGDGT-based SST records from the SW Pacific. These are related to a suite of pre-, syn-, and post-depositional processes that might alter the pelagic isoGDGT signal in marine sediments. In addition to the pelagic contribution, isoGDGT assemblages may include contributions from methanogenic (Blaga et al., 2009) and methanotrophic (Weijers et al., 2011; Zhang et al., 2011) archaea, deep-dwelling archaea (Taylor et al., 2013) and terrestrial sources (Hopmans et al., 2004; Weijers et al., 2006). Various approaches have been developed to recognize these contributions, leading to more reliable SST reconstructions. However, the influence of growth phase (Elling et al., 2014), and environmental ammonium and oxygen concentrations (Qin et al., 2015; Hurley et al., 2016) on sedimentary isoGDGT distributions are still poorly constrained.

Branched GDGTs (brGDGTs) produced by soil bacteria can be used to reconstruct mean annual air temperature (MAAT). The MBT'$_{5me}$ index (De Jonge et al., 2014a; Naafs et al., 2019; Dearing Crampton-Flood et al., 2020) represents the degree of methylation of the 5-methyl brGDGTs which strongly responds to MAAT. Studies on brGDGTs in marine sediments reveal that the MAAT evolution of Australian-New Zealand land masses followed the trends in deep- and surface ocean temperature remarkably well, but with lower absolute values than SST (Bijl et al., 2013a; Pancost et al., 2013). With improved analytical techniques (Hopmans et al., 2016), brGDGT isomers with a methylation on the 5- or the 6-position of the alkyl chain can now be separated and quantified (De Jonge et al., 2013). With this separation, the pH co-dependence of the brGDGT signal can be removed by only considering 5-methyl brGDGTs that only respond to temperature (De Jonge et al., 2014a; Naafs et al., 2017a). The separation of brGDGT isomers also allows the recognition and correction of potential contributions of aquatic brGDGTs to the soil-derived brGDGT signal stored in marine sediments that complicate the use of brGDGTs as continental paleothermometer in continental margin sediments (Peterse et al., 2009; Tierney and Russell, 2009; Zell et al., 2013; De Jonge et al., 2014b; 2015; Sinninghe Damsté, 2016; Dearing Crampton-Flood et al., 2018).

Deleted: Zachos et al, 2006; Frieling et al., 2017; Evans et al., 2018

Deleted: sw

Deleted: (Hollis et al., 2009; 2012; Bijl et al., 2009; 2013)…

Deleted: associated,

Deleted: relating

Deleted: I

Deleted: to the sedimentary isoGDGT pool have been determined…

Deleted: recognise

Deleted: identify

Deleted: These factors can be recognized in GDGT distributions, leading to better interpretation of TEX_{86}–based SST reconstructions

Deleted: as yet

Deleted: unknown

Deleted: provide reconstructions of

Deleted: for the MBT-index using t

Deleted: Peterse et al., 2012; Weijers et al., 2007;

Formatted: English (US)

Deleted: Based on

Deleted: supplied to

Deleted: ,

Deleted: continents

Deleted: much

Deleted: Albeit to a lesser extent than SST, southern high-latitude MAAT reconstructions remain warmer than model simulations (Huber and Caballero, 2011) as well, even when simulations replicate equatorial surface and global deep ocean temperatures (Cramwinckel et al., 2018). [[zou hier dus invoegen dat deze MAAT records op de oude methode zijn gebaseerd plus dat ze mogelijk een overprint van rivier- en/of mariene brGDGTs kunnen hebben]] …

Deleted: , isolating the

Deleted: relationship

Deleted: to recognize

Deleted: and correct for

Deleted: ; Peterse et al., 2009; Sinninghe Damsté, 2016; Tierney and Russell, 2009; Zell et al., 2013

Lipids from a related biomarker family, the branched glycerol monoalkyl glycerol tetraethers (brGMGTs), were identified in the marine realm in core-top sediments (Liu et al., 2012), oxygen minimum zones (Xie et al. 2014), and Paleogene sediments (Sluijs et al., 2020). In the terrestrial realm, they were described in peats (Naafs et al., 2018a) and East African lake sediments (Baxter et al 2019), the latter identifying 7 individual brGMGTs. The brGMGTs contain a covalent bond connecting the two alkyl chains, which is thought to enhance membrane stability at higher temperatures (Morii et al., 1998). The abundance of brGMGTs relative to that of brGDGTs, as well as the relative distribution of brGMGT isomers seems to vary with temperature in both the terrestrial (Naafs et al., 2018a; Baxter et al., 2019; Tang et al., 2021) and marine realms (Sluijs et al., 2020), although this is thus far only based on empirical relationships. The exact sources of these compounds in sedimentary archives and their temperature relation are as yet not fully understood. For example, brGMGTs in Paleogene Arctic Ocean sediments seem to be produced in a marine system with a strong oxygen minimum zone and substantial input of penecontemporaneous terrestrial matter (Sluijs et al., 2020). Similar to the temperature response of 5-methyl brGDGTs, the degree of methylation of acyclic brGMGTs ($HMBT_{acyclic}$) follows the TEX_{86} in the Paleogene Arctic record. However, the index brGMGTI, which was empirically calibrated to temperature using a suite of East African lake sediments (Baxter et al., 2019) does not (Sluijs et al., 2020).

1.3 Revisiting GDGTs, and investigating brGMGTs at Site 1172

From the new insights about the GDGT-based proxies, it is clear that assessing the reliability of previously published GDGT-based temperature reconstructions requires a detailed review of the depositional conditions. Moreover, the presence and proxy potential of brGMGTs the early Paleogene SW Pacific has not yet been studied. To this end, we have revisited the sedimentary record at ODP Site 1172 on the East Tasman Plateau (ETP), which contains an almost complete succession of late Cretaceous (Maastrichtian) to early Oligocene sediments (Brinkhuis et al., 2003; Schellenberg et al., 2004; Stickley et al., 2004a; Bijl et al., 2013b; 2014). We have undertaken new analyses of isoGDGTs, brGDGTs, and brGMGTs from the Maastrichtian and Paleocene section of the record, and re-analysed previously

Deleted: from later in
Formatted: Not Highlight
Deleted: in
Deleted: to some degree
Deleted: Naafs et al., 2018a;
Formatted: Not Highlight
Deleted: consistency of such signals in various terrestrial, lacustrine and marine realms,
Deleted: The degree of methylation of a specific subset of brGMGT compounds (Naafs et al., 2018a, Sluijs et al. 2020) is however similar to those in brGDGTs for w ... [5]
Deleted: The
Deleted: marine sediments from the
Deleted: do
Deleted: contain abundant
Deleted: brGMGTs
Deleted: (Sluijs et al., 2020)., and Tthese
Deleted: the
Deleted: ,
Deleted: terrestrial
Deleted: (Willard et al., 2019)
Deleted: T
Deleted: While t
Deleted: does show
Deleted: shows similar trends
Deleted:
Deleted: to
Deleted: ,
Deleted: tentatively
Deleted: tropical
Deleted: s
Deleted: The response of brGMGTs to environmer ... [6]
Deleted: revisit and a
Deleted: constraints on past environmental, ... [7]
Deleted: sw
Deleted: assessed
Deleted: a
Deleted: from the sw Pacific Ocean:
Deleted: late Cretaceous
Moved (insertion) [2]
Deleted: ;
Moved up [2]: Brinkhuis et al., 2003; Schellenberg et
Deleted: newly analysed

published sample sets using the chromatography method with improved compound separation (Hopmans et al., 2016). We critically evaluate the biomarker results using established indicators for pre-, syn- or post-depositional overprint of the primary sea surface and air temperature signals. In addition, we use dinoflagellate cyst assemblages and terrestrial palynomorph abundance as recorders of paleoenvironmental change on the continental shelf, for constraints on depositional, environmental and hydrological changes, in order to aid interpretations of the GDGT proxies. We also evaluate the nature, source and possible temperature affinity of the brGMGTs in our record. After this critical (re-)evaluation, we interpret the Maastrichtian to early Oligocene sea surface and air temperature, and paleoenvironmental evolution of the sw Pacific region.

Deleted: indices

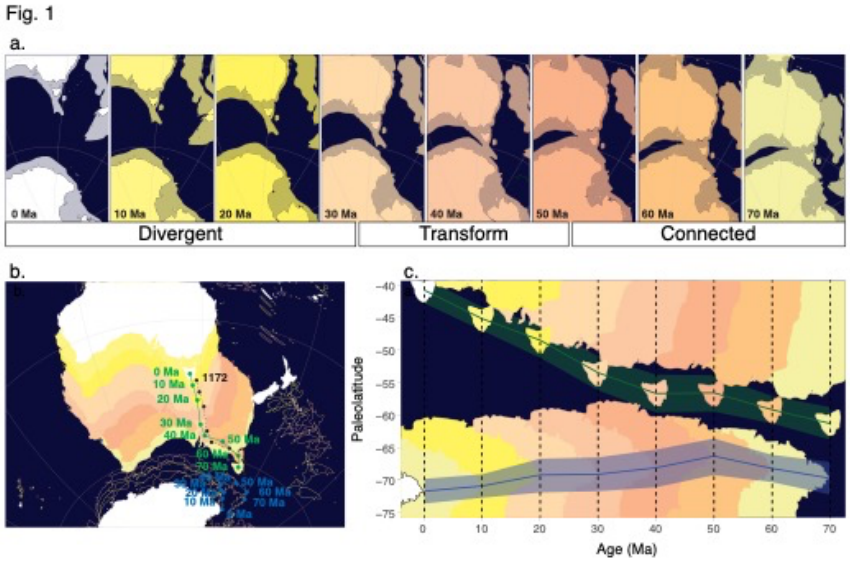

Figure 1. Absolute plate tectonic changes around Tasmania during the Maastrichtian to recent. a. Tasmanian Gateway (TG) opening in 8 time slices, present to 70 Ma. Relative tectonic motion between Australia and Antarctica is limited until about 53 Ma, transform until 34 Ma and divergent from 34 Ma onwards. b. Like a, but on an orthographic projection (compiled with Gplates, using paleomagnetic reference frame (Torsvik et al., 2012) from Seton et al. (2012)). Green and blue lines and dots represent the pathways of Tasmania and Cape Adare, respectively, black dashed line

Deleted: from 70 Ma to

Deleted: transfer

and dots represent the paleo-position of Site 1172. c. The absolute paleolatitude of Cape Adare, Antarctica (blue line, blue shading = uncertainty), as indicative of the plate tectonic motion around the pathway of the Tasman Current, and of Tasmania (green line, green shading = uncertainty), as indicative of the plate tectonic motion of the source area of the terrestrial organic matter, in 10 Myr time steps from 70–0 Ma. obtained from paleolatitude.org (Van Hinsbergen et al., 2015). Plate contours represent paleolatitude of present-day shorelines, for orientation (obtained from Gplates). Note that in visualizations b and c, submerged continental crust is not shown, but does limit TG opening.

2. Material

2.1 Site locality and tectonic evolution

Since the Cenomanian, the continental complex including Australia, Tasmania, ETP and the South Tasman Rise (STR) tectonically moved as one continental plate (Müller et al., 2000) – here referred to as Australia. True polar wander, although relatively poorly constrained, has caused absolute motions of the spin axis relative to the paleo-positions of the plate circuit (Torsvik et al., 2012; Van Hinsbergen et al., 2015). On a paleomagnetic reference frame, Antarctica and Australia rotated northwestward by 3° of latitude and over 3° longitude between 70 and 50 Ma (Fig. 1), with only little transform displacement between them. From 50 Ma onwards, the tectonic drift orientation of Antarctica shifted slightly more southwards than that of Australia, causing left transform motion between notably west of Cape Adare and west Tasmania (Fig. 1; Williams et al., 2019). Although this divergence effectively opened the Tasmanian Gateway (TG) to surface flow of the Antarctic Counter Current close to the early-middle Eocene boundary (Bijl et al., 2013a), probably through subsidence of the Antarctic continental margin and STR, rapid northward movement of Australia and southward movement of East Antarctica did not start before about 40 Ma (Fig. 1; Cande and Stock, 2004; Seton et al., 2012). Yet, a connection between Australian and Antarctic continental blocks persisted until 34 Ma when transform motion between STR and Wilkes Land changed into spreading and ocean crust formation (Cande and Stock, 2004; Seton et al., 2012).

Deleted: plate

Deleted: relative to the spin axis of the Earth

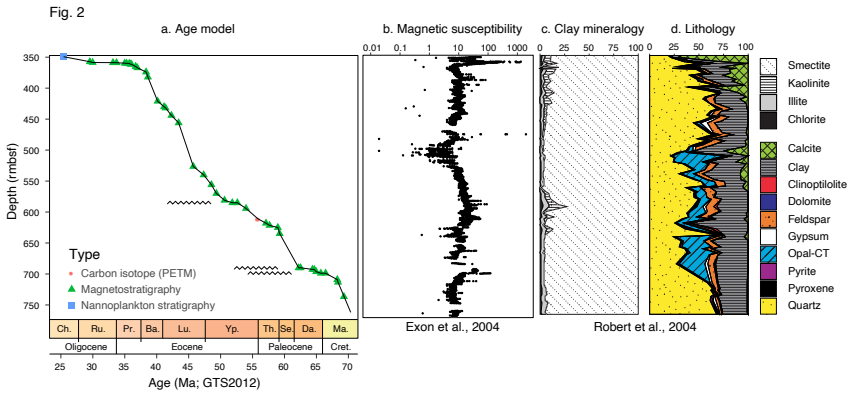

Figure 2. a. Age tie points used to construct the age model for ODP Site 1172, based on stable carbon isotopic (red dot; Sluijs et al., 2011), magnetostratigraphic (green triangles; Stickley et al., 2004a; Bijl et al., 2010; Houben et al., 2019), and nannofossil (blue square; Houben et al., 2019) age constraints. Black wobbly lines represent hiatuses. b. Shipboard magnetic susceptibility from Exon et al. (2001). c. Clay mineralogy and d. smear slide-based lithological observations from Robert (2004).

2.2 Lithology

A 760 meter thick sediment sequence was recovered at ODP Site 1172, on the western part of the ETP, east of Tasmania, Australia (Exon et al., 2001). We studied the interval from 760 meters below sea floor (mbsf) to about 350 mbsf in a composite (Röhl et al., 2004a) of Hole A and D. The carbonate ooze from 350 mbsf upwards did not yield any GDGTs. The studied succession consists broadly of green-grey silty claystones from 760 to ~505 mbsf, grading into dark grey to black silty claystones from 636 – 625 mbsf, then a return of the greenish grey silty claystones, which is interrupted by a more lithified unit at 610 mbsf (Exon et al., 2001; Röhl et al., 2004a, b; Schellenberg et al., 2004; Sluijs et al., 2011). The silty claystones turn gradually and cyclically lighter from 570 mbsf upwards until ~361 mbsf, with gradually more calcium carbonate and biogenic silica preserved (Röhl et al., 2004a). The clay mineralogy is dominated by smectite but contains progressively more kaolinite above

Deleted: e
Deleted: s
Deleted: Bijl et al., 2010;
Formatted: Not Highlight
Deleted: ; Stickley et al., 2004a
Deleted: s
Deleted: Shore-based
Deleted: c
Deleted: diatoms

~500 mbsf (Fig. 2; Exon et al., 2001; Robert, 2004). Grey silty claystones give way to a green glauconitic horizon between 360.1 and 357.3 mbfs (Exon et al., 2001). Above this greensand, carbonate oozes continue further upwards. The record is quasi-continuously bioturbated by zoophycos (Exon et al., 2001). We follow the depth corrections published in (Sluijs et al., 2011) for Cores 12R–31R, based on the correlation of core-log and downhole log magnetic susceptibility.

2.3 Age model

For age tie points (Table S1; Fig. 2), we use the identification of the PETM (Sluijs et al., 2011) and Middle Eocene Climatic Optimum (MECO; Bijl et al., 2010) and robust biostratigraphical constraints from the Eocene–Oligocene Boundary interval (Houben et al., 2019; Sluijs et al., 2003). In the intervals in between these tie points, the age model is based on magnetostratigraphy, which in the early Eocene suffers from a strong normal overprint (Dallanave et al., 2016). Despite the overprint, there is a paleomagnetic signal preserved in the inclination data (Fuller and Touchard, 2004). Biostratigraphic constraints from calcareous nannofossils, diatoms and dinocysts (Stickley et al., 2004a; Bijl et al., 2013b) are broadly consistent with nearby sites (Dallanave et al., 2016).

The nature of the sediments and depositional setting (see below) implies that small hiatuses may exist between the age tie points (Röhl et al., 2004a). Indeed, hiatuses were already identified across the Cretaceous–Paleogene Boundary (Schellenberg et al., 2004), in the mid-Paleocene (Bijl et al., 2013b; Hollis et al., 2014), early Eocene (Bijl et al., 2013b) and in the middle Eocene (Röhl et al., 2004a), corresponding to spikes in magnetic susceptibility (Fig. 2). The section across the Eocene–Oligocene transition is strongly condensed (Stickley et al., 2004a, b; Houben et al., 2019).

2.4 Depositional setting

From the lithology (Robert, 2004) and palynological content (Brinkhuis et al., 2003), the Maastrichtian–Eocene part of the record is interpreted to represent a shallow-marine, mid-continental shelf depositional setting, with gradual deepening in the middle Eocene based on an increase in calcium carbonate content (Fig. 2; Röhl et

Deleted: Exon

Deleted: relies

Deleted: some intervals

Deleted: , calibrated using nannofossil- diatom- and dinocyst biostratigraphy (Bijl et al., 2013b; Stickley et al., 2004). …

Deleted: does seem to be

Deleted: , and

Deleted: b

Deleted: (from

Deleted: biostratigraphy;

Deleted: Bijl et al., 2013b;

Deleted: increases

Deleted: Houben et al., 2019;

Deleted: was

al., 2004a). The late Eocene greensands were initially interpreted as indicating deepening and current inception as a result of widening of the TG (Stickley et al., 2004b). Later studies have related the greensands to invigorated ocean circulation and winnowing (Houben et al., 2019), with no deepening required. Volcanic activity of the Balleny plume in the late Eocene (Hill and Moore, 2001) might have influenced bathymetric changes of the ETP, in addition to the tectonic stresses that act on diverging plates in the TG area.

The regional tectonic evolution has implications for interpreting the marine and terrestrial temperature record at this site, because it influenced regional oceanography and climatic conditions in the hinterland. Field data and model simulations indicate that with a closed TG, the Tasman Current, a strong western boundary current of the proto-Ross gyre, bathed the plateau with Antarctic-derived surface waters (Huber et al., 2004; Bijl et al., 2011; 2013b; Sijp et al., 2014; 2016). Palynological evidence confirms that the Proto-Ross Gyre influence persisted at the ETP until the late Eocene (Warnaar et al., 2009; Bijl et al., 2011). This means that despite northward tectonic drift, the same strong western boundary current bathed the site during the Maastrichtian to late Eocene (Sijp et al., 2016), with perhaps some intermittent influence of East Australian Current waters from the north (Bijl et al., 2010; Cramwinckel et al., 2020). This ended when the proto-Leeuwin Current started to flow through the progressively widening TG (Fig. 1), bringing the ETP under the influence of more northerly sourced surface waters (Stickley et al., 2004b; Houben et al., 2019).

Persistent terrigenous input (Brinkhuis et al., 2003) arguably requires a large terrestrial catchment area, and the ETP seems too small (~50,000 km²) to have had vast areas above sea level. Seismic information from the East Tasman Saddle, connecting the Tasmanian Margin to the ETP, does not suggest there was a deep basin in between (Hill and Exon, 2004). Therefore, Tasmanian-sourced detrital material could reach the ETP. Paleocene–Eocene terrestrial palynomorph assemblages contain common Permian–Triassic elements (Contreras et al., 2014); the Permian–Triassic upper Parmeener group contains thick terrestrial (coal) deposits and comprises the surface lithology of most of eastern Tasmania today. Therefore, the source area for the terrestrial organic matter (OM) and detrital input was likely

Deleted: have been

Deleted: evidenc

Deleted: strong

Deleted: and not necessarily

Deleted: of the site

Deleted: played a profound role in the

Deleted: catchment area

Deleted: Huber et al., 2004;

Deleted: ; Warnaar et al., 2009

Deleted: early

Deleted: ; Stickley et al., 2004b

Moved down [5]: The source area for the terrestrial organic matter (OM) and detrital input was likely Tasmania.

Deleted: Moreover,

Tasmania. Minor contributions could have derived from rivers flowing from southeast Australia. Also, the Cretaceous-Paleocene ETP might have received perhaps a minor component of Antarctic-sourced terrestrial OM input, in addition to the dominant Tasmanian source. The regional palynology (Truswell, 1997; Macphail, 2000; 2002; Carpenter et al., 2012; Pross et al., 2012; Contreras et al., 2013; 2014), the abundance of peatlands (Holdgate et al., 2009), and the felsic lithology (Moore et al., 2013) suggests the hinterland catchment contained acidic, wet soils and peats.

2.5 Samples

For this study, we used lipid extracts that have been analysed for GDGTs previously (Bijl et al., 2009; Sluijs et al., 2011; Hollis et al., 2014; Houben et al., 2019). We augmented these with 69 new extracts of sediments from the Maastrichtian and the Paleocene, to extend and improve the temporal resolution of the record. Unfortunately, not all archived samples from the PETM interval (Sluijs et al., 2011) could be located, and the interval was reanalysed in a lower resolution (6 samples over the PETM interval). For the remaining PETM, we used the published peak areas (Sluijs et al., 2011) to calculate TEX_{86}, which is warranted given the new analytical technique does not affect isoGDGT peak area ratios (Hopmans et al., 2016). For palynology, we collated and revisited data presented in (Brinkhuis et al., 2003; Bijl et al., 2010; 2013b; Sluijs et al., 2011; Houben et al., 2019) and generated higher-resolution data for the Maastrichtian and Paleocene.

3. Methods

3.1 Organic geochemistry

3.1.1 Extraction, column separation and analysis

Earlier work (Bijl et al., 2009; 2010; 2013a; Sluijs et al., 2011; Houben et al., 2019) presented in detail the extraction, Al_2O_x column separation and filtering techniques used for the samples. We followed the same procedures for the processing of the new samples. We reanalysed all available polar fractions using the double column UHPLC-MS approach as described in (Hopmans et al., 2016). In short, processing involved extraction with a Dionex accelerated solvent extractor using

Deleted: Although that same formation might be present in the ETP subsurface as well, it was probably covered with sediment throughout the Cenozoic (Hill and Moore, 2001).

Deleted: R

Moved (insertion) [6]

Moved (insertion) [5]

Moved up [6]: Seismic information from the East Tasman Saddle, connecting the Tasmanian Margin to the ETP, does not suggest there was a deep basin in between (Hill and Exon, 2004). Therefore, Tasmanian-sourced detrital material could reach the ETP.

Deleted: drained into the Gippsland and Bass Basins, and that terrigenous material is unlikely to have reached the ETP. Seismic information from the East Tasman Saddle, connecting the Tasmanian Margin to the ETP, does not suggest there was a deep basin in between (Hill and Exon, 2004). Therefore, Tasmanian-sourced detrital material could reach the ETP. The source area for the terrestrial organic matter (OM) and detrital input was likely Tasmania. Seismic information from the East Tasman Saddle, connecting the Tasmanian Margin to the ETP, does not suggest there was a deep basin in between (Hill and Exon, 2004). Therefore, Tasmanian-sourced detrital material could reach the ETP. The

Deleted: was close enough to the Antarctic margin during the Maastrichtian–early Eocene to

Deleted: ; Truswell, 1997

Deleted: , Betts, and Hall

Deleted: ,

Deleted: ; Sluijs et al., 2011

Deleted: Brinkhuis et al., 2003;

Deleted: ; Sluijs et al., 2011

Deleted: ; Sluijs et al., 2011

dichloromethane:methanol (DCM:MeOH) 9:1 (v/v), column separation of the total lipid extract using solvent mixtures hexane:DCM 9:1 (v/v), hexane:DCM 1:1 (v/v) and DCM:MeOH 1:1 (v/v) for apolar, ketone and polar fractions, respectively. Polar fractions were filtered using a 0.45 µm polytetrafluorethylene filter and analysed using an Agilent 1260 Infinity series HPLC system coupled to an Agilent 6130 single-quadrupole mass spectrometer.

Deleted: ,

Formatted: Font: (Default) Cambria, Font colour: Black

3.1.2 Data analysis: indices, overprints

Since the discovery of isoGDGTs as proxy for SST (see Schouten et al. (2013) for a review), several non-SST effects have been identified that may affect the distribution of isoGDGTs in the sediment. Several indices have been developed to identify most of the known sources of overprints (Table 1). As well as identifying potential overprints, these indices can provide additional paleoenvironmental information.

Deleted: Next to signalling SST-unrelated influences on the isoGDGT pool, these indices also provide information on the prevailing marine and paleoenvironmental and depositional conditions.

Table 1: Indices from iso- and brGDGTs and brGMGTs. For the chemical structure of these components see Fig. 3.

Index name	Equation	Proxy for	Cut-off value	Source
TEX_{86}	$\frac{GDGT2 + GDGT3 + Cren'}{GDGT1 + GDGT2 + GDGT3 + Cren'}$	Sea surface temperature	-	(Schouten et al., 2002)
BIT index	$\frac{IIIa + IIIa' + IIa + IIa' + Ia}{Cren + IIIa + IIIa' + IIa + IIa' + Ia}$	Terrestrial input	>0.4? Site-dependent	(Hopmans et al., 2004)
fcren'	$\frac{\%Cren`}{\%Cren` + \%Cren}$	Non-thermal contribution of crenarchaeol isomer	0.25	(O'Brien et al., 2017)
Methane Index	$\frac{GDGT1 + GDGT2 + GDGT3}{GDGT1 + GDGT2 + GDGT3 + Cren + Cren'}$	Contribution by methane-metabolising archaea	>0.3	(Zhang et al., 2011)
AOM ratio	$GDGT2/Cren$	Contribution by anaeropbic methane oxydizers	>0.2	(Weijers et al., 2011)
GDGT2/3 ratio	$GDGT2/GDGT3$	Contribution by deep-dwelling archaea	>5	(Taylor et al., 2013)

Methano-genesis	$GDGT0/Cren$	Contribution by methanogenic archaea	>2.0	(Blaga et al., 2009)
Ring index (RI)	0*%GDGT0 + 1*%$GDGT1$ + 2*%$GDGT2$ + 3*%$GDGT3$ + 4*%$Cren$ + 4*%$Cren'$	Non-pelagic GDGT composition	ΔRI >0.3*	(Zhang et al., 2016)
MBT'_{5me}	$\frac{IIIa + IIIb + IIIc}{IIIa + IIIb + IIIc + IIa + IIb + IIc + Ia}$	Mean annual air temperature	-	(De Jonge et al., 2014a)
CBT'	$\frac{IIIb + IIb' + IIc' + Ia'}{IIIa + IIa + Ia}$	(soil-)pH	-	(De Jonge et al., 2014a)
$\#rings_{tetra}$	$\frac{Ib + 2 * Ic}{Ia + Ib + Ic}$	Marine in situ brGDGT production	>0.7	(Sinninghe Damsté, 2016)
$\#rings_{penta}$	$\frac{IIb + IIb' + 2 * IIc + 2 * IIc'}{IIa + IIa' + IIb + IIb' + IIc + IIc'}$		-	
$\#rings_{penta5}$	$\frac{IIb + 2 * IIc}{IIa + IIb + IIc}$		-	
$\#rings_{penta6}$	$\frac{IIb' + 2 * IIc'}{IIa' + IIb' + IIc'}$		-	
IR	$\frac{IIa' + IIb' + IIc' + Ia'}{IIa + IIa' + IIb + IIb' + IIc + IIc' + Ia + Ia'}$	River in situ brGDGT production	Depends on soil value	(De Jonge et al., 2014b)
IR_{hexa}	$\frac{Ia'}{Ia + Ia'}$		-	(Sinninghe Damsté, 2016)
IR_{penta}	$\frac{IIa' + IIb' + IIc'}{IIa + IIa' + IIb + IIb' + IIc + IIc'}$			
brGMGTI	$\frac{H1020c + H1034a + H1034c}{\mathrm{H1020b + H1020c} + H1034a + H1034b + H1}$	Temperature, oxygenation?	In lakes	(Baxter et al., 2019)
%brGMGT, $\%brGMGT_{acyclic}$	$\frac{[brGMGT]}{[brGMGT] + [brGDGT]} \times 100$		In peats, lakes	(Baxter et al., 2019)
	$\frac{[brGMGT]}{[Ia + IIa + IIIa + brGMGT]} \times 100$			(Naafs et al., 2018a)
$HMBT_{acyclic, all}$	$\frac{H1020a + H1020b + H1}{H1020a + H1020b + H1020c + H1034a + H}$		In peats	(Naafs et al., 2018a)
$HMBT_{acyclic}$	$\frac{H1020c}{H1020c + 1034b + H1048}$		In Arctic Ocean sediments	Sluijs et al., 2020, sensu Naafs et al., 2018a)

* Cutoff depends on TEX_{86} value. ΔRI = RI_{TEX} – RI, where RI_{TEX} = -0.77*TEX_{86} + 3.32*TEX_{86}^2 + 1.59

Formatted: Not Highlight

Formatted: Not Highlight

Formatted: Not Highlight

Formatted: Not Highlight

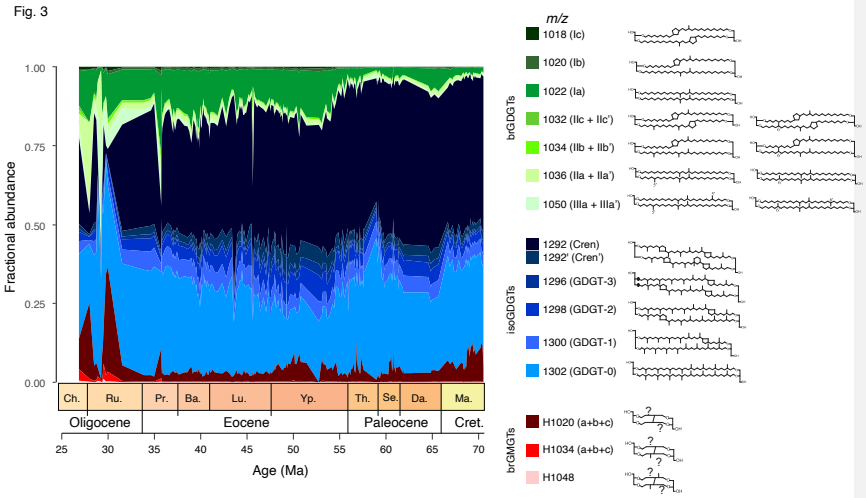

Figure 3. Variations in fractional abundances of the various branched (green) and isoprenoid (blue) GDGTs, and branched GMGTs (red) at ODP Site 1172.

All of the ratios that signal biases express the influence of this bias relative to modern "normal" or idealized compositions. For the branched and isoprenoid tetraether (BIT) index, it was proposed that the closed sum ratio between brGDGTs, which were thought to derive exclusively from soils, and the isoGDGT crenarchaeol, which was thought to be produced exclusively by marine archaea, could be an indicator for the relative contribution of soil organic matter (OM) into marine sediments (Hopmans et al., 2004). However, it was subsequently shown that crenarchaeol, but critically also other isoGDGTs are also produced on land (Weijers et al. (2006), and that a large contribution of soil-OM to marine sediments can cause a bias in TEX_{86}. Weijers et al. (2006) used an end-member model to calculate the potential bias in TEX_{86}-based SST reconstructions in the Congo Fan and this shows significant bias (>2°C) for BIT above 0.3. However, it is rather arbitrary to assign a cut-off for BIT based on the magnitude of the SST bias alone, as this bias depends primarily on the difference between the isoGDGT composition of the soil and marine endmembers. As a consequence, there is no uniform value for BIT index above which

Deleted: F

Deleted: and

Deleted: al

Deleted: The abundance of overprinted components is divided over either a total sum of overprinted and non-overprinted components (closed sum; e.g., methane index, IR) or over only the non-overprinted (ratio; GDGT2/3 ratio, AOM ratio). The complication is that a change in index value can be caused by changes in the denominator or numerator. This is particularly evident in the interpretation of…

Deleted:

Deleted: . I

Deleted: cut-off

TEX_{86} should be discarded. Secondly, because the BIT index is a closed sum, the index is equally affected by increased production of crenarchaeol as it is by the input of brGDGTs. Although this could be verified with absolute concentrations of GDGTs, these are not always presented. Third, brGDGTs are produced in situ in the marine realm (Peterse et al., 2009; Sinninghe Damsté, 2016). The corollary of this is that the cut-off value for BIT to infer an overprint in the isoGDGT-based SST signal should be assumed to differ per environmental setting, and perhaps also through time if the setting changes significantly (e.g., Sluijs et al., 2020). As a result, cut-offs have been set higher (e.g., 0.4; Bijl et al., 2013a) when no relationship between TEX_{86} and BIT index values is detected. This approach is also not without complications, because the abundance and composition of isoGDGTs (including crenarchaeol) in soil material varies (Weijers et al., 2006; De Jonge et al., 2015; De Jonge et al., 2016; Naafs et al., 2019; Sluijs et al., 2020). This implies that for samples with intermediate to high BIT (Weijers et al., 2006), a terrestrially-derived isoGDGT contribution with a variable isoGDGT composition or a TEX_{86}-signature close to the original pelagic isoGDGT signal would become undetectable in a TEX_{86}-BIT index crossplot. In some paleo-environmental settings that evidently lack high input of soil-OM, BIT index values are high (Leutert et al., 2020). For reasons given above, this could either mean very low crenarchaeol production in the marine realm, or in situ production of brGDGTs. These two scenarios make for a completely different paleoenvironmental interpretation, and fail to indicate whether the brGDGTs can be used to reconstruct MAAT of the hinterland, or whether isoGDGTs can be used for reliable paleothermometry. For that, it is important to assess the sources of brGDGTs, as brGDGTs produced in rivers (Zell et al., 2013; De Jonge et al., 2014b) or the (coastal) marine environment (Peterse et al., 2009; Sinninghe Damsté, 2016) may contribute and thereby bias the initial soil-derived brGDGT signal, affecting the reliability of MAAT reconstructions. Fortunately, production of brGDGTs in the marine realm can be recognized based on the weighed number of rings of the tetramethylated brGDGTs, quantified in the $\#rings_{tetra}$, where values >0.7 indicate a purely marine source of the brGDGTs (Sinninghe Damsté, 2016). The $\#rings_{tetra}$ in coastal marine sediments can subsequently be used to determine and correct for the contribution of marine brGDGTs to the temperature signal of the soil-derived brGDGTs (Dearing Crampton-Flood et al., 2018). Similarly,

Deleted: Dearing Crampton-Flood et al., 2019; Peterse et al., 2009; Sinninghe Damsté, 2016

Deleted: majorly

Deleted: were

Deleted: was

Deleted: This in turn implies that i

Deleted: n

Deleted: the

Formatted: Subscript

Deleted: will not be uniform, and might

Deleted: impossible

Deleted: to

Deleted:

Deleted: or

Deleted: ; Zell et al., 2013

Deleted: Dearing Crampton-Flood et al., 2019; Peterse et al., 2009; Sinninghe Damsté, 2016

brGDGTs that are produced in rivers are characterized by a relatively high abundance of the 6-methyl brGDGTs relative to the 5-methyl brGDGTs, expressed as the Isomerization Ratio (IR; De Jonge et al., 2014b).

For the other indices for overprints, cut-off values may not be as uniformly applicable to all depositional settings either. Leutert et al. (2020) showed that modern samples exceeding cut-off values for the GDGT2/3 ratio and methanogenesis index do not have anomalous TEX_{86} index values in the modern core-top dataset based on the Ring index. This suggests that the TEX_{86} index value is not equally influenced by non-thermal contributions in all depositional settings. As a result, evaluating non-thermal contributions on TEX_{86} index values should consider the depositional and environmental setting along with the cut-off values.

3.1.3 Calibrations for TEX_{86} and MBT'_{5me}

Several calibrations have been proposed to convert TEX_{86} index values to sea surface temperatures. For higher temperatures, it remains uncertain if the TEX_{86}-SST relationship is linear or exponential for values above the modern calibration (O'Brien et al., 2017; Tierney et al., 2017; Cramwinckel et al., 2018; Hollis et al., 2019). Following recent recommendations (Hollis et al. 2019), we here apply several calibrations to convert our TEX_{86} values to SSTs. We apply an exponential calibration (Kim et al., 2010) even though it suffers from a regression dilution bias (Tierney and Tingley, 2015), and two linear calibrations; one on the warm part (>15°C) of the core-top dataset (O'Brien et al., 2017) and one using Bayesian statistics (BAYSPAR; Tierney and Tingley, 2015) to convert our TEX_{86} values to SSTs. We chose these calibrations to present the appropriate uncertainty related to calibration function, particularly for TEX_{86} values exceeding those of the modern core-top data. For MAAT reconstructions, we use the Bayesian $BayMBT_0$ of Dearing Crampton-Flood et al. (2020). We will compare the calibrations for both proxies to middle Eocene $U^{K'}_{37}$-based SSTs (from Bijl et al., 2010, but using BAYSPLINE calibration of Tierney and Tingley, 2018) and to Paleocene–early Eocene sporomorph-based MAAT estimates (Contreras et al., 2014) from the same site.

Table 2. Calibration equations for TEX_{86} and MAAT

Deleted: overprinting
Deleted: indices
Deleted: An extensive number of
Deleted: has
Formatted: Subscript
Deleted: At the heart of the calibration discussion is the uncertainty whether the TEX_{86}-to-SST relationship continues in a linear way beyond the modern SST range, or in an exponential way (Hollis et al. 2019).
Deleted: The answer to that is beyond the scope of this paper, and we refer to (Cramwinckel et al., 2018; Hollis et al., 2019; O'Brien et al., 2017; Tierney et al., 2017) for detailed discussions, specifically about using TEX_{86} in regions with SSTs warmer than modern.
Deleted: for which we acknowledge that
Deleted: this calibration
Deleted: BAYSPAR produces a linear calibration based on a subset of the core top data with similar GDGT assemblages as the measured TEX_{86}, with a user-defined tolerance. The larger the subset of core tops (i.e., when the number of identified core-top analogues to the sample TEX_{86} values is large), the closer the Bayesian calibration will approach a global linear regression.
Deleted: in order
Deleted: full
Deleted: scope of
Deleted: in the absolute SST reconstructions
Deleted: for the part of the record with
Formatted: Subscript
Deleted: index
Deleted: ocean
Deleted: Deming regression of the soil-specific calibration of Naafs et al. (2017b; $MAAT_{soil}$) and the
Deleted: The latter follows the approach of BAYSPAR, but then for MBT'_{5me}.

Calibration	Equation	Type	Proxy for	Source
SST_{exp} (TEX_{86}^{H})	68.4 * log10(TEX_{86}) + 38.6	Exponential	Mean annual SST (0–20m)	(Kim et al., 2010)
SST_{lin}	58.8 * TEX_{86} – 11.18	Linear	Mean annual SST (0–20m)	(O'Brien et al., 2017)
BAYSPAR	TEX_{86}, Prior mean = 20, prior std = 10, search tolerance = 0.15	Bayesian linear	Mean annual SST (0-20m)	(Tierney and Tingley, 2015)
$BayMBT_0$	MBT'_{5me}, Prior mean = 20, prior std = 15	Bayesian linear	Mean annual air temperature (excluding days >0°C)	(Dearing Cramptor-Flood et al., 2020)

Deleted: (regression dilution)

Formatted: Subscript

Deleted: $MAAT_{soil}$

Formatted: Subscript

Deleted: (Naafs et al., 2017b)

Deleted: 40.01 * MBT'_{5me} -15.25

Deleted: Linear, Deming regression

Deleted: Mean annual air temperature (for days above freezing)

Formatted: Font: 10 pt

Deleted: $BayMBT_0$ ... [8]

3.1.4 R-script for data analysis and evaluation

To facilitate systematic calculation of GDGT ratios, data analysis, visualization, and evaluation, we constructed a set of R markdowns (https://github.com/bijlpeter83/RGDGT.git) that can be applied to any time- or depth series of isoGDGT, brGDGT and/or brGMGT data. The R script loads peak areas of GDGTs/GMGTs from Microsoft excel spreadsheets, calculates and plots fractional abundances, overprinting indices and paleotemperature time or depth series.

3.2 Palynology

3.2.1 Sample processing

Palynological sample processing techniques were published in the original papers describing these datasets (Brinkhuis et al., 2003; Bijl et al., 2010; 2013b; Sluijs et al., 2011; Houben et al., 2019). We followed the same procedure for the new Maastrichtian–Paleocene samples. These publications do utilize different sieve mesh sizes (10 or 15 µm) but given all counted dinocysts are larger than 15 µm, this has not led to differences in the dinocyst results.

Deleted: Brinkhuis et al., 2003;

Deleted: ; Sluijs et al., 2011

Deleted: . The different

Deleted: indicate

Deleted: differences

Deleted: in the employed

3.2.2 Taxonomy

We used the taxonomic framework cited in Williams et al., (2017) in our counts down to the species level, with one exception. For the Wetzelielloidae subfamily, we follow Bijl et al. (2017), for reasons stated therein. We follow the supra-generic classification of Fensome et al. (1993), also for genera described post-1993.

Deleted: also

Deleted: based on

Deleted: .;

Deleted: G

Deleted: g

Deleted: were added into that classification

Deleted: accordingly

3.2.3 Ecological affinities of dinocyst eco-groups

In this paper, dinocysts are plotted in eco-groups and complexes, which group species with similar ecologic affinities based on modern (for extant taxa) and empirical (for extant and extinct taxa) data (Sluijs et al., 2005; Frieling and Sluijs, 2018). The species of which the ecologic affinity was not assessed previously were included into larger groups based on shared morphological characteristics; primarily tabulation, archaeopyle and cyst- and process shapes. For example, the "*Apectodinium* complex" is equated to "Wetzellioids" following Frieling et al. (2014; see Table S2 for taxonomic grouping). We directly compare dinocyst- and terrestrial palynomorph indices with GDGT-based indices (following the approach of Frieling and Sluijs, 2018) to arrive at multi-proxy reconstructions of SST, river runoff and distance to shore (Table 3). For this, we resampled and binned GDGT-based indices to the sample resolution of the dinocyst data. Some dinocyst groups have affinities for multiple environmental parameters, due to the strong co-variance of environmental gradients on an inshore-to-offshore transect. Therefore, the complete dinocyst assemblage (including absence of presence) and knowledge of the geographic setting is used to reconstruct changes in paleoenvironmental conditions from dinocysts.

Table 3. Environmental parameters, and their corresponding GDGT indices and dinocyst eco-groups, based on Sluijs et al. (2005), Frieling and Sluijs (2018) and Sluijs and Brinkhuis (2009).

Environmental parameter	**GDGT index**	**Dinocyst eco-group**
Sea surface temperature	TEX_{86}	%Thermophiles (Wetzellioideae, *Hafniasphaera* spp., *Florentinia reichartii*, *Polysphaeridium* spp, *Homotryblium* spp., *Heteraulacacysta* spp., *Eocladopyxis* spp., *Dinopterygium* spp.)
Runoff, fresh water, salinity	IR, BIT	%*Senegalinium* cpx, %*Phthanoperidinium* spp., %Terrestrial palynomorphs
Distance to shore	BIT, #ringstetra	%Open marine (*Apectodinium* spp., *Impagidinium* spp., *Operculodinium* spp.,

Deleted: we present our results
Deleted: s
Deleted: dinocyst
Deleted: Frieling and Sluijs, 2018;
Formatted: Not Highlight

		Spiniferites spp.), %*Glaphyrocysta* cpx., %Epicystal Goniodomids (*Polysphaeridium* spp, *Homotryblium* spp., *Heteraulacacysta* spp., *Eocladopyxis* spp., *Dinopterygium* spp.), %Terrestrial palynomorphs

3.2.4 Diversity and variability indices

To gain insight into the diversity and variability of the dinocyst assemblage through time, we employ several indices (Table 4), and compare their results at species and eco-group level. We note that diversity in dinocyst taxonomy is complicated because dinocysts are dominantly produced during the hypnozygotic phase of the dinoflagellate life cycle following sexual reproduction. Only ~15% of modern dinoflagellates have this cyst stage (Fensome et al., 1993). This leaves a large proportion of the biological group unrepresented in the fossil record, including, for example, coral and foraminifer symbionts, but also many free-swimming taxa. Dinocyst diversity is therefore a biased indicator for plankton diversity. As a further complication, taxonomic divisions of cysts, although strongly related to dinoflagellate morphology and taxonomy, is fully based on the morphology of dinocysts. Even modern dinoflagellate-dinocyst relationships are often ambiguous. Some dinoflagellate species produce various cyst morphologies (Rochon et al., 2008) that represent multiple cyst genera or species. Some of these cyst morphological variations are the result of ecology (Mertens et al., 2011). This complicates comparing cyst datasets on the species level and affects assessing biological diversity based on cysts. On the genus level, taxonomic division of cysts is in most cases based on plate tabulation, which is the morphologic feature that has the closest relationship to dinoflagellate biological diversity (Fensome et al., 1993). However, ecologic or biogeographic affinities have been established for some dinocysts on a species level (e.g., Frieling and Sluijs, 2018), which does suggest subtle morphological features may have biologic and ecologic significance. The eco-groups we use here are the result of extensive reviews of empirical data. These groups combine dinocyst genera and

Deleted: ecogroup

Deleted: since

Deleted: features

Deleted: ,

Deleted: which

Deleted: more closely related

Deleted: can therefore only be used as an

Deleted:

Deleted: dinocyst-producing dinoflagellates

Deleted: not un

species with fundamentally similar plate tabulations, and thus probably group cysts of closely affiliated biological dinoflagellate species, and, as such also ecologic affinities. For our diversity calculations we use both the ungrouped data on species level and the diversity in dinocyst eco-groups.

As the simplest approximation of biological diversity, the richness (R) sums dinocyst taxa. Furthermore, several diversity measures were calculated using the R package Vegan (Oksanen et al., 2015). Fisher's alpha (α), Shannon index (H') and Simpson index (D). Finally, we employed the Σcv metric (Gibbs et al., 2012), which we here dub the "Gibbs index", which provides a measure for assemblage variability. Together, these metrics give insight into changing stability and diversity of these regional dinocyst assemblages over the Maastrichtian to early Oligocene.

Deleted: ecogroups

Deleted: in terms of dinocyst taxa was summed

Deleted: .

Deleted: Of these,

Deleted: is based on the count data, whereas the

Deleted: derive from the relative abundance data

Deleted: and

Deleted: can

Table 4. Diversity and variability indices for (fossil) assemblages. In the Shannon and Simpson indices, p_i represents the proportional abundance of the i^{th} taxon of the total amount of taxa R. The Gibbs index summates the coefficients of variation (SD/mean) of all taxa (i to R) over a certain rolling window $t_1 \rightarrow t_2$. In Fisher's alpha, the α parameter is estimated from the dataset in which S is the expected number of species with an abundance of n. x represents a nuisance parameter estimated from the dataset, generally between 0.9 and 1. While the Gibbs index is calculated over a rolling window, the other indices are calculated per sample.

Index	Equation	Source
Shannon index (H')	$H' = \sum_{i=1}^{R} p_i * \ln p_i$	(Shannon, 1948)
Simpson index (D)	$D = \sum_{i=1}^{R} p_i^2$	(Simpson, 1949)
Gibbs index (Σcv)	$\Sigma\text{cv} = \sum_{i=1}^{R} \left(\frac{\text{SD}_{i,t_1 \rightarrow t_2}}{\text{mean}_{i,t_1 \rightarrow t_2}} \right)$	(Gibbs et al., 2012)
Fisher's alpha (α)	$S_n = \frac{\alpha x^n}{n}$	(Fisher et al., 1943)

3.3 Comparison of GDGT and dinocyst assemblage data

Both dinocyst eco-groups and GDGT indices bear information on SST, runoff (~salinity), nutrients and marine primary productivity, and relative distance to shore (Table 4). As dinocyst and GDGT analyses were performed on partly separate datasets, the highest resolution dataset (dinocysts) was linearly resampled to the depth intervals of the GDGT data to facilitate inter-comparison.

4. Results

4.1 GDGTs

The resulting dataset has an average temporal resolution of ~130 kyrs for the time interval between 70 and 30 Ma. IsoGDGTs dominate the pool of GDGTs (particularly GDGT-0 and crenarchaeol), with a gradual increasing relative abundance of brGDGTs (particularly Ia) throughout the record (Fig. 3). BrGMGTs are in low (<10%) relative abundance, except in the Oligocene, where they account for up to 30% of the total pool of tetraether lipids.

4.1.1 Isoprenoidal GDGTs

Before the TEX_{86} index results (Fig. 4a) can be interpreted in terms of SST, we assess whether the isoGDGTs are primarily derived from the sea surface, or have received contributions from non-pelagic sources. Across the Ypresian, the BIT index (Fig. 4b) increases from values around 0.1 in the underlying sediments to values at times exceeding 0.4. Most EECO and middle Eocene values, however, have BIT index values between 0.2 and 0.35. The remaining sediments have BIT index values of around 0.3, with the exception of some upper Eocene and Oligocene sediments that occasionally have values around 0.75. There is no correlation between TEX_{86} and BIT index in our entire dataset (R^2=0.0067 ; p=0.15). None of the samples have fcren' (Fig. 4c) values above the cut-off of 0.25, which excludes non-thermal contributions of the crenachaeol isomer to the isoGDGTs. In fact, the consistent trend in fcren' and the TEX_{86} (Fig. 4) demonstrates the temperature sensitivity of cren'. With the exception of 6 samples in the Oligocene, all samples have methane index values below the conservative cut-off value of 0.3 (Fig. 4d), although in the early and middle Eocene, methane index values do approach the cut-off. AOM ratio values suggest an overprint from anaerobic methane oxidisers in one sample in the early Eocene that also has a

Deleted: ecogroups

Deleted: GDGT/GMGT

Formatted: Superscript

Deleted: suggesting no non-

Deleted: temperature related

Deleted: (

Deleted:)

Deleted: index

Deleted: and confirms that discarding it from the index as was done for the cold-temperature index TEX_{86}^{L} (Kim et al., 2010) is not justified here

high BIT index, and 5 samples from the Oligocene where isoGDGTs supposedly received a contribution of anaerobic methane oxidisers (Fig. 4e). As a result, these samples were not used for SST reconstruction.

Values signalling a deeper water column overprint (GDGT2/3 ratio) fall below 5 for most of the data (Fig. 4f), which was expected given the depositional setting on a continental shelf. A total of 5 samples has GDGT2/3 values exceeding 5, 4 of which also had other indications of overprinted isoGDGT signals. We discard eight TEX_{86} datapoints because GDGT-0/crenarchaeol ratios are above 2 (Fig. 4g). One of these is from the PETM, with a value just above the cut-off. The others represent Oligocene samples.

In total, 18 samples fall outside the range of RI values that characterize modern pelagic-derived isoGDGT compositions (ΔRI >0.3; Fig. 4h, or 95% confidence interval; Fig. 5). Nine of these 18 come from the interval >43 Ma and have no other indications of overprints. These samples fall just outside the 95% confidence interval limits (Fig. 5) and do follow the overall RI/TEX_{86} trend, but we here discard them to be conservative. The other 9 samples with too high ΔRI come from the late Eocene-Oligocene and have BIT index values over 0.4. Two of these samples have no other overprint indication, the other 7 have multiple other overprints. One sample has RI values above the range of modern samples (with no other overprinting indications), the others have too low RI values. Eight samples with normal RI values do have overprints based on the other indices: BIT index values slightly over 0.4 (6 samples), GDGT2/3 ratio values over 5 (1 sample), and AOM ratio over 0.2 (1 sample). Following Leutert et al. (2020) we retained the samples with normal RI values and high BIT or GDGT2/3 ratio values. After considering all these potential biases, and retaining those with normal isoGDGT distributions, we discard a total of 19 samples. Most discarded samples are from the Oligocene and are excluded based on multiple overprint criteria.

Deleted: for TEX_{86}.

Fig. 4

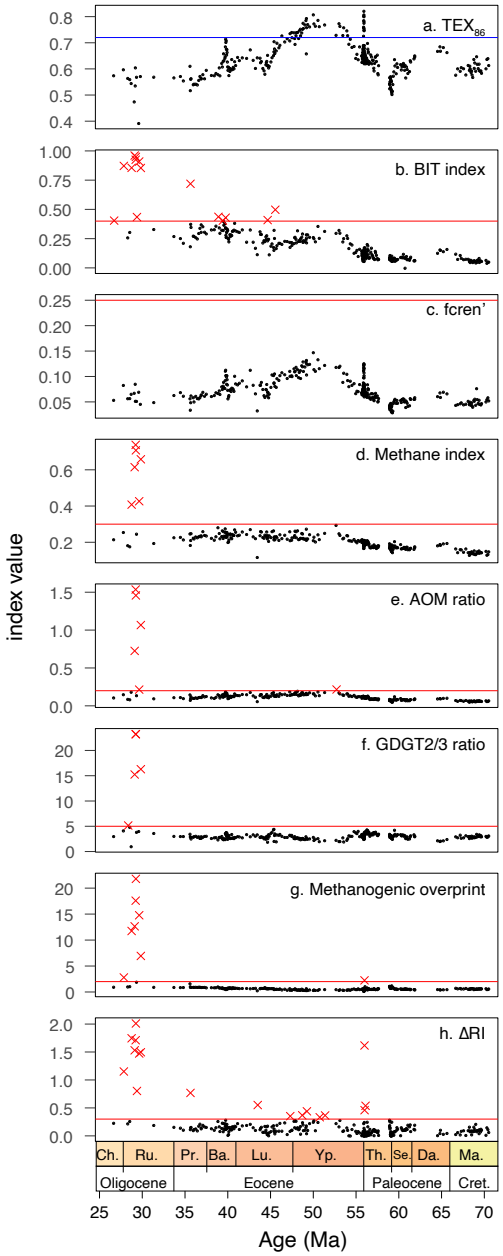
a. TEX86
b. BIT index
c. fcren'
d. Methane index
e. AOM ratio
f. GDGT2/3 ratio
g. Methanogenic overprint
h. ΔRI
index value
Ch.
Ru.
Pr.
Ba.
Lu.
Yp.
Th.
Se.
Da.
Ma.
Oligocene
Eocene
Paleocene
Cret.
Age (Ma)

1036

Figure 4. TEX_{86} index and indices to identify overprints. For the equations of these indices see Table 1. Red line indicates the cut-off value, red crosses indicate samples exceed the cutoff a. TEX_{86} (Schouten et al., 2002), with blue line indicating the maximum modern core-top value (~0.72). b. BIT index (Hopmans et al., 2004). c. fcren' (O'Brien et al., 2017), no samples discarded; d. Methane index (Zhang et al., 2011), $n_{discarded}$ = 6. e. AOM ratio (Weijers et al., 2011), $n_{discarded}$ = 6. f. GDGT2/3 (Taylor et al., 2013), conservative cut-off of 5, $n_{discarded}$ = 4, one sample retained for absence of anomalous Ring index values (see text). g. Methanogenesis (Blaga et al., 2009), cut-off of 2.0, $n_{discarded}$ = 8. h. ΔRI $n_{discarded}$ = 18.

Fig.5

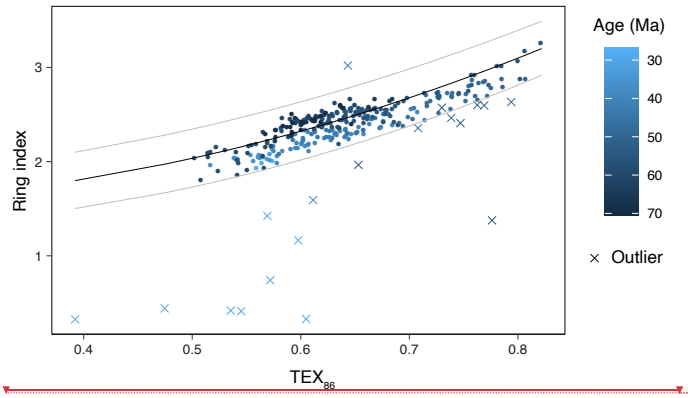

Figure 5. Ring index (RI) versus TEX_{86}. Dots indicate RI/TEX_{86} values for samples that are retained, crosses indicate samples that are discarded (see Fig. 4). Color of all datapoints indicates age of the sample, from Maastrichtian (dark blue) to Oligocene (light blue). Black and grey curves represent the RI/TEX_{86} ratio in modern core top samples and 95% confidence interval, respectively (see Table 1).

4.1.2 Branched GDGTs

Before brGDGT distributions can be interpreted in terms of air temperature, we assess whether they are primarily derived from soils, or have received

Deleted: overprinting

Formatted: Not Highlight

Formatted: Not Highlight

Deleted: Values signalling a deeper water column overprint (GDGT2/3 ratio) fall below 5 for most of the data (Fig. 4f), which was expected given the depositional setting on a continental shelf. A total of 5 samples has water GDGT2/3 values exceeding 5, 4 of which also had other indications of overprinted isoGDGT signals. We discard eight TEX_{86} datapoints because GDGT-0/crenarchaeol ratios are over above 2 (Fig. 4g). One of these is from the PETM, with a value just above the cut-off. The others represent Oligocene samples.¶
In total, 18 samples fall outside the range of RI values that characterize modern pelagic-derived isoGDGT compositions (ΔRI >0.3; Fig. 4h, or 95% confidence interval; Fig. 5). Nine of these 18 come from the interval >43 Ma and have no other indications of overprints. These samples fall just outside the 95% confidence interval limits (Fig. 5) and do follow the overall RI/TEX_{86} trend, but we here discard them to be conservative. The other 9 samples with too high ΔRI come from the late Eocene-Oligocene and have BIT index values over 0.4. Two of these samples have no other overprint indication, the other 7 have multiple other overprints. One sample has RI values above the range of modern samples (with no other overprinting indications), the others have too low RI values. Eight samples with normal RI values do have overprints based on the other indices: BIT index values slightly over 0.4 (6 samples), GDGT2/3 ratio values over 5 (1 sample), and AOM ratio over 0.2 (1 sample). Following Leutert et al. (2020) we retained the samples with normal RI values and high BIT or GDGT2/3 ratio values. Aft ... [9]

Fig.5

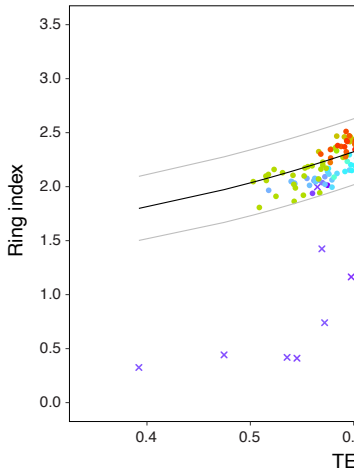

Deleted:

Deleted: relationship of

Deleted: ,

Deleted: ¶

contributions from river-, or marine in situ production. The relative abundance of tetra-, penta- and hexamethylated brGDGTs in the samples from 1172 deviates from that in modern and Paleogene soils and peats (Fig. 6): it has either comparatively less tetra-, less penta-, or more hexamethylated brGDGTs, and the data split into 2 clusters. The largest cluster follows the distribution observed in modern soils and peats with an offset (Fig. 6). This generally indicates brGDGT contributions from sources other than soils. The smaller second cluster, containing exclusively mid-to-late Paleocene samples, is indeed close to that of modern continental shelf sediments (Berau delta and Svalbard; Sinninghe Damsté, 2016; Dearing Crampton-Flood et al., 2019) for which in situ brGDGT production substantially exceeds soil contributions. This would generally suggest that the smaller cluster, and perhaps also the larger cluster of samples, have contributions from marine in situ brGDGT production. However, unlike those modern marine sediments, our entire record does not show elevated #rings$_{tetra}$ values that are associated to marine *in situ*-produced brGDGTs (Fig. 7). Instead, the low #rings$_{tetra}$ values on our record (<0.3) suggest that brGDGTs have a terrestrial source.

Deleted: and Berau delta

Deleted: ; Sinninghe Damsté, 2016

Deleted: -

Deleted: T

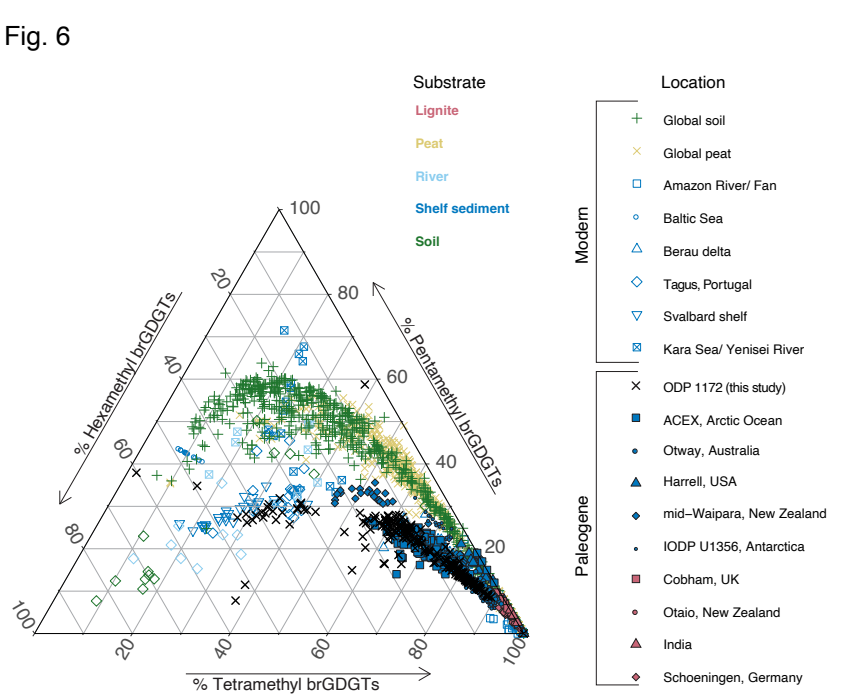

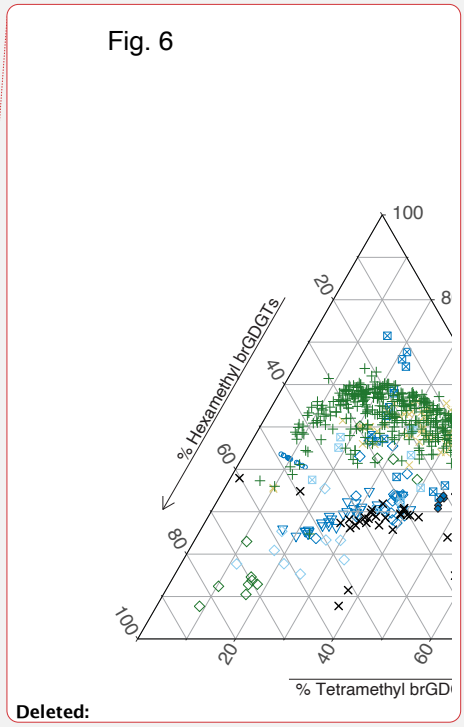

Deleted:

Figure 6. Ternary diagram showing fractional abundance of tetra-, penta- and hexamethylated brGDGTs from modern soils (Dearing Crampton-Flood et al., 2020), peats (Naafs et al., 2017b), rivers (Tagus River, Portugal (Warden et al., 2016) and Yenisei River (De Jonge et al., 2015)) and marine sediments (Kara Sea (De Jonge et al., 2015), Svalbard (Dearing Crampton-Flood et al., 2019), Berau delta (Sinninghe Damsté, 2016), Portugal (Warden et al., 2016), Baltic Sea (Warden et al., 2018), and Amazon Fan (Zell et al., 2014)), Paleogene lignites (Cobham, Schoeningen, India and Otaio (Naafs et al., 2018b)) and Paleogene marine sediments (Arctic Ocean, IODP Arctic Coring Expedition ACEX (Willard et al., 2019), Otway Basin, Australia (Huurdeman et al., 2020), Gulf of Mexico coastal plain, Harrel core (Sluijs et al., 2014), New Zealand (Pancost et al., 2013) and Antarctic Margin IODP Site U1356 (Bijl et al., 2013a)). Data from ODP Site 1172 in black crosses.

Fig.7

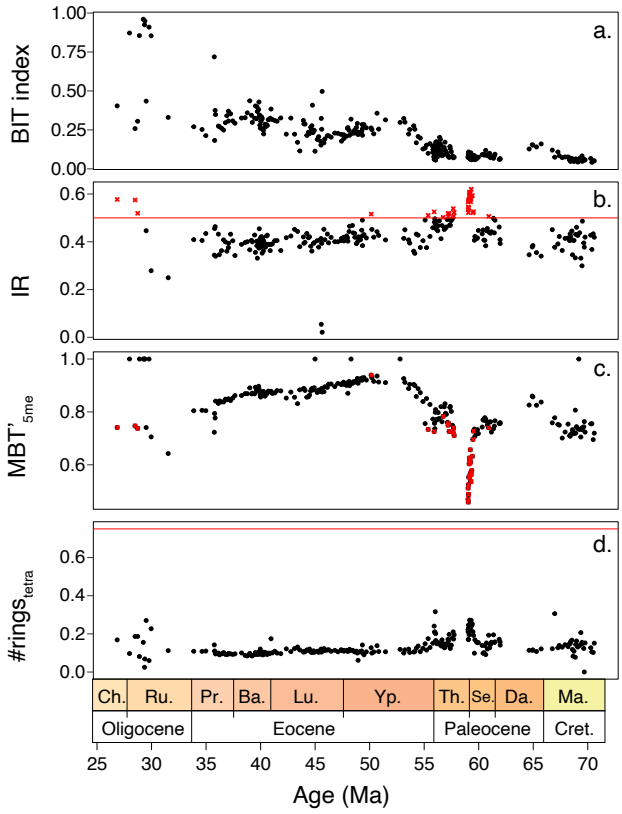

Figure 7. a. BIT index, b. IR (with cut-off value of the Australian soil IR of 0.5 and discarded MAAT samples in red crosses), c. MBT'_{5me} and d. $\#rings_{tetra}$ from Site 1172.

In the modern soil- and peat brGDGT dataset $\#rings_{penta}$ and $\#rings_{tetra}$ follow a coherent 1:1 correlation (Fig. 8a). At Site 1172, however, $\#rings_{tetra}$ is below 0.3, whereas $\#rings_{penta}$ ranges up to 0.6. This diverts from the 1:1 line but brings the brGDGT dataset from Site 1172 within the area of other Paleogene marine brGDGT datasets (Fig. 8a). This is consistent with the relative abundances of tetra-, penta- and hexamethylated brGDGTs plotted in the ternary diagram, where all Paleogene data plotted offset to that in modern soils. $\#rings_{tetra}$ and $\#rings_{penta}$ for the 5- (Fig. 8b) and

Fig.7

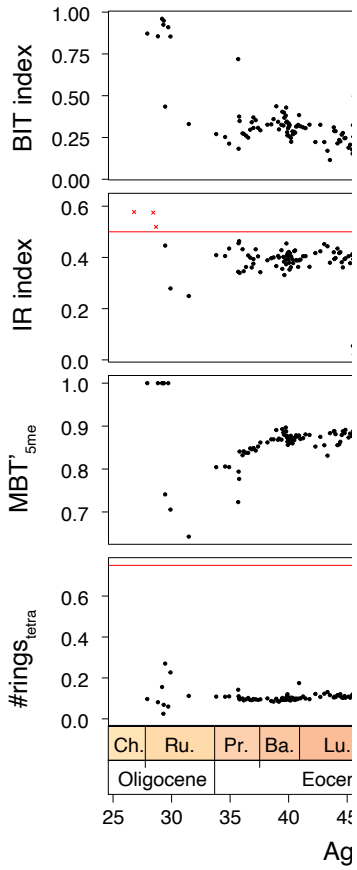

Deleted:

Deleted: and

Formatted: Subscript

Deleted: Notably, Iin

Deleted: are below 0.7 and

Deleted: Values >0.7 suggest brGDGTs cannot come purely from soils (Sinninghe Damsté 2016). All samples from 1172 are below 0.7 for both these indices, which suggests a terrestrial origin is likely, and a strong contribution by marine in situ produced brGDGT is unlikely. We do note that while

6-methyl brGDGTs (Fig. 8c) separately shows that the diversion of the 1172 data from modern soils and peats is primarily caused by a larger degree of cyclisation of the 6-methyl brGDGTs.

The samples within the Paleocene cluster have relatively high IR. The IR in our record averages ~0.4, but is elevated between 62 Ma and 54 Ma, with peak values in the mid-Paleocene up to 0.6 (Fig. 7). Although both the IR_{penta} and IR_{hexa} are well within the range of the modern soil and peat data (Fig. 8d) they exceed the two available datapoints from modern southeast Australian soils, which have IR values of maximum 0.5 (De Jonge et al., 2014a), suggesting a contribution by non-soil sources (be it marine or river in situ production; De Jonge et al., 2014a). Given that the relatively low #rings$_{tetra}$ values argue against a large contribution from marine in situ production, we suggest that river-produced 6-me brGDGTs have contributed to the GDGT pool in the Paleocene samples with high IR. Therefore, for MBT'$_{5me}$ calculation, we eliminate all brGDGT samples in our record that have IR values above that of Australian soils.

Deleted: , suggesting an influence by river brGDGT production…

Deleted: do

Moved (insertion) [4]

Deleted: T

Deleted: and settings affected by marine or river in situ production (Svalbard, Kara / Yenisei), and plot far away from lignite deposits.

Deleted: Although based on

Deleted: only

Deleted: ,

Deleted: . Hence, any values exceeding that of the corresponding hinterland soils could indicate

Formatted: Subscript

Deleted: indices

Deleted: -

Moved up [4]: The IR_{penta} and IR_{hexa} are well within the range of the modern soil and peat data (Fig. 8d) and settings affected by marine or river in situ production (Svalbard, Kara / Yenisei), and plot far away from lignite deposits.¶

Fig.8

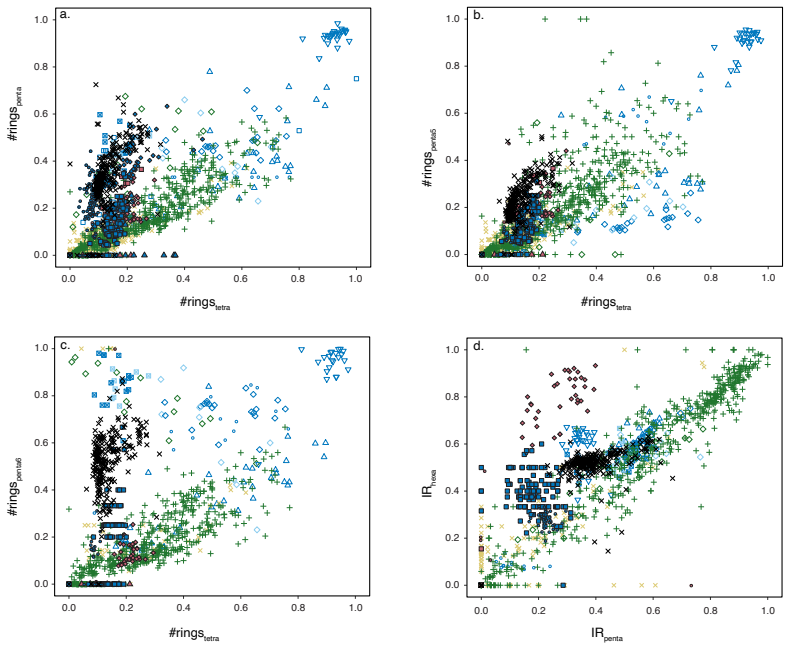

Figure 8. Crossplots of various brGDGT indices. a. #rings$_{tetra}$ *vs.* #rings$_{penta}$, #rings$_{tetra}$ *vs.* #rings$_{penta5}$, #rings$_{tetra}$ *vs.* #rings$_{penta6}$, IR$_{penta}$ *vs.* IR$_{hexa}$. For color and symbol legend see Figure 6.

Finally, the consistent offset in brGDGT composition in Paleogene marine sediments relative to modern soils can potentially be explained by non-soil contributions even though many (most) indices suggest soil-dominated sourcing. Notably, not only Paleogene marine sediments from Site 1172 are offset from present-day soils, but this extends to other sites as well, including Paleogene lignites that are not influenced by marine contributions. We suggest that there may be an additional evolutionary- or bacterial community factor that is at least in part responsible for the observed offset brGDGT distributions during the Paleogene. Except where indices suggest non-soil contributions, Paleogene marine sediments may contain a dominant soil-derived brGDGT signal in spite of their offset composition.

Deleted: T

Deleted: thus argue

Deleted: ,

Deleted: and argue that, with some exceptions

Deleted: do

4.2 SST and MAAT reconstructions

4.2.1 SST

By removing all samples with potential overprint from the record we can now assess the trends in TEX_{86}-based SST (Fig. 9a). Reconstructed SSTs differ by up to 4 °C between the exponential SST_{exp} and the linear SST_{lin} calibration in the warmest intervals, and progressively less with lower SSTs (Fig. 9a). The BAYSPAR method, which uses a linear relation between SST and TEX_{86} yields the lowest SSTs for the low TEX_{86} values in the Maastrichtian, Paleocene and middle–late Eocene, and SSTs between those based on the linear and exponential calibrations for the highest TEX_{86} index values (Fig. 9a). $U^{K'}_{37}$-based SSTs (Bijl et al., 2010, with BAYSPLINE calibration) around the MECO are in best agreement with the high SSTs derived from the linear TEX_{OBL} calibration, although in this TEX_{86} range all calibrations yield SSTs within error (Fig. 9a).

In general, Maastrichtian (70.5–66.7 Ma) SSTs show a gradual cooling trend towards the late Maastrichtian–early Danian hiatus of ~800 kyrs. The early Danian (~65 Ma) is roughly 3 °C warmer than the late Maastrichtian (~67 Ma). The mid-Paleocene (62–59 Ma) shows two cooling steps: a ~2 °C cooling at 62 Ma, followed by a return to higher SSTs roughly at 60 Ma, and a ~5 °C cooling to minimum values of around 18°C around 59.5 Ma, where the record is truncated by a hiatus.

A hiatus straddling the early Thanetian (59.0–57.7 Ma) likely obscures the onset of late Paleocene warming out of the mid-Paleocene temperature minimum. Background latest Paleocene SSTs fluctuate considerably, but the PETM warming clearly stands out (Sluijs et al., 2011), with a magnitude (5-7 °C depending on the calibration) comparable to that in other mid- to high latitude sections and similar to the global average (Frieling et al., 2017). Post-PETM SSTs drop back to pre-PETM values completely, followed by renewed warming towards the EECO. The magnitude of warming is 6 to 11 °C depending on the choice of calibration. Smaller early Eocene hyperthermal events, cannot be confidently identified at Site 1172.

Highest SSTs of the EECO are slightly lower than peak PETM values in all calibrations, consistent with other records (Hollis et al., 2019; Inglis et al., 2020).

Deleted: to

Formatted: Subscript

Deleted: generates

Deleted: in

Deleted: most consistent

Deleted: based on

Deleted: if represented in our record, do not clearly stand out…

However, a hiatus between 52.7 and 51.4 Ma may conceal peak EECO temperatures (Hollis et al., 2019; Lauretano et al., 2018). A gradual SST decline marks the end of the EECO around 49.2 Ma, which is broadly coeval with cooling inferred from benthic foraminiferal isotope records (Lauretano et al., 2018) and proxy records from New Zealand (Dallanave et al., 2016; Crouch et al., 2020).

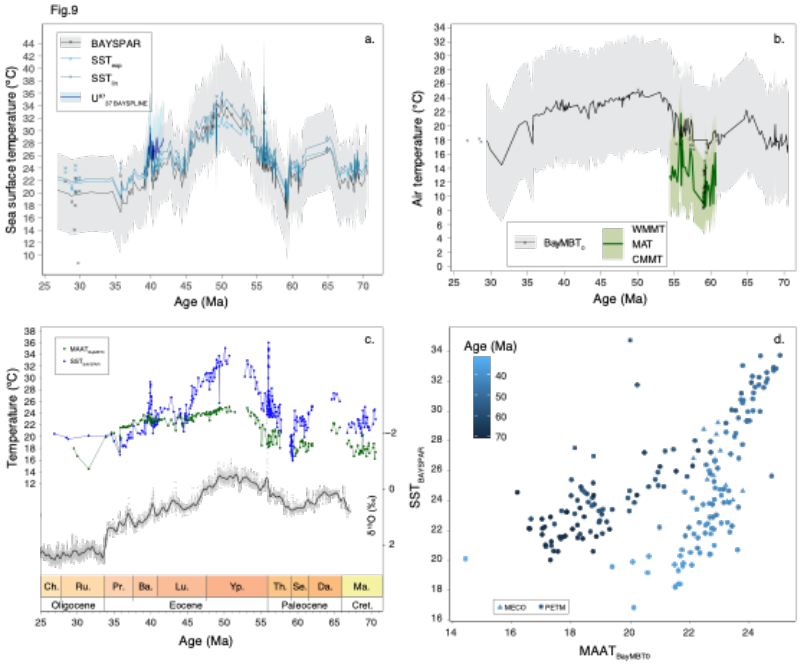

Figure 9. Paleothermometers. a. TEX_{86} based SST reconstructions, using a Bayesian (BAYSPAR; black, with 90% confidence interval in grey envelope; Tierney and Tingley, 2015) an exponential (SST_{exp}; light blue; Kim et al., 2010) and a linear (SST_{lin}; dark blue; O'Brien et al., 2017) calibration. Also plotted are $U^{K'}_{37}$ -based SSTs (thick blue line; from Bijl et al., 2010, recalculated using BAYSPLINE of Tierney and Tingley, 2018). Discarded samples are indicated by the crosses. b. brGDGT-based MAAT reconstructions using the Bayesian calibration ($BayMBT_0$; black, with 90% uncertainty interval in grey envelope; Dearing Crampton-Flood et al., 2020). Discarded samples are indicated in crosses. Also plotted are pollen-based NLR-

Deleted: commences around 49.2 Ma and

Deleted: terminates

Deleted: is used to mark

Deleted: top

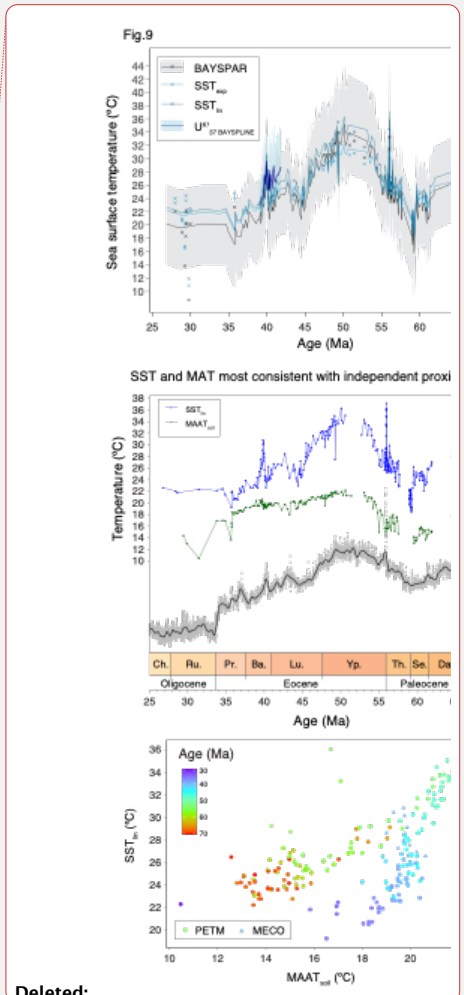

Deleted:

Deleted: confidence

Deleted: and soil ($MAAT_{soil}$; light green; Naafs et al., 2017b) calibrations

approach mean annual (MAT) reconstructions (thick dark green, with light green envelope representing coldest and warmest month mean temperatures; from Contreras et al., 2014). c. SST and MAAT reconstructions using the Bayesian calibrations calibrations, with the CENOGRID benthic foraminifer oxygen isotope splice of Westerhold et al., 2020 (10pnt LOESS smooth in grey, 500 pnt LOESS smooth in black). d. cross-correlation between SST and MAAT, using the calibrations shown in c.

Post-EECO cooling is gradual and of small magnitude (2 °C from peak EECO values) until about 46.4 Ma, after which it accelerates (5 °C) between 46.2 Ma and 44.4 Ma. The age model in this particular interval is uncertain, due to a questionable assignment of chron C21n (Bijl et al., 2010; 2013b). Following the minimum SSTs at 44.4 Ma, SSTs rise again towards a plateau at 42.7 Ma. An SST minimum of ~22 °C is observed just prior to the MECO, at 40.2 Ma, followed by MECO warming of about 5–7 °C at 39.9 Ma. Post-MECO cooling seems more gradual than MECO warming, although this might be the result of fine-scale sedimentation rate changes (Bijl et al., 2010), which are not accounted for in our age model. SSTs are almost identical to those for the MECO at nearby Site 1170 on the South Tasman Rise (Cramwinckel et al., 2020). Post-MECO cooling transitions into gradual late Eocene cooling, down to a minimum of ~19 °C at 35.7 Ma. The following latest Eocene to Oligocene TEX_{86}-based SSTs (35–27 Ma) are 3 °C warmer, with surprisingly no cooling across the Eocene–Oligocene transition (Houben et al., 2019).

4.2.2 MAAT

After excluding samples with IR values above those of local soils, we present MBT'_{5me}-based MAAT reconstructions. MAAT evolution reveals late Maastrichtian-early Danian warming of 3°C, gradual 4°C cooling towards the mid-Paleocene, gradual 8°C warming towards the EECO, with a conspicuous absence of warming at the PETM. Gradual cooling of 4°C starts at 49.5 Ma and continues into the Late Eocene. MAAT reaches a minimum at 43 Ma, followed by a plateau-phase. There is little warming that can be associated to the MECO. MAAT shows a conspicuous transient 3 °C cooling in the Late Eocene, at the onset of glauconite deposition. The Eocene-Oligocene

Deleted: that are most consistent with independent proxies from this site (Bijl et al., 2010; Contreras et al., 2014)

Deleted: loess

Deleted: loess

Deleted: lin

Deleted: soil

Deleted: e. SST and MAAT reconstructions using the calibrations that are, in absolute temperature, most consistent with each other, with the CENOGRID benthic foraminifer oxygen isotope splice of Westerhold et al., 2020 (10pnt loess LOESS smooth in grey, 500 pnt loess smooth in black). f. cross-correlation between SST_{exp} and $BayAYMBT_0$.¶

Deleted: part of the sequence

Deleted: complicated

Deleted: problematic

Deleted: S

Deleted: reached

Deleted: associated to

Deleted: These differ substantially (up to 5°C) per calibration chosen (Fig. 9b). The $MAAT_{soil}$ calibration yields consistently cooler MAATs (2–3°C) compared to the $BAYMBT_0$ calibration (Fig. 9b), which may be because the $MAAT_{soil}$ is calibrated against average temperature of the days above freezing, while $BAYMBT_0$ is calibrated against mean annual temperature. Both MAAT calibrations fall between the MAT and the warmest month mean temperature reconstruction of the sporomorph nearest living relative (NLR)-based temperature reconstruction (Contreras et al., 2014), and calibration errors largely overlap. ¶
Independent of the calibration chosen,

Transition is characterized by another 5°C cooling, except during the late Eocene, SST is overall warmer than MAAT (Fig. 9c). This difference is largest during the EECO (up to 9°C).

Deleted: MAAT

Deleted:

Formatted: Subscript

Fig. 10

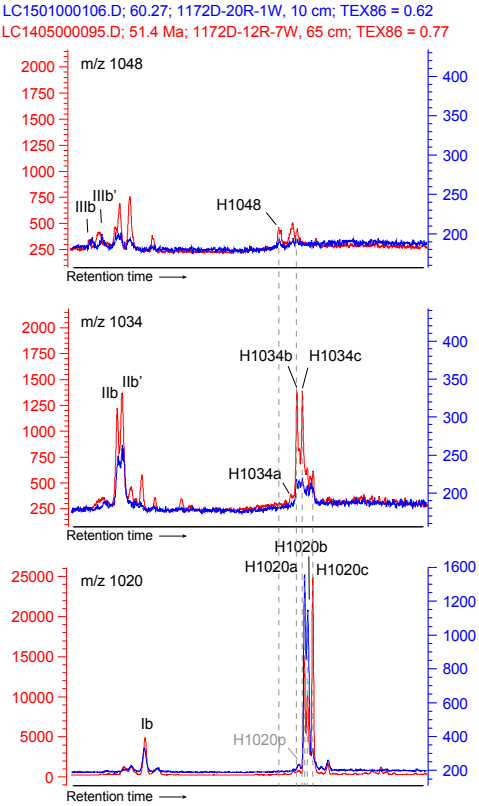

Figure 10. Stack of 2 UHPLC-MS chromatograms (1172D-12R-7W, 65cm; 51.41 Ma in red and 1172D-20R-1W, 10cm; 60.27 Ma in blue) of *m/z* 1048, 1034 and 1020 traces between ~40 and ~60 minutes retention time, showing the pattern of peaks corresponding to brGDGTs and brGMGTs. Peak labels refer to the molecular structures in Fig. 3. Note that not all peaks are 3x baseline.

Deleted:

4.3 brGMGTs

We detected brGMGTs throughout the record (see Fig. 10 for typical chromatograms). The exact molecular structure and position of the C-C bridge is still unknown but based on visual comparison with chromatograms of brGMGTs in African lake sediments (Baxter et al., 2019), (traces of) all 7 known brGMGTs can be identified. Next to H1020a, b, and c as most abundant brGMGTs, also H1034a, b and c are detected, although in some samples in the Maastrichtian, individual peaks could not be separated. Traces of H1048 can be seen at times, suggesting presence of this compound as well, albeit in low relative abundance. Next to these previously described peaks, we here recognized several other peaks that consistently occur at Site 1172: one compound that elutes just prior to H1020a, which we term H1020p (Fig. 10).

The fractional abundances of the H1020 isomers show qualitatively similar relations to temperature as in the East African lake dataset of Baxter et al. (2019): the relative abundance of H1020b has a negative relationship with MAAT, while H1020c has a positive relationship (Fig. 11). In addition, H1020a seems negatively correlated with MAAT in our data, although this compound does not show any relation to temperature in lakes (Baxter et al., 2019). The relative abundances of the H1034 isomers do not show a clear relationship with MAAT (Fig. 11), similar as in the tropical lake dataset, where the scatter increases at lower (H1034b) or higher (H1034a, c) temperatures (Baxter et al., 2019).

Downcore trends in brGMGTI are primarily controlled by the relative abundance of H1020c and closely follow those in both SST and MAAT. Upon cross-correlation, we note that brGMGTI has a higher correlation with MAAT (R = 0.89) than with SST (R=0.57; Fig. 12). Interestingly, the correlations between brGMGTI and temperature indices only hold for part of the dataset. Samples with high IR values, for which brGDGT-based MAAT is influenced by a fluvial brGDGT contribution, fall outside the correlation (grey crosses in Fig. 12). In addition, we also note that brGMGTI approaches 0 at reconstructed MAAT of 15°C. The correlation with temperature (both MAAT and SST) is divided into 2 clusters. BrGMGTI values for samples from the younger part of the record, with BIT index <~0.3, seem to correlate

Deleted: ¶

Deleted: ~1 minute after H1048 elutes, two more peaks appear which we here term H1048b-1 and H1048b-2 (Fig. 10). Because these have so far unknown affinities or molecular structure and occur at or around detection limit, we do not include them here further in our calculations....

Deleted: abundance

Formatted: Indent: First line: 1.27 cm

1424 better to temperature than those from the older part of the record, with BIT index
1425 values >~0.3 (Fig. 12). In the Oligocene, where many isoGDGT signals were evidently
1426 overprinted, the %brGMGTs increases (Fig. 3, 12d), and the brGMGT composition is
1427 characterized by a relatively higher abundance of H1020c, H1034b and H1048
1428 compared to the rest of the record (Fig. 3; 12).

Fig. 11

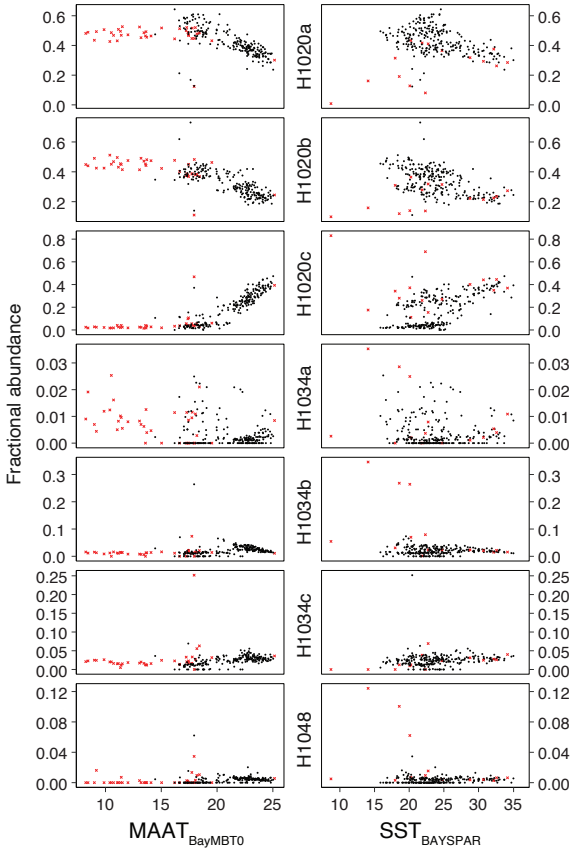

1429

1430 Figure 11. Fractional abundances of brGMGTs plotted against $MAAT_{soil}$ and SST_{lin}. Red
1431 crosses are those samples that have non-thermal overprints on the
1432 paleotemperatures.

1433

Deleted:

Fig. 11

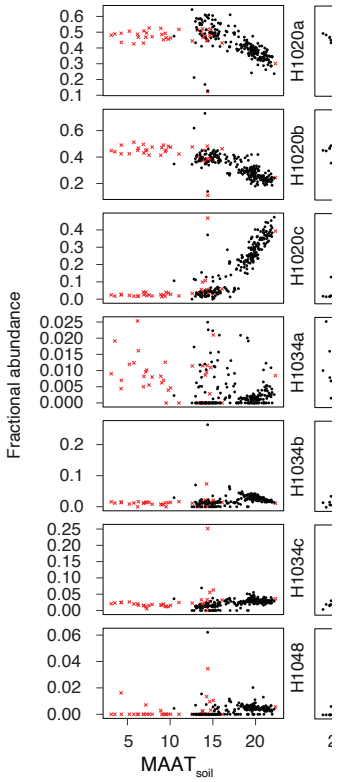

There is no clear relationship between %brGMGTs and brGDGT-based MAAT (Fig. 12h, i). This differs from the Paleocene-Eocene Arctic Ocean record (Sluijs et al., 2020), where the brGMGTI has no correlation to temperature, while %brGMGTs do. This may indicate differences in sources of brGMGTs between the sites, differences in oceanographic settings, or a non-temperature control on their distribution. In constrast, $HMBT_{acyclic}$ appears to show similar trends to the brGDGT-based MAAT (Fig. 12g), as is also seen in the Arctic Ocean (Sluijs et al., 2020).

Deleted: Downcore trends in brGMGTI are primarily controlled by the relative abundance of H1020c and closely follow those in both SST and MAAT. Upon cross-correlation, we note that brGMGTI has a higher correlation with MAAT (R = 0.89) than with SST (R=0.57; Fig. 12). Interestingly, the correlations between brGMGTI and temperature indices only hold for part of the dataset. Samples with high IR values, for which brGDGT-based MAAT is influenced by a fluvial brGDGT contributioncould not be reliably interpreted, fall outside the correlation (grey crosses in Fig. 12). This is probably due to the supposed contribution of river-derived brGDGTs that may bias MAAT towards lower temperatures. In addition, we also note that brGMGTI approaches 'saturation' (brGMGTI = 0) at reconstructed MAAT of 15°C. The correlation with temperature (both MAAT and SST) is divided into 2 clusters. BrGMGTI values for samples from the younger part of the record, with BIT index <~0.3, seem to correlate better to temperature than those from the older part of thae record, with BIT index values >~0.3 (Fig. 12). In the Oligocene, where many isoGDGT signals were evidently overprinted, the %brGMGTs increases (Fig. 3, 12d), and the brGMGT composition is characterized by a relatively higher abundance of H1020c, H1034b and H1048 compared to the rest of the record (Fig. 3; 12). ¶

Deleted: MBT'_{5me}

Deleted: slightly

Deleted: does seem

Deleted: MBT'_{5me}

Deleted: like

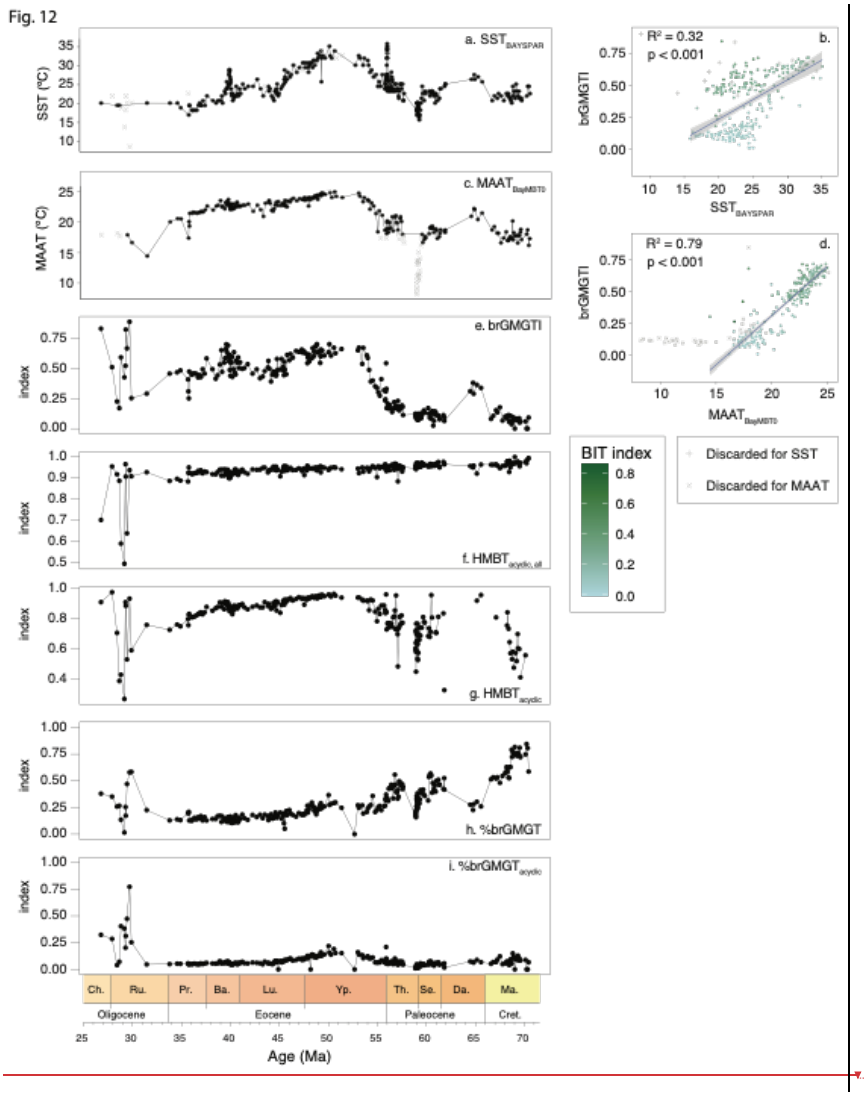

Deleted:

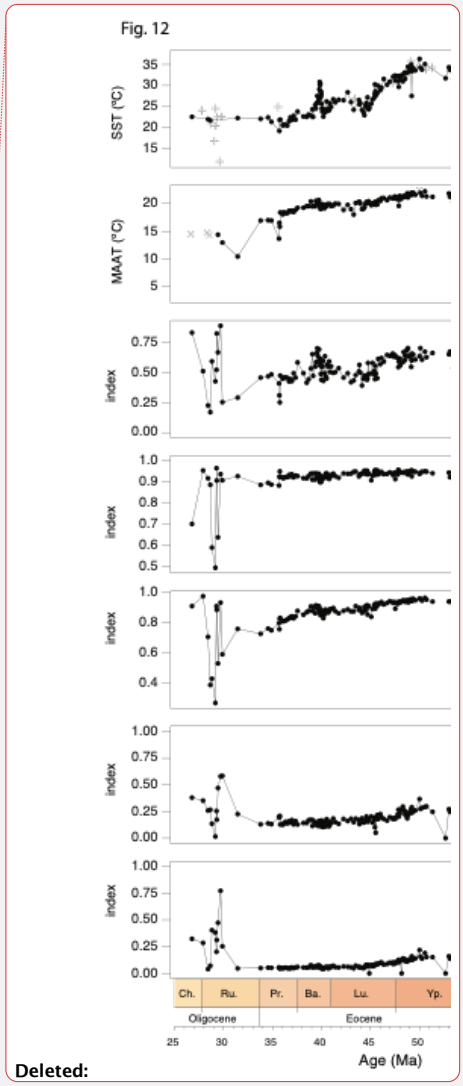

Figure 12. Time series and crossplots of brGMGT-based indices with MAAT and SST reconstructions. (a) SST_{lin} (b) crossplot of SST_{lin} and brGMGTI, (c) $MAAT_{soil}$, (d) crossplot of $MAAT_{soil}$ and brGMGTI, (e) brGMGTI, (f) $HMBT_{acyclic, all}$, (g) $HMBT_{acyclic}$, (h) %brGMGT (Baxter et al., 2019), (i) $\%brGMGT_{acyclic}$ (Naafs et al., 2018a). For equations see Table 1). Colour variable in the crossplots indicate the BIT index value.

4.4 Palynology

4.4.1 Assemblages

Dinocyst assemblages are dominated by *Manumiella* spp. throughout the Maastrichtian, together with Goniodomideae (notably *Dinopterygium* spp.), and *Cerebrocysta* cpx. (Fig. 13). From the late Maastrichtian onwards, *Senegalinium* cpx. increases gradually in relative abundance, interrupted by acmes of *Palaeoperidinium pyrophorum* in the Danian and *Glaphyrocysta* cpx. in the lower Selandian. *Senegalinium* cpx. is most abundant during the mid-Paleocene and the Paleocene–Eocene transition, while the PETM itself is characterised by abundant *Apectodinium* (~30%) and common *Senegalinium* cpx. and Goniodomideae (Sluijs et al., 2011). After the PETM, *Senegalinium* cpx. abundance temporarily increases, and followed by high abundance of *Deflandrea* cpx, *Spinidinium* cpx and *Elytrocysta* spp. with minor contributions of various other genera, e.g., *Wetzeliella*, *Hystrichokolpoma*, Goniodomideae (Fig. 13). From 45 Ma to ~37 Ma, *Enneadocysta* spp. abundance oscillated with *Deflandrea* cpx. and *Spinidinium*/*Vozzhennikovia* cpx, with contributions of *Phthanoperidinium* spp. (Röhl et al., 2004a). Protoperidinioid dinocysts become common in the late Eocene, around 35.5 Ma (Houben et al., 2019; Sluijs et al., 2003; Fig. 13).

Deleted: Relative abundances of

Deleted: reach maximum values

Deleted: during

Deleted: s

Deleted: are

Deleted: then replaced

Deleted: and low abundances of

Deleted: alternates

Deleted: dominance

Deleted: appear commonly

Fig. 13

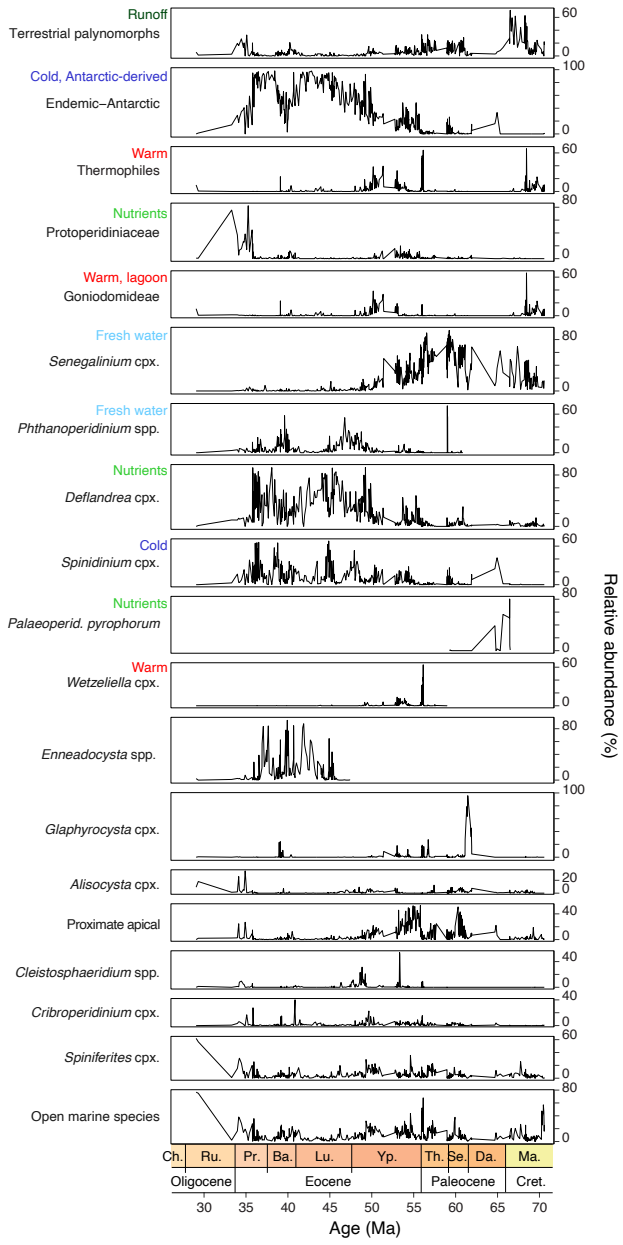

1510

Deleted: ¶

4.4.2 Diversity and variability¶

Together with the changing assemblage composition are some strong and coherent changes in all diversity and variability indices (Fig. 14). First, results are highly similar for the full species-level dataset and the grouped assemblages, indicating robustness of both the grouping and diversity analysis. The Maastrichtian–Paleocene assemblages are characterized by relatively low diversity, which increases towards the EECO, as variability indicated by the Gibbs index decreases. After this, diversity drops and variability increases during middle–late Eocene cooling ~49–38 Ma, with an interruption around 41–39 Ma. Towards the top of the record, both diversity and variability increase. ¶

¶

Figure 13. Dinocyst eco-groups and %terrestrial palynomorphs from Site 1172. From left to right, eco-groups are ordered in an in-shore-to-offshore transect. Relative abundance ticks represent 20%.

Deleted: ecogroups

Deleted: ecogroups

4.4.2 Diversity and variability

Together with the changing assemblage composition, some strong and coherent changes in diversity and variability indices are observed (Fig. 14). First, results are highly similar for the full species-level dataset and the grouped assemblages, indicating robustness of both the grouping and diversity analysis. The Maastrichtian–Paleocene assemblages are characterized by relatively low diversity, which increases towards the EECO, as variability indicated by the Gibbs index decreases. After this, diversity drops and variability increases during middle–late Eocene cooling ~49–38 Ma, with an interruption around 41–39 Ma. Towards the top of the record, both diversity and variability increase.

Formatted: Indent: First line: 1.27 cm

Fig. 14

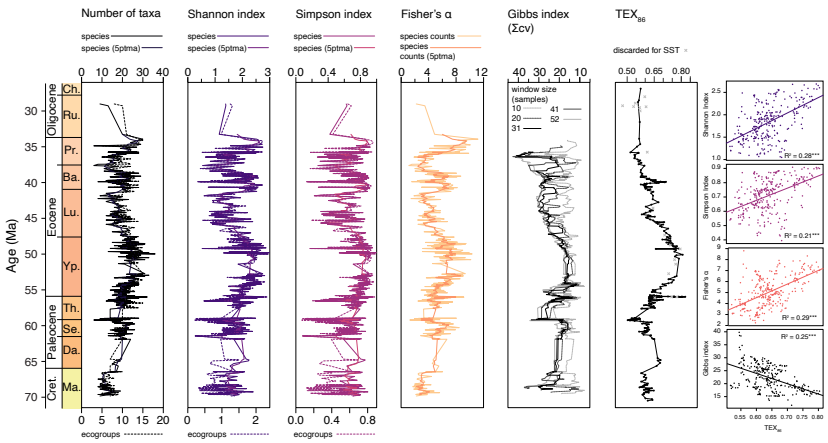

Figure 14. Dinocyst taxonomic diversity and variability through time. From left to right are plotted number of taxa (black), Shannon index (purple), Simpson index (pink), Fisher's alpha (orange) (species-based dataset in solid lines; eco-grouped dataset in dashed lines) and Gibbs index (note the reversed axis; different window

Deleted: ecogroup

sizes in grey-black). TEX_{86} plotted for comparison. Grey crosses indicate samples that have non-pelagic or non-thermal contributions. Crossplots show correlation of these indices with TEX_{86}.

5. Discussion

5.1 Air and sea surface temperature evolution compared

The near-shore depositional setting of our record should have recorded a coastal terrestrial environment, with MAATs similar to the local SSTs. Indeed, the brGDGT-based MAAT record shows strong similarities to SST particularly in multi-million year trends (Fig. 9). Specifically, the early Danian is warmer than the Maastrichtian, and both records show a 2-step Paleocene cooling, late Paleocene warming towards peak values in the EECO, and middle–late Eocene cooling. On shorter time scales both records, occasionally even on sample-to-sample level, show synchronous variability (Fig. 9). The Bayesian calibrations for MAAT and SST generate overlapping median temperatures for the colder middle-late Eocene and Paleocene, but in the warmer Eocene time intervals SSTs remain consistently warmer (by ~8 °C). The lower MAATs cannot be explained by a saturation of the MBT'_{5me} index that is underlying the paleothermometer, as maximum recorded MBT'_{5me} values are around 0.85 in the EECO. The large calibration errors of BAYSPAR (± 6 °C) and $BayMBT_0$ (±8 °C) in principle could resolve the offset. However, applying the extremes in calibration error to make them consistent with each other would make both profoundly inconsistent to the independent SST and MAAT estimates from the same samples. More importantly, the colder MAAT compared to SST seems to be a consistent feature in many regions where TEX_{86} and MBT'_{5me} were applied together (see e.g., Hollis et al., 2019 and compare Willard et al., 2019 and Sluijs et al., 2020). The offset between MAAT and SST would have been more variable between sites if it were only the result of calibration errors. TEX_{86} -based SSTs in the southwest Pacific realm have been on the high end of many multi-proxy-based temperature reconstructions for the Eocene (Hollis et al., 2012), and therefore may be assumed to have an as yet poorly understood warm bias. However, the consistency of TEX_{86}-based SSTs with other SST proxies for specific time intervals and locations (Bijl et al., 2010; Hines et al., 2017) suggests the SST-MAAT offset cannot be easily reconciled by

Deleted: a

Deleted: captured

Deleted: similar

Deleted: e

Deleted: c, d

Deleted: The independent SST (based on alkenones; Bijl et al., 2010) and air temperature reconstructions (based on pollen assemblages; Contreras et al., 2014) show the best fit with the absolute SST values derived from the linear calibration for TEX_{86} (BAYSPAR or SST_{lin}; generating the highest SST estimates), and MAATs based on the calibration using Deeming regression ($MAAT_{soil}$), respectively. These are the two calibrations with the largest absolute temperature offset, particularly in the warm EECO (Fig. 9c). If the local terrestrial climate in the nearby river catchment is largely controlled by ocean temperature, the absolute mean annual SST and MAAT should be broadly similar in the integrated signal of our samples. This could be an argument to choose transfer functions for SST and MAAT whereby absolute temperature estimates overlap most: SST_{exp} and the Bayesian $BayAYMBT_0$. These

Deleted:

Deleted: absolute

Deleted: Accounting for t

Deleted: TEX_{86} SST (±2.5 °C)

Deleted:

Deleted: the large calibration error bar of

Deleted: AY

Deleted: 3.8

Deleted: ,

Deleted: but

Deleted: although a

Deleted: to the SST and MAAT recordsTEX_{86} and MBT'_{5me} …

Deleted: other

Deleted: proxies

Deleted: based on different proxies applied to

Deleted: from

only invoking a warm bias in TEX_{86}, as was also shown by Hollis et al. (2012). MAAT reconstructions on the other hand have been broadly consistent with nearest living relative based temperature reconstructions on pollen assemblages in many applications in the Eocene (Pross et al., 2012; Contreras et al., 2013; 2014; Pancost et al., 2013; Willard et al., 2019), but both brGDGT and plant-based temperature estimates are arguably prone to cold biases at the high-temperature end (e.g. Naafs et al. 2018b, Van Dijk et al., 2020). In addition, it may be that the same evolutionary or bacterial community factors that make Paleogene brGDGT assemblages deviate from that in modern soils, may also cause a deviation in the calibration to MAAT. This may resolve some of the offset between MAAT and SST reconstructions. Although this implies that quantitative MAAT estimates based on MBT'_{5me} in non-analogue settings such as the present one should be interpreted with care, the strong temperature dependence in Paleogene brGDGTs cannot be ignored.

Another surprising result is that the brGDGT-based MAAT record does not capture PETM and MECO warming (Fig. 9b), while pollen-based MAAT does. This is remarkable for several reasons: (1) brGDGTs were measured on the same samples as isoGDGTs, which precludes a sampling bias; (2) SST changes of longer duration (Maastrichtian–Danian warming, mid-Paleocene cooling and early Eocene warming towards the EECO) are represented in the MAAT record; (3) The duration of PETM (~150-250 kyrs; Röhl et al., 2007, Zeebe & Lourens, 2019) and MECO (~400 kyrs; Bohaty et al, 2009) is too long to explain the absence in MAAT warming with a lag in soil-derived OM delivery to the ocean (up to several kyr, see, e.g., Feng et al., 2013; Schefuß et al., 2016; Huurdeman et al., 2020); (4) seems incompatible with the fact that other low-amplitude, shorter-term SST changes are reflected in the MAAT record (Fig. 9), which suggests that soil-derived OM did capture short-term climate variability on the time resolution of the samples; (5) Other brGDGT-based records from the region do show a temperature response during the PETM (Hollis et al., 2012; Pancost et al., 2013, Huurdeman et al. 2020). A lack of MAAT rise during the PETM and the MECO could be explained by a switch from brGDGT sourcing from soils to (peaty) lakes, which are notoriously cold-biased (Tierney et al., 2010). Paleocene–Eocene peats are abundant in southeast Australia (Holdgate et al., 2009), and it is possible that a contribution from peat lakes at times of global warming, contributed

Deleted: .
Deleted: Contreras et al.,
Deleted: Pross et al., 2012;
Deleted: taken
Deleted: c
Deleted: independent of the calibration chosen.
Deleted: c, d
Deleted: PETM
Deleted: in
Deleted: in
Deleted: in various proxies including brGDGTs

to a dampening of the proxy-response. This may also explain the lack of response at the EECO and explain why MBT'$_{5me}$ does not reach saturation in that interval. The final option, which, although unlikely, cannot be excluded, is that a dominant fraction of the brGDGT was produced in situ and subdues the temperature response during these warming phases.

The subdued middle-late Eocene cooling in the air temperature record compared to the strong decrease in SST is particularly clear when cross-plotting SST *versus* MAAT (Fig. 9d): the relationship between the two proxies is different in the Maastrichtian–early Eocene compared to the middle–late Eocene. This may be related to the start of a progressive northward tectonic drift of the Tasmanian hinterland, which occurred around the same time (Fig. 1). A similar subdued MAAT record relative to SST cooling was observed in records from New Zealand (Pancost et al., 2013; Crouch et al., 2020), which was also moving northward at that time. This puts the hinterland of the soil-derived brGDGTs into warmer climate zones throughout the middle–late Eocene, while the ETP remained under influence of the Antarctic-derived Tasman Current (TC) through that time (Huber et al., 2004; Sijp et al., 2016). The TC cools and likely strengthens in the middle and late Eocene. The terrestrial climate cooled as well, but this signal will be subdued if the soil material is sourced from a progressively lower-latitude environment as Australia drifted northward. Yet, one would expect that the close coupling between coastal and offshore temperatures in near-shore environments would subdue such tectonic effects in mean annual temperature reconstructions.

Both marine and terrestrial temperature records diverge once more during the late Eocene–Oligocene, when they show a sharp cooling of 2–3 °C at the onset of greensand deposition, at ~35.5 Ma. Whereas this is merely a continuation of progressive late Eocene cooling in the SST record, the decrease in MAAT is more pronounced compared to the middle–late Eocene trends. Another 3–4 °C MAAT drop occurs sometime between the late Eocene and the early Oligocene (likely associated with the Eocene–Oligocene transition), while SSTs revert to warmer, middle Eocene-like values. The continued sea surface warmth across the EOT has been related to persistent influence of the proto-Leeuwin Current (Houben et al., 2019), which apparently retained a constant temperature across the EOT. Since MAAT decreased

Deleted: c,

Deleted: land

Deleted: -

Deleted: seawater

Deleted: not capture such

Deleted: The correlation between b

Deleted: proxies

Deleted: change

Deleted: s

Deleted: strongly accelerated

Deleted: returns

Deleted:

Deleted: in this interval

while SSTs remained high, the influence of regional oceanographic changes did not appear to impact climate changes in the source region of brGDGTs during this time interval. Later, at 30 Ma, MAAT does rise in the region, which could be related to either the progressive northward movement of the site, or a response to widespread warming in the early Oligocene (e.g., Westerhold et al., 2020). This is surprising given the proximity of the sediment record to the coastline, but it represents further evidence that hinterland MAAT and near-shore SST trends can be decoupled under certain circumstances. MAAT temperatures from Site 1172around EOT are somewhat colder than those from Southern Australia (Lauretano et al., 2021) although calibration error bars do overlap.

Minimum mid-Paleocene SSTs are lower than those for the early Oligocene at Site 1172. However, the site migrated northward by ~7 ° of latitude between the mid-Paleocene and the early Oligocene (Fig. 1) and the oceanographic regime changed with throughflow of the proto-Leeuwin Current through the TG in the Late Eocene (Houben et al., 2019). More remarkably, the mid-Paleocene SSTs approach those of the warmest interglacial intervals of Oligocene Wilkes Land Margin, east Antarctica (Hartman et al., 2018), at a similar paleolatitude as the Paleocene ETP. This suggests that mid-Paleocene Antarctic-proximal temperatures were similar to those at times of major Antarctic glaciation during EOT. Previous work has indeed presented widespread evidence for low sea level during this time interval (e.g., Guasti et al., 2006; Frieling et al., 2014; 2018; Hollis et al., 2014), which combined with low SSTs suggests the presence of some continental ice on the Antarctic continent during this mid-Paleocene interval.

5.2 BrGMGTs

The continuous presence of brGMGTs in our record appears unrelated to depositional conditions, and distributional changes of brGMGT isomers do not correlate to varying relative contributions of terrestrial material. This suggests that at least part of the brGMGTs has a marine origin, in line with observations from modern sediments and water columns (Liu et al., 2012, Xie et al., 2014) and from Paleogene Arctic Ocean sediments (Sluijs et al., 2020). Their sparse presence in modern mineral

Deleted: s

Deleted: Guasti et al., 2006;

Deleted: ¶

Formatted: Indent: First line: 1.27 cm

Deleted: or

Deleted: relative abundance changes

Deleted: s

Deleted: ,

Deleted: suggesting

Deleted: ve

Deleted: . This confirms previous

Deleted: the

soils (Peterse, F., pers obs., based on metadata from De Jonge et al., 2019; Kirkels et al., 2020) seems to confirm this, although abundant occurrence in peats and lakes (Naafs et al., 2018a, Baxter et al. 2019, Tang et al., 2021) shows clear potential for terrestrial input. Despite the uncertainties in sourcing of brGMGTs, we find signals in the brGMGTs at Site 1172 resemble those from East African lakes. For example, the brGMGT index (brGMGTI), which was derived to quantify the relationship between brGMGT composition and MAAT in surface sediments of East African lakes (Baxter et al., 2019), seems to be correlated to temperature in our record as well (Fig. 12b, d). In addition, H1020c is practically absent in the cold mid-Paleocene part of our record, similar to in cold (<12°C), high-altitude lakes (Baxter et al. 2019), which suggests that the biosynthesis of H1020c occurs only above a certain temperature, or that the microbes that biosynthesize H1020c do not live at low temperatures. However, contrasting to in lakes, site 1172 lacks H1048 isomers in the cold mid-Paleocene interval, illustrating that there are also differences between fresh water and marine depositional settings.

The HMBT record does not reflect a temperature signal when using all brGMGT isomers in the calculation (Fig. 12f), as H1020 isomers are by far the most abundant brGMGTs at Site 1172, and any change in the abundance of H1020c is compensated by both H1020b and H1020a in our record. In contrast, only using the H1020c and H1034b isomers does show some correlation to temperature in our record (Fig. 12g).

%brGMGT does not show a clear relationship with temperature (Fig. 12h, i), in contrast to observations in modern peats (Naafs et al., 2018a) and lake sediments (Baxter et al., 2019). We do note the extremely high %brGMGT (~80%) in the Maastrichtian and Oligocene, much higher than seen elsewhere. We also do not see a clear inverse relationship between %brGMGT and BIT index, as in the Arctic Eocene record of Sluijs et al. (2020). There, it does correlate with SST, which we do not see either. These discrepancies may be because of the complexity in the sources of brGDGTs in the records.

BrGMGTs are more abundant and different in composition in the Oligocene, compared to the rest of the record. This coincides with abundant signs of overprints in all br- and isoGDGT indices, which may indicate a source change of brGMGTs in this

Deleted: et al.

Deleted: comm

Deleted: is also in line with this,

Deleted: a strong resemblance

Deleted: with the signals

Deleted: tropical

Deleted: T

Deleted: temperature relation of

Deleted: lake temperatures

Deleted: 12a

Deleted: –

Deleted: , although the better correlation of brGMGTI with MAAT than with SST (Fig. 12a–d) seems to be at odds with the presumed marinesuggest a terrestrial source of brGMGTs in our record. Despite all potential complications, our study provides additional evidence that a temperature signal may be governing the distribution of the different brGMGT isomers, as proposed by (Baxter et al., 2019), but there are differences as well. For instance,

Deleted: altogether

Deleted: . There are numerous ways in which this can be explained, e.g.,

Deleted: , or the site receives brGMGTs from a different catchment in colder climates. Indeed, H1020c was almost absent in the cold (<12°C), high-altitude tropical lake samples (Baxter et al. 2019)

Deleted: those cold lakes did have high relative abundance of H1048 (Baxter et al., 2019), which our record also …

Deleted: the

Deleted: modern lakes

Deleted: our

Deleted: , which following the chromatographic peak identification of Sluijs et al. (2020) match the compounds used to derive the HMBT index based on brGMGTs in peats (Naafs et al., 2018),

Deleted: a

Deleted: as calculated in Naafs et al., (2018) or as in Baxter et al., (2019)

Deleted: anywhere

Deleted: so far

Deleted: is

Deleted: the relative abundance

Deleted: , which does not necessarily reflect the … [10]

Deleted: The higher relative abundance and cha … [11]

Deleted: b

Deleted: higher

Deleted: that

interval, e.g., related to the same changes in contribution that cause the overprints in isoGDGTs. The differences in brGMGT signals between our record, the Eocene Arctic Ocean record and modern sediments demonstrate that more research is needed on their modern sources and environmental dependencies to further assess their use and value in paleoclimate studies.

5.3 Integrated environmental and climatological reconstruction

5.3.1 Sea level and ecosystem response to SST changes

The abundance of temperature-responsive dinocyst eco-groups qualitatively confirm our SST trends. The thermophile dinocyst eco-group shows higher relative abundance at higher SSTs (Fig. 15). This eco-group has been empirically linked to SST in a global compilation of late Paleocene-early Eocene records (Frieling and Sluijs, 2018), and we here see the same relationship for the longer early Paleogene. The somewhat muted response of the dinocyst assemblages to the large EECO SST rise is consistent with that in other SW Pacific records and microfossil groups (Crouch et al., 2020), and might be related to the already warm background conditions upon which this warming took place. Moreover, the abundance of SST-insensitive dinocysts in the assemblage and absence of typical cold-indicators could further explain the muted response. The relationship between isoGDGT-based SSTs and relative abundance of the supposedly cold-affiliated endemic dinocysts (Bijl et al., 2011) is not as clear. This might be because the majority of dinocyst species within the Endemic-Antarctic dinocyst eco-group are restricted to the Eocene (Bijl et al., 2011). The absence of endemic-Antarctic dinocysts in the cold mid-Paleocene is interesting, given that some endemic species had already appeared (Bijl et al., 2013b). It might be that the strong fresh-water influence negatively affected their proliferation in the mid-Paleocene. Indeed, from 50 Ma onwards, SST has a negative correlation with the %endemic Antarctic dinocyst abundance in the record (Fig. 15; see Bijl et al., 2011), which may indicate a more distinct biogeographical separation through the development of stronger meridional gradients or evolutive adaptation of the endemic dinocyst community to more polar environments following the extreme warmth of the EECO.

We particularly note the correlation between TEX_{86}-based SST and the relative abundance of more open ocean-affiliated dinocysts (Fig. 15), which suggests that SST

Deleted: paleoreconstructions
Deleted: ¶
Deleted: paleo
Deleted: -
Deleted: associated
Deleted: based on its strong affinity to high SST
Deleted: the
Deleted: here confirm this
Deleted: sw
Deleted: temperature rise
Deleted: akes
Deleted: ecogroup
Deleted: ve
Deleted: evolved then
Deleted: s
Deleted: ¶
Deleted: does
Deleted: ve
Deleted: strong
Deleted: 13

correlates with regional sea level. The thermophilic and Open Ocean eco-groups share some outer neritic species. However, the strong covariance is caused by the absence of other Open Ocean species, such as *Impagidinium* spp., *Spiniferites* spp., and *Operculodinium* spp. Moreover, sea level trends derived from Open Ocean dinocysts are supported by weight % $CaCO_3$ in these sediments in the middle Eocene (Röhl et al., 2004a), on orbital and longer time scales. SST-induced sea level changes hint at steric effects as driver. Indeed, because of the flatness of continental shelf areas during long-term greenhouse climates (Somme et al., 2009) small changes in regional sea level will cause large changes in distance to shore and associated characteristics, including e.g. salinity, nutrients and suspended sediment loads, which subsequently shapes the dinocyst assemblages.

The SST control on dinocyst assemblages is further demonstrated in diversity and assemblage variability indices. Throughout the long time interval covered by our record, dinocyst richness and diversity show a remarkably similar pattern to TEX_{86}-based SST. Species richness, as well as diversity expressed in the Shannon and Simpson indices and Fisher's alpha reach a maximum during the prolonged warmth of the EECO and drop during middle–late Eocene cooling. These relationships are demonstrated by modest correlation coefficient between diversity and TEX_{86} (Fig. 14). This pattern holds for the long-term trends, as well as for the short-term PETM, but, surprisingly, not for the MECO. Dinocyst diversity is known to peak mid-way an inshore-to-offshore transect in the modern and Eocene oceans (Brinkhuis, 1994; Pross and Brinkhuis, 2005). As our assemblages indeed consist of many mid-shelf species, the correlation between diversity and SST might thus be indirectly related through habitat size, with expansion of the flat shelf area and thereby increase in shelf niches during the EECO (Somme et al., 2009). Variability as indicated by the Gibbs index records the opposite pattern to diversity for the long-term trends into and out of the EECO (Fig 14). That is, the lower-diversity assemblages in general have a higher variability, or sample-to-sample fluctuations within the relative abundances. This indicates that the higher diversity dinocyst assemblages might be more ecologically resilient.

Formatted: Font: Italic
Formatted: Font: Italic
Deleted:
Deleted: in
Formatted: Font: Italic
Deleted: further
Formatted: Subscript
Formatted: Indent: First line: 0 cm

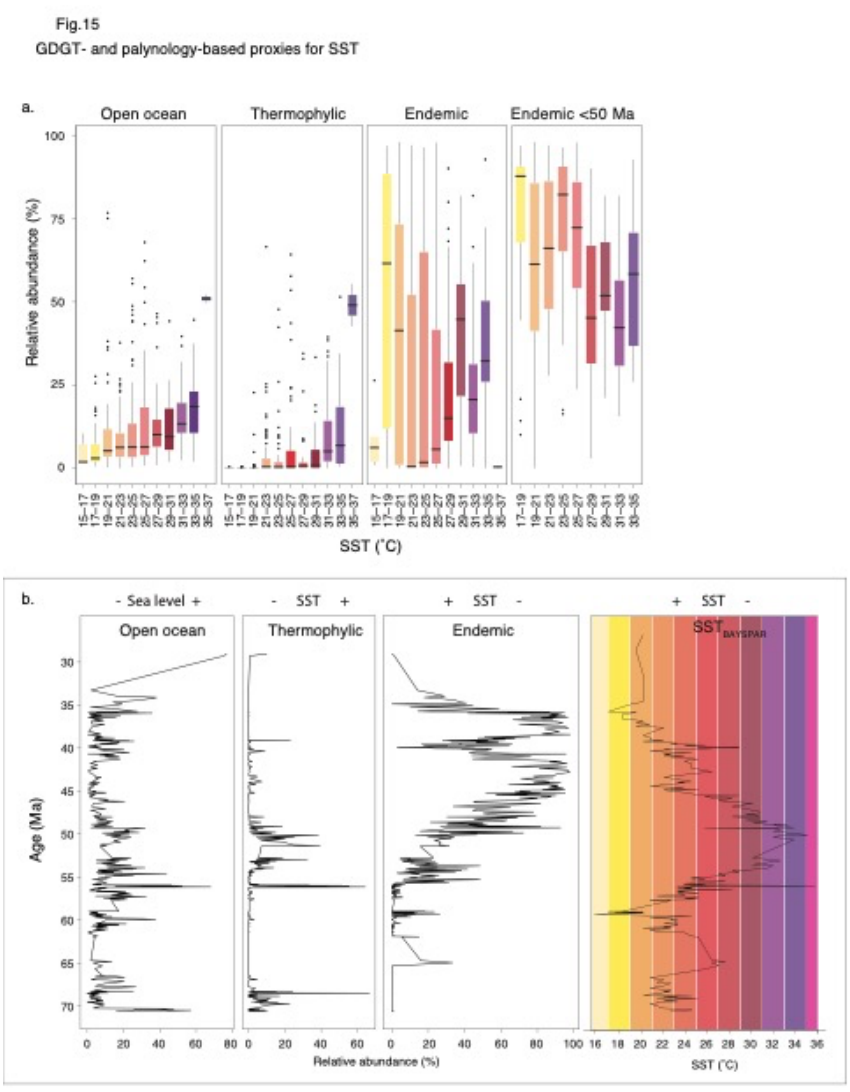

Deleted:

Fig.15
GDGT- and palynology-based proxies for SST
a.
Open ocean
Thermophylic
Relative abundance (%)
b.
- Sea level +
- SST +
Open ocean
Thermophylic
Age (Ma)

Figure 15. isoGDGT- and palynology-based proxies for SST. a. relative abundance of Open ocean, thermophylic and endemic-Antarctic dinocyst eco-groups (for groups see Table 3; total dataset and samples <50Ma only) plotted against linearly interpolated (resampled) TEX_{86}-based SST, in 2 degree bins. Median (black bars), lower-to-upper quartiles (25–75 percentile; coloured envelopes), lower to upper

Deleted: o

Deleted: o

whiskers (95% confidence intervals; black lines), outlier samples (black dots). b. Time series of the same dinocyst eco-groups and SST.

5.3.2 Marine environmental response to runoff changes

Senegalinium cpx. abundance broadly correlates with the IR (Fig. 16), which signals input of river-produced brGDGTs. *Senegalinium* cpx. is generally thought to have tolerated low salinity environments (Sluijs and Brinkhuis, 2009; Barke et al., 2011). These two proxies together confirm a large input of fresh water at this site during the mid-to-late Paleocene in line with high relative abundance of terrestrial palynomorphs, low abundances of open ocean dinocysts and high IR values (Fig. 16). Interestingly, *Phthanoperidinium* spp., which is also generally associated with low-salinity to near fresh-water conditions (Sluijs and Brinkhuis, 2009; Barke et al., 2011; Frieling and Sluijs, 2018) does not correlate with IR (Fig. 16). Because we find different species of *Phthanoperidinium* spp. than those previously associated to fresh-water conditions (e.g., Barke et al., 2011), it could be that the fresh-water tolerance of *Phthanoperidinium* spp. was not shared among all species. It could also be that some species of *Phthanoperidinium* spp. were slightly less euryhaline than *Senegalinium*, contrary to the species noted by Barke et al. (2011).

Tasmania was located at latitudes between 55° and 60° S, in the middle of the region of strong westerly winds, within the range of low atmospheric pressure and received a large amount of precipitation during the Paleocene (Huber and Caballero, 2011). River input from Tasmania and perhaps also Australia could have reached the site. Interestingly, while Tasmania migrated northwards only a few degrees latitude between 60 and 40 Ma (Fig. 1), under warmer temperature conditions as in the mid-Paleocene, the freshwater input decreased, based on both *Senegalinium* cpx., terrestrial palynomorph abundance (decimated abundance from 50 Ma onwards) and the IR (decrease to normal values around 54 Ma; Fig. 16). This suggests either a rerouting of river input or a change in hinterland precipitation regime. Support for the latter comes from clay mineralogical data, showing an increase in kaolinite starting at 50 Ma (Fig. 2; Robert, 2004). Kaolinite forms abundantly at the base of acidic peats (Staub and Cohen, 1978; Korasidis et al., 2019) and in old, leached soils, which were ubiquitous in the Eocene Australian hinterland (Holdgate et al., 2009).

Deleted: ecogroups

Deleted: The SST control on dinocyst assemblages is further demonstrated in diversity and assemblage variability indices. Throughout the long time interval covered byin our record, dinocyst richness and diversity show a remarkably similar pattern to TEX_{86}-based SST. Species richness, as well as diversity expressed in the Shannon and Simpson indices and Fisher's alpha reach a maximum during the prolonged warmth of the EECO and drop during middle–late Eocene cooling. These relationships are demonstrated by modest correlation coefficient between diversity and TEX_{86} (Fig. 13). This pattern holds for the long-term trends, as well as for the short-term PETM, but not for the MECO. Dinocyst diversity is known to vary in an inshore-to-offshore transect in the modern and Eocene (Brinkhuis, 1994; Pross and Brinkhuis, 2005). As our assemblages indeed consist of many mid-shelf species, the strong correlation between diversity and SST might thus be indirectly related through habitat size, with expansion of the flat shelf area and thereby increase in shelf niches during the EECO (Somme et al., 2009). Variability as indicated by the Gibbs index records the opposite pattern to diversity for the long-term trends into and out of the EECO (Fig 14). That is, the lower-diversity assemblages in general have a higher variability, or sample-to-sample fluctuations within the relative abundances. This indicates the higher diversity dinocyst assemblages might be more ecologically resilient.¶

Deleted: ; Sluijs et al., 2005; Sluijs and Brinkhuis, 2009

Deleted: ; Sluijs and Brinkhuis, 2009

Deleted: to

Deleted: is

Deleted: drying of the

While the hinterland could well retain the kaolinite-rich clays during the Maastrichtian and Paleocene, because the site was under a year-round high precipitation regime, it was less efficient in doing so when the hinterland experienced seasonally more variable climatic conditions as Australia migrated northward. The increase in kaolinite delivery to Site 1172 is hence interpreted as a signal of enhanced soil (or peat) erosion from the catchment areas in Tasmania and SW, as a result of a (seasonally?) more variable climate regime.

5.4 Environmental and climatological changes in the catchment

The long-term trends in the BIT index are at odds with all the river runoff indicators in our data (Fig. 7). BIT remains low during the interval in which increased river water discharge is inferred, but increases when this river-runoff signal decreases. This is unexpected because the BIT index should reflect high input of soil-derived brGDGTs into the marine sediments, associated with increased discharge (Hopmans et al., 2004). There are two ways to explain this signal. The BIT index could be responding to marine crenarchaeol production, rather than to the terrestrial brGDGT flux. Indeed, marine productivity could have been spurred by runoff and associated nutrient delivery to the coastal zone during the Paleocene, and decreased in the Eocene, thereby lowering and increasing BIT index values, respectively. Another explanation is that the BIT index has been influenced by in-river crenarchaeol production, although crenarchaeol concentrations in rivers are normally negligible compared to those produced in the marine realm (Zell et al., 2013). Decreasing BIT index values with increasing river-and soil input has been related to climate in the catchment in the late Quaternary Zambezi river (Lattaud et al., 2017), where hinterland vegetation and seasonality in precipitation controls soil-OM input to the marine realm. Studies of modern soil-river-ocean pathways in the Amazon River system show that whereas river-suspended brGDGTs in its upper tributaries during the wet season reflect catchment soils (Kirkels et al., 2020), the lower Amazon contains increasing contributions of *in situ* produced brGDGTs, especially during the dry season, when soil mobilisation is limited (Zell et al., 2013). In addition, soil-derived brGDGTs appear to be rapidly lost upon entering a river, and are only effectively transferred to the ocean floor in catchments with a distinct rainy

Deleted: drier,

Deleted: presumed

Deleted: with

Deleted: ,

Deleted: as

Deleted: indicated by

Deleted: the high IR and abundance of *Senegalinium*

Deleted: and

Deleted: input

Deleted: ,

Deleted: affecting

Deleted: riverine

Deleted:

Deleted: in the river (Zell et al., 2013)

Deleted: the river-producedine

Deleted: that

Deleted: (ref; of Zell et al hier naartoe verplaatsen)

Deleted: catchment dynamics

Deleted: involving

Deleted: dynamics

Deleted: ling

Deleted: on

Deleted: brGDGTs in

Deleted: receive

Formatted: Font: Italic

Deleted: ,

season or during periods with heavy rainfall (e.g. Weijers et al., 2007b; Guo et al., 2020). The marine surface sediments of the Amazon fan consequently contain a mix of soil, fluvial, and marine brGDGTs (Zell et al., 2014). Thus, we here propose the following scenario to explain the BIT index trends for Site 1172: In the early Paleocene–early Eocene, year-round precipitation caused strong fresh-water delivery into the SW Pacific. Soil-derived brGDGTs were partly remineralized in the river catchment, and the strongly diluted soil-derived OM was dominated by river-produced brGDGTs, which suppressed the BIT index. This explains the unexpectedly cold MAATs derived from the mid-Paleocene samples with high IR. The high fluvial discharge also promoted pelagic isoGDGT production, including crenarchaeol, due to associated nutrient delivery, further lowering the BIT index. Later in the early Eocene, precipitation in the hinterland decreased and became more seasonal as the hinterland gradually drifted out of the zone of intense precipitation. This led to a more effective transfer of soil-derived brGDGTs and kaolinite to the mearine realm, increasing the BIT index at the ETP.

Deleted: Kim et al., 2012;

Deleted: and m

Deleted: riverine

Deleted: In a high-precipitation, soil-rich environment like the Amazon basin, this can only occur if the river-produced brGDGT production progressively exceeds the soil-derived brGDGTs input in river water along the trajectory of the river, or when the soil-derived brGDGTs are preferentially remineralized during river transport. W

Deleted:

Deleted: early

Deleted: excessive,

Deleted: -fed river runoff

Deleted: sw

Deleted: and crenarchaeol, both in river production and on the continental shelf

Deleted: riverine

Deleted: input did

Deleted: : both crenarchaeol

Deleted: (which

Deleted: decreaseds

Deleted: ed

Deleted:) and isoGDGTs in general

Deleted: In

Deleted: This reduced river discharge, but at the same time the moreand

Deleted: T dynamic climate regime northward drift of the resulted in the development of a caused more seasonal precipitation regime that which enhanced soil mobilisation increased destabilization of in Australian and Tasmania during the wet seasonn .

Deleted: soils, leading to a higher abundance of

Deleted: from destabilized soils in the river discharge, and relatively little river-produced brGDGTs (because enhanced soil-OM content increased turbidity) and river-produced crenarchaeol

Deleted: which

Deleted: e

Deleted: d

Fig. 16

GDGT- and palynology-based proxies for runoff

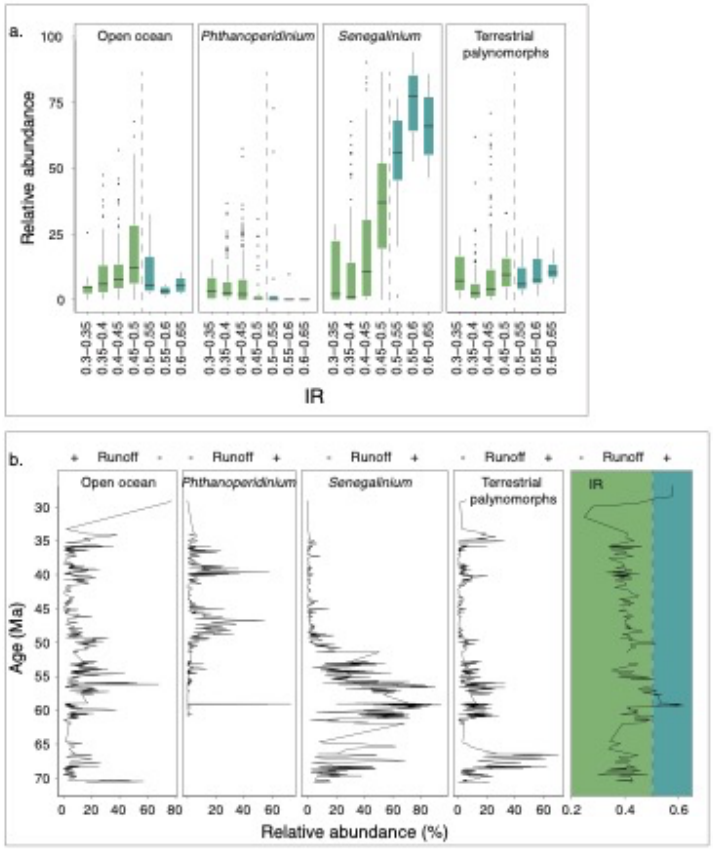

Figure 16. BrGDGT- and palynology-based proxies for river runoff. a. relative abundance of Open Ocean, *Phthanoperidinium* spp., *Senegalinium* cpx. (for groups see Table 3) and terrestrial palynomorphs in 0.05 index unit bins of the resampled IR. Dashed line separates elevated IR bins from non-elevated IR bins. Median (black bars), lower-to-upper quartiles (25–75 percentile; coloured envelopes), lower to upper whiskers (95% confidence intervals; black lines), outlier samples (black dots). b. Time series of the same palynology eco-groups and the IR.

Deleted: ecogroups

6. Conclusions

We have analysed GDGT- and dinoflagellate cyst data in samples from the Maastrichtian–lower Oligocene sediments at ODP Site 1172. IsoGDGTs represent a pelagic signal throughout the Maastrichtian–Eocene but are influenced by sedimentary-produced isoGDGTs in the Oligocene. BrGDGTs at this site are likely primarily soil- or peat-derived, albeit evolutionary changes in brGDGT producers may be responsible for Paleogene-specific brGDGT signals. Exceptions are the mid-Paleocene, where in river-produced brGDGTs influence the record, and the Oligocene, where marine in situ brGDGTs dominate. TEX_{86} and MBT'_{5me} records reveal the SST and MAAT evolution of the region, respectively, within the range of independent existing paleotemperature reconstructions from the same samples. A temperature offset between the SST and MAAT proxies remains poorly reconciled with the coastal proximity of the site but is likely a combined effect of evolutionary trends in MBT'_{5me}-MAAT relationships and a disparate integration of climate signals by both proxies. The subdued air temperature cooling in the middle Eocene compared to the SST cooling could in part reflect progressive northward tectonic drift of the hinterland, while SSTs responded to stronger progressive cooling of southern-sourced surface waters. Strong MAAT cooling occurred step-wise at 35.5 Ma and around the Eocene–Oligocene transition. The absence of SST cooling around the Eocene–Oligocene transition seems to suggest some disconnection between oceanographic reorganisations and regional MAAT changes. The absence of a MAAT response at the PETM and MECO remains unresolved but might be related to shifting sources of brGDGTs during these warm phases.

The relatively high IR and low $\#rings_{tetra}$ confirm inferences from dinocyst assemblages of an inner mid-shelf depositional setting. We reconstruct strong river-runoff in the mid-Paleocene–earliest Eocene at this site, and normal open-marine conditions thereafter. The latter reflects increased seasonality in precipitation in the catchment as the continent tectonically migrates northwards during the middle and late Eocene, out of the region of year-round precipitation. The correlation between SST changes, dinoflagellate cyst assemblages and biodiversity metrics suggest temperature-controlled sea level changes influenced the site, probably through steric effects. We find corroborating evidence for a temperature signal in brGMGT

Deleted: critically reviewed
Deleted: the
Deleted: and
Deleted: our
Deleted: prodcution
Deleted: distribution
Deleted: have altered the
Deleted: soil
Deleted: composition
Deleted: -produce
Deleted: d
Deleted: ine
Deleted: produced
Deleted: consistent with
Deleted: differences
Deleted: remained continuously influenced by the Antarctic-derived Tasman Current
Deleted: s
Deleted: ,
Deleted: characteristic of
Deleted: n
Deleted: y
Deleted: a drying and
Deleted: strong
Deleted: during the middle and late Eocene
Deleted: and changes

assemblages, further demonstrating the potential to develop novel proxies with more extensive studies of modern distributions.

Deleted: n

Deleted: affinities

Deleted: biomarker associations

7.Supplements

- Table S1: Age tie points
- Table S2: grouping of dinocysts in eco-groups

Deleted: ecogroups

8. Data availability

Raw GDGT/GMGT and palynological data presented in this paper, as well as R markdown code for data analysis and visualization can be found on Github (https://github.com/bijlpeter83/RGDGT.git). Data was deposited at zenodo under DOI:10.5281/zenodo.4471204.

9. Author contributions

AS (PETM) and PKB (part) prepared samples for GDGT analyses. PKB (part), AS (PETM) and CB (part) integrated UHPLC-MS results. AS (PETM) and PKB (part) analysed palynological samples. All authors contributed to the interpretation of the OG results, and PKB, AS, JF and MC interpreted dinocyst results. PKB wrote the R script for data analyses and visualization, drafted the figures and wrote the paper with input from all authors.

10. Acknowledgements

This research used samples from the Ocean Drilling Program, which was funded through U.S. National Science foundation under the management of joined oceanographic institutions, inc. We thank Klaas Nierop, Desmond Eefting and Natasja Welters for technical/analytical support. PKB acknowledges funding through NWO Vernieuwingsimpuls Veni grant no. 863.13.002. This work was carried out under the program of the Netherlands Earth System Science Centre (NESSC), financially supported by the Dutch Ministry of Education, Culture and Science. MC and AS thank the Ammodo Foundation for funding unfettered research of laureate AS. PB and AS thank the European Research Council for Starting Grant 802835 OceaNice and Consolidator Grant 771497 SPANC, respectively. We thank Chris Hollis and an

anonymous reviewer for constructive, critical reviews which greatly improved the paper.

11. References

Anagnostou, E., John, E. H., Edgar, K. M., Foster, G. L., Ridgwell, A., Inglis, G. N., et al.: Changing atmospheric CO_2 concentration was the primary driver of early Cenozoic climate, Nature, 533, 380-384, doi:10.1038/nature17423, 2016.

Anagnostou, E., John, E.H., Babila, T.L., Sexton, P.F., Ridgwell, A., Lunt, D.J., Pearson, P.N., Chalk, T.B., Pancost, R.D., Foster, G.L.: Proxy evidence for state-dependence of climate sensitivity in the Eocene greenhouse, Nature Communications, 11(1): art. no. 4436, 2020.

Barke, J., Abels, H. A., Sangiorgi, F., Greenwood, D. R., Sweet, A. R., Donders, T., et al.: Orbitally forced Azolla blooms and middle Eocene Arctic hydrology: Clues from palynology, Geology, 39, 427-430, 2011.

Baxter, A. J., Hopmans, E. C., Russell, J. M., and Sinninghe Damsté, J. S.: Bacterial GMGTs in east african lake sediments: Their potential as palaeotemperature indicators, Geochimica et Cosmochimica acta 259: 155-169, doi:https://doi.org/10.1016/j.gca.2019.05.039, 2019.

Bijl, P. K., Bendle, A. P. J., Bohaty, S. M., Pross, J., Schouten, S., Tauxe, L., et al.: Eocene cooling linked to early flow across the Tasmanian Gateway, Proceedings of the National Academy of Sciences of the United States of America 110(24), 9645-9650, 2013a.

Bijl, P. K., Brinkhuis, H., Egger, L. M., Eldrett, J. S., Frieling, J., Grothe, A., et al.: Comment on 'Wetzeliella and its allies–the 'hole' story: A taxonomic revision of the

Formatted: Not Highlight

Formatted: English (US)

Formatted: Not Highlight

Formatted: English (US)

Formatted: Not Highlight

Formatted: English (US)

Formatted: Not Highlight

Formatted: Not Highlight

Deleted: ¶

Deleted: Beerling, D. J., and Royer, D. L.: Convergent Cenozoic CO_2 history, Nature Geoscience, 4, 418-420, 2019. ¶

Paleogene dinoflagellate subfamily Wetzelielloideae' by Williams et al. (2015). Palynology, 41(3), 423-429. doi:10.1080/01916122.2016.1235056, 2017.

Bijl, P. K., Houben, A. J. P., Schouten, S., Bohaty, S. M., Sluijs, A., Reichart, G.J., et al.: Transient middle Eocene atmospheric carbon dioxide and temperature variations, Science 330, 819-821, 2010.

Bijl, P. K., Pross, J., Warnaar, J., Stickley, C. E., Huber, M., Guerstein, R., et al.: Environmental forcings of Paleogene Southern Ocean dinoflagellate biogeography, Paleoceanography 26, PA1202, 2011.

Bijl, P. K., Schouten, S., Brinkhuis, H., Sluijs, A., Reichart, G.J., and Zachos, J. C.: Early Palaeogene temperature evolution of the southwest Pacific Ocean, Nature 461, 776-779, 2009.

Bijl, P. K., Sluijs, A., and Brinkhuis, H.: A magneto- chemo- stratigraphically calibrated dinoflagellate cyst zonation of the early Paleogene South Pacific Ocean, Earth-Science Reviews 124, 1-31, 2013b.

Bijl, P. K., Sluijs, A., and Brinkhuis, H.: Erratum to "A magneto- and chemostratigraphically calibrated dinoflagellate cyst zonation of the early Paleogene South Pacific Ocean" [Earth sci. rev. 124 (2013) 1-31], Earth-Science Reviews 134, 160-163. doi:10.1016/j.earscirev.2014.03.010, 2014.

Blaga, C. I., Reichart, G.-J., Heiri, O., and Sinninghe Damsté, J. S.: Tetraether membrane lipid distributions in water-column particulate matter and sediments: A study of

47 European lakes along a north-south transect, Journal of Paleolimnology 41(3), 523-540, doi:10.1007/s10933-008-9242-2, 2009

Bohaty, S. M., Zachos, J. C., and Delaney, M. L.: Foraminiferal Mg/Ca evidence for Southern Ocean cooling across the Eocene–Oligocene transition, EPSL, doi:https://doi.org/10.1016/j.epsl.2011.11.037 ,2012

Bohaty, S. M., Zachos, J. C., Florindo, F., and Delaney, M. L.: Coupled greenhouse warming and deep-sea acidification in the middle Eocene, Paleoceanography 24, doi:10.1029/2008PA001676, 2009

Brinkhuis, H.: Late Eocene to early Oligocene dinoflagellate cysts from the Priabonian type-area (northeast Italy); biostratigraphy and palaeoenvironmental interpretation, Palaeogeography, Palaeoclimatology, Palaeoecology 107, 121-163, 1994.

Brinkhuis, H., Sengers, S., Sluijs, A., Warnaar, J., and Williams, G. L.: Latest Cretaceous to earliest Oligocene, and Quaternary dinoflagellates from ODP site 1172, East Tasman Plateau, In N. Exon, and J. P. Kennett (Eds.), Proceedings of the Ocean Drilling Program, scientific results, volume 189. College Station, Texas: U.S. Government Printing Office, 2003.

Cande, S. C., and Stock, J. M.: Cenozoic reconstructions of the Australia-new Zealand-south Pacific sector of antarctica, In N. F. Exon, J. P. Kennett and M. Malone (Eds.), The Cenozoic Southern Ocean: Tectonics, sedimentation and climate change between australia and Antarctica (pp. 5-18) Geophysical Monograph Series, American Geophysical Union, 2004.

2287 Carpenter, R. J., Jordan, G. J., Macphail, M. K., and Hill, R. S.: Near-tropical early Eocene
2288 terrestrial temperatures at the Australo-Antarctic margin, western Tasmania,
2289 Geology, 40(3), 267-270, doi:10.1130/G32584.1, 2012

2290 Contreras, L., Pross, J., Bijl, P. K., Koutsodendris, A., Raine, J. I., van de Schootbrugge, B.,
2291 et al.: Early to middle Eocene vegetation dynamics at the Wilkes Land Margin
2292 (Antarctica), Review of Palaeobotany and Palynology 197, 119-142, 2013.

2293 Contreras, L., Pross, J., Bijl, P. K., O'Hara, R. B., Raine, J. I., Sluijs, A., et al.: Southern
2294 high-latitude terrestrial climate change during the Palaeocene-Eocene derived
2295 from a marine pollen record (ODP site 1172, East Tasman Plateau), Climate of the
2296 Past, 10(4), 1401-1420, doi:10.5194/cp-10-1401-2014, 2014.

2297 Cramwinckel, M. J., Huber, M., Kocken, I. J., Agnini, C., Bijl, P. K., Bohaty, S. M., et al.:
2298 Synchronous tropical and deep ocean temperature evolution in the Eocene,
2299 Nature 559, 382-386, 2018.

2300 Cramwinckel, M. J., Woelders, L., Huurdeman, E. P., Peterse, F., Gallagher, S. J., Pross, J.,
2301 et al.: Surface-circulation change in the Southern Ocean across the Middle Eocene
2302 Climatic Optimum: Inferences from dinoflagellate cysts and biomarker
2303 paleothermometry, Climate of the Past, , 1-34, 2020

2304 Creech, J. B., Baker, J. A., Hollis, C. J., Morgans, H. E. G., and Smith, E. G. C.: Eocene sea
2305 temperatures for the mid-latitude southwest Pacific from Mg/Ca ratios in
2306 planktonic and benthic foraminifera, Earth and Planetary Science Letters, 299,
2307 483-495, 2010.

Crouch, E. M., Shepherd, C. L., Morgans, H. E. G., Naafs, B. D. A., Dallanave, E., Phillips, A., et al.: Climatic and environmental changes across the Early Eocene Climatic Optimum at mid-Waipara River, Canterbury Basin, New Zealand, Earth-Science Reviews, 200, doi:10.1016/j.earscirev.2019.102961, 2020.

Dallanave, E., Bachtadse, V., Crouch, E. M., Tauxe, L., Shepherd, C. L., Morgans, H. E. G., et al.: Constraining early to middle Eocene climate evolution of the southwest Pacific and Southern Ocean. Earth and Planetary Science Letters, 433, 380-392. doi:10.1016/j.epsl.2015.11.010, 2016

De Jonge, C., Hopmans, E. C., Stadnitskaia, A., Rijpstra, W. I. C., Hofland, R., Tegelaar, E., et al.:Identification of novel penta- and hexamethylated branched glycerol dialkyl glycerol tetraethers in peat using HPLC-MS2, GC-MS and GC-SMB-MS, Organic Geochemistry 54, 78-82, doi:10.1016/j.orggeochem.2012.10.004, 2013.

De Jonge, C., Hopmans, E. C., Zell, C. I., Kim, J. -., Schouten, S., and Sinninghe Damsté, J. S.: Occurrence and abundance of 6-methyl branched glycerol dialkyl glycerol tetraethers in soils: Implications for palaeoclimate reconstruction, Geochimica et Cosmochimica Acta, 141, 97-112. doi:10.1016/j.gca.2014.06.013, 2014a.

De Jonge, C., Stadnitskaia, A., Cherkashov, G., and Sinninghe Damsté, J. S.: Branched glycerol dialkyl glycerol tetraethers and crenarchaeol record post-glacial sea level rise and shift in source of terrigenous brGDGTs in the Kara Sea (Arctic Ocean), Organic Geochemistry 92, 42-54, doi:10.1016/j.orggeochem.2015.11.009, 2016.

2329 De Jonge, C., Stadnitskaia, A., Hopmans, E. C., Cherkashov, G., Fedotov, A., and
2330 Sinninghe Damsté, J. S.: In situ produced branched glycerol dialkyl glycerol
2331 tetraethers in suspended particulate matter from the Yenisei River, eastern
2332 Siberia, Geochimica et Cosmochimica Acta, 125, 476-491,
2333 doi:10.1016/j.gca.2013.10.031, 2014b.

2334 De Jonge, C., Stadnitskaia, A., Hopmans, E. C., Cherkashov, G., Fedotov, A., Streletskaya,
2335 I. D., et al.: Drastic changes in the distribution of branched tetraether lipids in
2336 suspended matter and sediments from the Yenisei River and Kara Sea (Siberia):
2337 Implications for the use of brGDGT-based proxies in coastal marine sediments,
2338 Geochimica et Cosmochimica Acta 165, 200-225, doi:10.1016/j.gca.2015.05.044,
2339 2015.

2340 De Jonge, C., Radujković, D., Sigurdsson, B. D., Weedon, J. T., Janssens, I., and Peterse,
2341 F.: Lipid biomarker temperature proxy responds to abrupt shift in the bacterial
2342 community composition in geothermally heated soils, Org Geochem, 137, 894
2343 103897, https://doi.org/10.1016/j.orggeochem.2019.07.006, 2019.

2344 Dearing Crampton-Flood, E., Peterse, F., Munsterman, D., Sinninghe Damsté, J.S.: Using
2345 tetraether lipids archived in North Sea Basin sediments to extract North Western
2346 European Pliocene continental air temperatures, Earth and Planetary Science
2347 Letters, 490: pp. 193-205, 2018.

2348 Dearing Crampton-Flood, E., Peterse, F., and Sinninghe Damsté, J. S.: Production of
2349 branched tetraethers in the marine realm: Svalbard fjord sediments revisited,
2350 Organic Geochemistry 138 doi:10.1016/j.orggeochem.2019.103907, 2019.

Formatted: Not Highlight
Formatted: English (US)
Formatted: Not Highlight
Formatted: English (US)
Formatted: Not Highlight
Formatted: English (US)
Formatted: Not Highlight
Formatted: English (US)
Formatted: English (US)
Formatted: English (US), Not Highlight

2351 Dearing Crampton-Flood, E., Tierney, J. E., Peterse, F., Kirkels, F M S A, and Sinninghe
2352 Damsté, J. S. BayMBT: A bayesian calibration model for branched glycerol dialkyl
2353 glycerol tetraethers in soils and peats, Geochimica Et Cosmochimica Acta, 268,
2354 142-159, doi:10.1016/j.gca.2019.09.043, 2020.

2355 Douglas, P. M. J., Affek, H. P., Ivany, L. C., Houben, A. J. P., Sijp, W. P., Sluijs, A.,
2356 Schouten, S., Pagani, M.: Pronounced zonal heterogeneity in Eocene southern
2357 high latitude sea surface temperatures, PNAS 111 (18), 6582-6587, 2014.

2358 Elling, F. J., K.nneke, M., Lipp, J. S., Becker, K. W., Gagen, E. J., and Hinrichs, K.-U.: Effects
2359 of growth phase on the membrane lipid composition of the thaumarchaeon
2360 Nitrosopumilus maritimus and their implications for archaeal lipid distributions
2361 in the marine environment, Geochim Cosmochim Ac, 141, 579-597,
2362 https://doi.org/10.1016/j.gca.2014.07.005, 2014.

2363 Evans, D., Sagoo, N., Renema, W., Cotton, L. J., Müller, W., Todd, J. A., et al.: Eocene
2364 greenhouse climate revealed by coupled clumped isotope-Mg/Ca thermometry,
2365 Proceedings of the National Academy of Sciences of the United States of America,
2366 115(6), 1174-1179. doi:10.1073/pnas.1714744115, 2018.

2367 Exon, N. F., Kennett, J. P., and Malone, M.: Proceedings of the Ocean Drilling Program,
2368 initial reports, volume 189, College Station, Texas: U.S. Government Printing
2369 Office., 2001.

2370 Feng, X, Vonk, J.E., van Dongen, B.E., Gustafsson, Ö., Semiletov, I.P., Dudarev, O.V.,
2371 Wang, Z., Montluçon, D.B., Wacker, L., Eglinton, T.I.: Differential mobilization of

terrestrial carbon pools in Eurasian Arctic river basins, PNAS 110 (35) 14168-14173; https://doi.org/10.1073/pnas.1307031110 , 2013.

Fensome, R. A., Taylor, F. J. R., Norris, G., Sarjeant, W. A. S., Wharton, D. I., and Williams, G. L.: In Dinkins G. (Ed.), A classification of modern and fossil dinoflagellates, Salem: Micropalaeontology, Special Paper, 1993.

Fisher, R. A., Corbet, A. S., and Williams, C. B.: The relation between the number of species and the number of individuals in a random sample of an animal population, Journal of Animal Ecology, 12(1), 42-58, doi:10.2307/1411, 1943.

Foster, G. L., Royer, D. L., and Lunt, D. J.: Future climate forcing potentially without precedent in the last 420 million years, Nature Communications, 8, 14845, 2017.

Frieling, J., Gebhardt, H., Huber, M., Adekeye, O. A., Akande, S. O., Reichart, G.J., et al.: Extreme warmth and heat-stressed plankton in the tropics during the Paleocene-Eocene Thermal Maximum. Science Advances, 3(3) doi:10.1126/sciadv.1600891, 2017.

Frieling, J., Huurdeman, E. P., Rem, C. C. M., Donders, T. H., Pross, J., Bohaty, S. M., et al.: Identification of the Paleocene-Eocene boundary in coastal strata in the Otway Basin, Victoria, Australia, Journal of Micropalaeontology, 37(1), 317-339, doi:10.5194/jm-37-317-2018, 2018.

Frieling, J., Iakovleva, A. I., Reichart, G. J., Aleksandrova, G. N., Gnibidenko, Z. N., Schouten, S., et al.: Paleocene–Eocene warming and biotic response in the epicontinental west Siberian Sea, Geology, doi:10.1130/G35724.1, 2014.

2393 Frieling, J., and Sluijs, A.: Towards quantitative environmental reconstructions from
2394 ancient non-analogue microfossil assemblages: Ecological preferences of
2395 Paleocene – Eocene dinoflagellates, Earth-Science Reviews, 185, 956-973,
2396 doi:10.1016/j.earscirev.2018.08.014, 2018.

2397 Fuller, M., and Touchard, Y. On the magnetostratigraphy of the East Tasman Plateau,
2398 timing of the opening of the Tasmanian Gateway and paleoenvironmental
2399 changes, In N. Exon, J. P. Kennett and M. Malone (Eds.), The Cenozoic Southern
2400 Ocean. tectonics, sedimentation and climate change between Australia and
2401 Antarctica (pp. 127-151), Washington: American Geophysical Union (AGU)
2402 Geophysical Monograph series, 2004.

2403 Gibbs, S. J., Bown, P. R., Murphy, B. H., Sluijs, A., Edgar, K. M., Pälike, H., et al.: Scaled
2404 biotic disruption during early Eocene global warming events, Biogeosciences,
2405 9(11), 4679-4688, 2012.

2406 Guasti, E., Speijer, R. P., Brinkhuis, H., Smit, J., and Steurbaut, E.: Paleoenvironmental
2407 change at the Danian-Selandian transition in Tunisia: Foraminifera, organic-
2408 walled dinoflagellate cyst and calcareous nannofossil records, Marine
2409 Micropaleontology, 59, 210-229, 2006.

2410 Guo, J., Glendell, M., Meersmans, J., Kirkels, F., Middelburg, J.J., Peterse, F.: Assessing
2411 branched tetraether lipids as tracers of soil organic carbon transport through the
2412 Carminowe Creek catchment (southwest England), Biogeosciences, 17 (12): pp.
2413 3183-320, 2020.

Formatted: Not Highlight
Formatted: English (US)
Formatted: Not Highlight
Formatted: English (US)
Formatted: Not Highlight
Formatted: English (US)
Formatted: Not Highlight
Formatted: English (US)
Formatted: English (US)
Formatted: English (US), Not Highlight

2414 Hartman, J. D., Bijl, P. K., Sangiorgi, F., Peterse, F., Schouten, S., Salabarnada, A., et al.:
2415 Paleoceanography and ice sheet variability offshore Wilkes Land, Antarctica –
2416 part 3: Insights from Oligocene–Miocene TEX_{86}-based sea surface temperature
2417 reconstructions, Climate of the Past, 14, 1275–1297, 2018.

2418 Hill, P. J., and Exon, N. F.: Tectonics and basin development of the offshore Tasmanian
2419 area; incorporating results from deep ocean drilling, In N. F. Exon, J. P. Kennett
2420 and M. Malone (Eds.), The Cenozoic Southern Ocean; tectonics, sedimentation
2421 and climate change between Australia and Antarctica (Geophysical Monograph
2422 Series 151 ed., pp. 19-19), Washington, D.C., U.S.A.: American Geophysical Union,
2423 2004.

2424 Hill, P. J., and Moore, A. M. G.: Geological framework of the South Tasman Rise and
2425 East Tasman Plateau, Geoscience Australia, 2001/40, 2001.

2426 Hines, B. R., Hollis, C. J., Atkins, C. B., Baker, J. A., Morgans, H. E. G., and Strong, P. C.:
2427 Reduction of oceanic temperature gradients in the early Eocene southwest
2428 Pacific Ocean, Palaeogeography, Palaeoclimatology, Palaeoecology, 475, 41-54,
2429 doi:10.1016/j.palaeo.2017.02.037, 2017.

2430 Holdgate, G. R., McGowran, B., Fromhold, T., Wagstaff, B. E., Gallagher, S. J., Wallace, M.
2431 W., et al.: Eocene-Miocene carbon-isotope and floral record from brown coal
2432 seams in the Gippsland Basin of southeast Australia, Global and Planetary
2433 Change, 65(1-2), 89-103, doi:10.1016/j.gloplacha.2008.11.001, 2009

2434 Hollis, C. J., Crouch, E. M., Morgans, H. E. G., Handley, L., Baker, J. A., Creech, J., et al.:
2435 Tropical sea temperatures in the high latitude South Pacific during the Eocene,
2436 Geology, 37(2), 99-102, 2009.

2437 Hollis, C. J., Dunkley Jones, T., Anagnostou, E., Bijl, P. K., Cramwinckel, M. J., Cui, Y., et
2438 al.: The DeepMIP contribution to PMIP4: Methodologies for selection,
2439 compilation and analysis of latest paleocene and early Eocene climate proxy data,
2440 incorporating version 0.1 of the DeepMIP database, Geoscientific Model
2441 Development, 12(7), 3149-3206, doi:10.5194/gmd-12-3149-2019, 2019

2442 Hollis, C. J., Tayler, M. J. S., Andrew, B., Taylor, K. W., Lurcock, P., Bijl, P. K., et al.:
2443 Organic-rich sedimentation in the south Pacific Ocean associated with late
2444 Paleocene climatic cooling, Earth-Science Reviews, 134, 81-97, 2014.

2445 Hollis, C. J., Taylor, K. W. R., Handley, L., Pancost, R. D., Huber, M., Creech, J. B., et al.:
2446 Early Paleogene temperature history of the southwest Pacific Ocean: Reconciling
2447 proxies and models, Earth and Planetary Science Letters, 349–350(0), 53-66,
2448 doi:10.1016/j.epsl.2012.06.024, 2012

2449 Hopmans, E. C., Schouten, S., and Sinninghe Damsté, J. S.: The effect of improved
2450 chromatography on GDGT-based palaeoproxies, Organic Geochemistry, 93, 1-6,
2451 doi:10.1016/j.orggeochem.2015.12.006, 2016.

2452 Hopmans, E. C., Weijers, J. W. H., Schefuß, E., Herfort, L., Sinninghe Damsté, J. S., and
2453 Schouten, S.: A novel proxy for terrestrial organic matter in sediments based on
2454 branched and isoprenoid tetraether lipids, Earth and Planetary Science Letters,
2455 224, 107-116, 2004.

Houben, A. J. P., Bijl, P. K., Sluijs, A., Schouten, S., and Brinkhuis, H.: Late Eocene Southern Ocean cooling and invigoration of circulation preconditioned Antarctica for full-scale glaciation, Geochemistry, Geophysics, Geosystems, 20, https://doi.org/10.1029/2019GC008182, 2019.

Huber, M., Brinkhuis, H., Stickley, C. E., Döös, K., Sluijs, A., Warnaar, J., et al.: Eocene circulation of the Southern Ocean: Was Antarctica kept warm by subtropical waters? Paleoceanography, 19, 4026, 2004.

Huber, M., and Caballero, R.: The early Eocene equable climate problem revisited, Climate of the Past, 7, 603-633, 2011.

Huber, M., and Thomas, E., Paleoceanography: The greenhouse world, in Encyclopedia of Ocean Sciences, pp 319–329, 2010.

Hurley, S. J., Elling, F. J., K.nneke, M., Buchwald, C., Wankel, S. D., Santoro, A. E., Lipp, J. S., Hinrichs, K.-U., and Pearson, A.: Influence of ammonia oxidation rate on thaumarchaeal lipid composition and the TEX_{86} temperature proxy, Proceedings of the National Academy of Sciences, 113, 7762-7767, 10.1073/pnas.1518534113, 2016.

Huurdeman, E.P., Frieling, J., Reichgelt, T., Bijl, P.K., Bohaty, S.M., Holdgate, G.R., Gallagher, S.J., Peterse, F., Greenwood, D.R., Pross; J.: Rapid expansion of meso-megathermal rain forests into the southern high latitudes at the onset of the Paleocene-Eocene Thermal Maximum. Geology doi: https://doi.org/10.1130/G47343.1, 2020.

Formatted: Subscript

2477 Inglis, G. N., Farnsworth, A., Lunt, D., Foster, G. L., Hollis, C. J., Pagani, M., et al.: Descent
2478 toward the icehouse: Eocene sea surface cooling inferred from GDGT
2479 distributions, Paleoceanography, 30(7), 1000-1020,
2480 doi:10.1002/2014PA002723, 2015.

2481 Inglis, G. N., Bragg, F., Burls, N. J., Cramwinckel, M. J., Evans, D., Foster, G. L., Huber, M.,
2482 Lunt, D. J., Siler, N., Steinig, S., Tierney, J. E., Wilkinson, R., Anagnostou, E., de Boer,
2483 A. M., Dunkley Jones, T., Edgar, K. M., Hollis, C. J., Hutchinson, D. K., and Pancost, R.
2484 D.: Global mean surface temperature and climate sensitivity of the early Eocene
2485 Climatic Optimum (EECO), Paleocene–Eocene Thermal Maximum (PETM), and
2486 latest Paleocene, Clim. Past, 16, 1953–1968, https://doi.org/10.5194/cp-16-
2487 1953-2020, 2020.

2488 Kim, J. -., Meer, J. v. d., Schouten, S., Helmke, P., Willmott, V., Sangiorgi, F., et al.: New
2489 indices and calibrations derived from the distribution of crenarchaeal isoprenoid
2490 tetraether lipids: Implications for past sea surface temperature reconstructions,
2491 Geochimica et Cosmochimica Acta, 74, 4639-4654, 2010.

2492 Kirkels, F. M. S. A., Ponton, C., Galy, V., West, A. J., Feakins, S. J., and Peterse, F.: From
2493 Andes to Amazon: Assessing Branched Tetraether Lipids as Tracers for Soil
2494 Organic Carbon in the Madre de Dios River System, Journal of Geophysical
2495 Research: Biogeosciences, 125, e2019JG005270, 10.1029/2019jg005270, 2020.

2496 Korasidis, V. A., Wallace, M. W., Dickinson, J. A., and Hoffman, N.: Depositional setting
2497 for Eocene seat earths and related facies of the Gippsland Basin, Australia,
2498 Sedimentary Geology, doi:10.1016/j.sedgeo.2019.07.007, 2019

Deleted: ¶

Kozdon, R., Penman, D. E., Kelly, D. C., Zachos, J. C., Fournelle, J. H., & Valley, J. W.: Enhanced poleward flux of atmospheric moisture to the Weddell Sea region (ODP Site 690) during the Paleocene-Eocene Thermal Maximum, Paleoceanography and Paleoclimatology, 35, e2019PA003811, https://doi.org/10.1029/2019PA003811 , 2020

Lattaud, J., Dorhout, D., Schulz, H., Castañeda, I. S., Schefuß, E., Damsté, J. S. S., et al.: The C32 alkane-1,15-diol as a proxy of late Quaternary riverine input in coastal margins, Climate of the Past, 13(8), 1049-1061, doi:10.5194/cp-13-1049-2017, 2017.

Lauretano, V., Zachos, J. C., and Lourens, L. J.: Orbitally paced carbon and deep-sea temperature changes at the peak of the Early Eocene Climatic Optimum. Paleoceanography and Paleoclimatology, 33(10), 1050-1065, doi:10.1029/2018PA003422, 2018.

Lauretano, V., Kennedy-Asser, A.T., Korasidis, V.A., Wallace, M.W., Valdes, P.J., Lunt, D.J., Pancost, R.D., Naafs, B.D.A.: Eocene to Oligocene terrestrial Southern Hemisphere cooling caused by declining pCO_2. Nature Geoscience, 14 (9), pp. 659-664, DOI: 10.1038/s41561-021-00788-z

Leutert, T. J., Auderset, A., Martínez-García, A., Modestou, S., and Meckler, A. N.: Southern Ocean temperature evolution coupled to middle Miocene ice sheet expansion, Nature Geoscience 13, 634-639, 2020.

Formatted: English (US), Not Highlight
Formatted: Not Highlight
Formatted: English (US), Not Highlight
Formatted: Not Highlight
Formatted: Subscript, Not Highlight
Formatted: English (US), Not Highlight
Formatted: Not Highlight
Formatted: English (US), Not Highlight
Formatted: Not Highlight
Formatted: English (US), Not Highlight
Formatted: English (US), Not Highlight
Deleted: ¶

Liu, Z., Pagani, M., Zinniker, D., DeConto, R., Huber, M., Brinkhuis, H., Shah, S.R., Leckie, R.M., Pearson, A.: Global cooling during the eocene-oligocene climate transition, Science, 323 (5918): pp. 1187-1190, DOI: 10.1126/science.1166368, 2009

Liu, X., Lipp, J. S., Simpson, J. H., Lin, Y., Summons, R. E., and Hinrichs, K.: Mono- and dihydroxyl glycerol dibiphytanyl glycerol tetraethers in marine sediments: Identification of both core and intact polar lipid forms. Geochimica et Cosmochimica Acta, 89, 102-115. doi:https://doi.org/10.1016/j.gca.2012.04.053, 2012.

Lunt, D. J., Jones, T. D., Heinemann, M., Huber, M., LeGrande, A., Winguth, A., et al.: A model-data comparison for a multi-model ensemble of early Eocene atmosphere-ocean simulations: EoMIP, Climate of the Past, 8(5), 1717-1736, DOI: 10.5194/cp-8-1717-2012, 2012.

Lunt, D. J., Bragg, F., Chan, W.-L., Hutchinson, D. K., Ladant, J.-B., Morozova, P., Niezgodzki, I., Steinig, S., Zhang, Z., Zhu, J., Abe-Ouchi, A., Anagnostou, E., de Boer, A. M., Coxall, H. K., Donnadieu, Y., Foster, G., Inglis, G. N., Knorr, G., Langebroek, P. M., Lear, C. H., Lohmann, G., Poulsen, C. J., Sepulchre, P., Tierney, J. E., Valdes, P. J., Volodin, E. M., Dunkley Jones, T., Hollis, C. J., Huber, M., and Otto-Bliesner, B. L.: DeepMIP: model intercomparison of early Eocene climatic optimum (EECO) large-scale climate features and comparison with proxy data, Clim. Past, 17, 203–227, https://doi.org/10.5194/cp-17-203-2021, 2021.

Formatted: English (US)
Formatted: English (US)
Formatted: English (US)
Formatted: English (US)
Formatted: English (US)
Deleted: ¶
Formatted: English (US)
Formatted

2542 Macphail, M. K.: Australian palaeoclimates, cretaceous to tertiary, volume 1: Review
2543 of palaeobotanical and related evidence up to 2000, Canberra: Geology
2544 Department, Australian National University, 2000.

2545 Macphail, M. K.: ODP Leg 189 initial results: Terrestrial plant microfossils. Canberra:
2546 Geoscience Australia, 2002

2547 Mertens, K. N., Dale, B., Ellegaard, M., Jansson, I. -., Godhe, A., Kremp, A., et al.: Process
2548 length variation in cysts of the dinoflagellate protoceratium reticulatum, from
2549 surface sediments of the baltic-kattegat-skagerrak estuarine system: A regional
2550 salinity proxy, Boreas, 40(2), 242-255, DOI: 10.1111/j.1502-3885.2010.00193.x
2551 2011.

2552 Moore, D. H., Betts, P. G., and Hall, M.: Towards understanding the early Gondwanan
2553 margin in southeastern Australia, Gondwana Research, 23(4), 1581-1598,
2554 doi:10.1016/j.gr.2012.08.006, 2013.

2555 Morii, H., Eguchi, T., Nishihara, M., Kakinuma, K., König, H., Koga, Y.: A novel ether core
2556 lipid with H-shaped C80-isoprenoid hydrocarbon chain from the hyperthermophilic
2557 methanogen Methanothermus fervidus, Biochimica et Biophysica Acta 1390: 339-
2558 345, DOI: 10.1016/s0005-2760(97)00183-5 , 1998.

2559 Müller, R. D., Gaina, C., and Clark, S.: Seafloor spreading around Australia, In J. Veevers
2560 (Ed.), Billion-year earth history of Australia and neighbours in gondwanaland
2561 (2000) – BYEHA (pp. 1-1) School of Geosciences, University of Sydney, 2000

Formatted: English (US)

Formatted

Formatted: Indent: Left: 0 cm, Hanging: 0.75 cm

Formatted: Not Highlight

Formatted: Indent: Left: 0 cm, First line: 0 cm

Formatted: Not Highlight

Formatted: Not Highlight

Formatted: Not Highlight

Formatted: Not Highlight

Formatted: Not Highlight

Formatted: Not Highlight

Formatted: Not Highlight

Formatted: Default Paragraph Font, Font: Times New Roman, Font colour: Black,

Formatted: Not Highlight

Deleted: ¶

Naafs, B. D. A., Gallego-Sala, A. V., Inglis, G. N., and Pancost, R. D.: Refining the global branched glycerol dialkyl glycerol tetraether (brGDGT) soil temperature calibration, Organic Geochemistry, 106, 48-56, doi:10.1016/j.orggeochem.2017.01.009, 2017a.

Naafs, B. D. A., Inglis, G. N., Blewett, J., McClymont, E. L., Lauretano, V., Xie, S., et al.: The potential of biomarker proxies to trace climate, vegetation, and biogeochemical processes in peat: A review, Global and Planetary Change, 179, 57-79, doi:10.1016/j.gloplacha.2019.05.006, 2019.

Naafs, B. D. A., Inglis, G. N., Zheng, Y., Amesbury, M. J., Biester, H., Bindler, R., et al.: Introducing global peat-specific temperature and pH calibrations based on brGDGT bacterial lipids, Geochimica et Cosmochimica Acta, 208, 285-301, doi:10.1016/j.gca.2017.01.038, 2017b.

Naafs, B. D. A., McCormick, D., Inglis, G. N., and Pancost, R. D.: Archaeal and bacterial H-GDGTs are abundant in peat and their relative abundance is positively correlated with temperature, Geochimica Et Cosmochimica Acta, 227, 156-170, doi:10.1016/j.gca.2018.02.025, 2018a.

Naafs, B. D. A., Rohrssen, M., Inglis, G. N., Lähteenoja, O., Feakins, S. J., Collinson, M. E., et al.: High temperatures in the terrestrial mid-latitudes during the early Palaeogene, Nature Geoscience, 11(10), 766-771, doi:10.1038/s41561-018-0199-0, 2018b.

O'Brien, C. L., Robinson, S. A., Pancost, R. D., Sinninghe Damsté, J. S., Schouten, S., Lunt, D. J., et al.: Cretaceous sea-surface temperature evolution: Constraints from TEX_{86}

Deleted:

Formatted: Not Highlight

Formatted: Not Highlight

Formatted: English (US), Not Highlight

Formatted: Not Highlight

and planktonic foraminiferal oxygen isotopes, Earth-Science Reviews, 172, 224-247, doi:10.1016/j.earscirev.2017.07.012, 2017.

O'Brien, C. L., Huber, M., Thomas, E., Pagani, M., Super, J. R., Elder, L. E., et al.: The enigma of Oligocene climate and global surface temperature evolution, Proceedings of the National Academy of Sciences, 202003914, doi:10.1073/pnas.2003914117, 2020.

O'Connor, L. K., Robinson, S. A., Naafs, B. D. A., Jenkyns, H. C., Henson, S., Clarke, M., et al.: Late Cretaceous temperature evolution of the southern high latitudes: A TEX_{86} perspective, Paleoceanography and Paleoclimatology, 34(4), 436-454, doi:10.1029/2018PA003546, 2019.

Oksanen, J., Blanchet, F. G., Friendly, M., Kindt, R., Legendre, P., McGlinn, D., et al.: Vegan: Community ecology package, 2015.

Pancost, R. D., Taylor, K. W. R., Inglis, G. N., Kennedy, E. M., Handley, L., Hollis, C. J., et al.: Early Paleogene evolution of terrestrial climate in the SW Pacific, southern New Zealand, Geochemistry, Geophysics, Geosystems, 14(12), 5413-5429, DOI: 10.1002/2013GC004935, 2013.

Passchier, S., Bohaty, S. M., Jiménez-Espejo, F., Pross, J., Röhl, U., Van De Flierdt, T., et al.: Early Eocene to middle Miocene cooling and aridification of east Antarctica, Geochemistry, Geophysics, Geosystems, 14(5), 1399-1410, doi:10.1002/ggge.20106, 2013.

Formatted: English (US)

Formatted

Deleted:

Formatted: English (UK)

Passchier, S., Ciarletta, D. J., Miriagos, T. E., Bijl, P. K., and Bohaty, S. M.: An Antarctic stratigraphic record of stepwise ice growth through the Eocene-Oligocene transition, Bulletin of the Geological Society of America, 129(3-4), 318-330, doi:10.1130/B31482.1, 2017.

Peterse, F., Kim, J. -., Schouten, S., Kristensen, D. K., Koç, N., and Sinninghe Damsté, J. S.: Constraints on the application of the MBT-CBT paleothermometer at high latitude environments (Svalbard, Norway), Organic Geochemistry, 40, 692-699, https://doi.org/10.1016/j.orggeochem.2009.03.004, 2009.

Pross, J., & Brinkhuis, H., Organic-walled dinoflagellate cysts as paleoenvironmental indicators in the paleogene; a synopsis of concepts, Palaeontologische Zeitschrift, Band 79, 53-59, https://doi.org/10.1007/BF03021753, 2005.

Pross, J., Contreras, L., Bijl, P. K., Greenwood, D. R., Bohaty, S. M., Schouten, S., et al.: Persistent near-tropical warmth on the Antarctic continent during the early Eocene epoch, Nature, 488, 73-73, https://doi.org/10.1038/nature11300, 2012.

Qin, W., Carlson, L. T., Armbrust, E. V., Devol, A. H., Moffett, J. W., Stahl, D. A., and Ingalls, A. E.: Confounding effects of oxygen and temperature on the TEX_{86} signature of marine Thaumarchaeota, Proceedings of the National Academy of Sciences, 112, 10979-10984, 10.1073/pnas.1501568112, 2015.

Reichgelt, T., West, C.K., Greenwood, D.R.: The relation between global palm distribution and climate, Scientific Reports 8(1), DOI: 10.1038/s41598-018-23147-2, 2018.

Formatted: English (US)

Formatted

Deleted: Peterse, F., Meer, J. v. d., Schouten, S., Weijers, J. W. H., Fierer, N., Jackson, R. B., et al.: Revised calibration of the MBT-CBT paleotemperature proxy based on branched tetraether membrane lipids in surface soils. Geochimica Et Cosmochimica Acta, 2012.¶

Formatted: English (US)

Formatted

Formatted: English (US)

Formatted

Robert, C.: Cenozoic environments in the Tasmanian area of the Southern Ocean (ODP Leg 189): Inferences from bulk and clay mineralogy, Geophysical Monograph Series, 151, 127-151, DOI:10.1029/GM151, 2004.

Rochon, A., Lewis, J., Ellegaard, M., and Harding, I. C.: The gonyaulax spinifera (dinophyceae) "complex": Perpetuating the paradox? Review of Palaeobotany and Palynology, 155(1), 52-60, doi:https://doi.org/10.1016/j.revpalbo.2008.12.017, 2008.

Röhl, U., Brinkhuis, H., Stickley, C. E., Fuller, M., Schellenberg, S. A., Wefer, G., et al.: Sea level and astronomically induced environmental changes in middle and late Eocene sediments from the East Tasman Plateau. Geophysical Monograph Series, 151, 127-151, DOI:10.1029/GM151, 2004a.

Röhl, U., Brinkhuis, H., Sluijs, A., and Fuller, M.: On the search for the Paleocene/eocene boundary in the Southern Ocean: Exploring ODP Leg 189 Holes 1171D and 1172D, Tasman Sea, Geophysical Monograph Series, 151, 113-124, DOI:10.1029/GM151, 2004b.

Röhl, U., Westerhold, T., Bralower, T. J., and Zachos, J. C.: On the duration of the Paleocene-Eocene Thermal Maximum (PETM), Geochemistry, Geophysics, Geosystems, 8, Q12002, DOI: 10.1029/2007GC001784, 2007.

Salamy, K.A., Zachos, J.C.: Latest Eocene-Early Oligocene climate change and Southern Ocean fertility: Inferences from sediment accumulation and stable isotope data, Palaeogeogr., Palaeoclimatol., Palaeoecol. 145, 61–77, 1999.

Formatted: English (US)

Formatted

Deleted: ¶

Deleted: Röhl, U., Westerhold, T., Bralower, T. J., and Zachos, J. C.: On the duration of the Paleocene-Eocene Thermal Maximum (PETM), Geochemistry, Geophysics, Geosystems, 8, Q12002, 2007. ¶

Schefuß, E., Eglinton, T., Spencer-Jones, C. et al.: Hydrologic control of carbon cycling and aged carbon discharge in the Congo River basin, Nature Geosciences 9, 687–690, https://doi.org/10.1038/ngeo2778, 2016.

Schellenberg, S. A., Brinkhuis, H., Stickley, C. E., Fuller, M., Kyte, F. T., and Williams, G. L.: The Cretaceous/Paleogene transition on the East Tasman Plateau, southwestern Pacific, In N. Exon, J. P. Kennett and M. Malone (Eds.), The Cenozoic Southern Ocean; tectonics, sedimentation and climate change between Australia and Antarctica (pp. 93-112), Washington: Geophysical Monograph Series 151, DOI:10.1029/GM151, 2004.

Schouten, S., Hopmans, E. C., Schefuß, E., and Sinninghe Damsté, J. S.: Distributional variations in marine crenarchaeotal membrane lipids: A new tool for reconstructing ancient sea water temperatures? Earth and Planetary Science Letters, 204, 265-274, https://doi.org/10.1016/S0012-821X(02)00979-2, 2002.

Schouten, S., Hopmans, E. C., and Sinninghe Damsté, J. S., The organic geochemistry of glycerol dialkyl glycerol tetraether lipids: A review, Organic Geochemistry, 54, 19-61, doi:10.1016/j.orggeochem.2012.09.006, 2013.

Seton, M., Müller, R. D., Zahirovic, S., Gaina, C., Torsvik, T., Shephard, G., et al.: Global continental and ocean basin reconstructions since 200 Ma, Earth-Science Reviews, 113(3-4), 212-270, 2012.

Shannon, C. E.: A mathematical theory of communication, Bell System Technical Journal, 27(3), 379-423, doi:10.1002/j.1538-7305.1948.tb01338.x, 1948.

Formatted: English (US)

Formatted

Formatted: English (US)

Formatted

2680 Sijp, W. P., Von Der Heydt, A S, and Bijl, P. K.: Model simulations of early westward
2681 flow across the Tasman Gateway during the early Eocene, Climate of the Past,
2682 12(4), 807-817, doi:10.5194/cp-12-807-2016, 2016.

2683 Sijp, W. P., von der Heydt, A S, Dijkstra, H. A., Flögel, S., Douglas, P. M. J., and Bijl, P. K.:
2684 The role of ocean gateways on cooling climate on long time scales, Global and
2685 Planetary Change, 119, 1-22, doi:10.1016/j.gloplacha.2014.04.004, 2014.

2686 Simpson, E.: Measurement of diversity. Nature, 163, 688, 1949.

2687 Sinninghe Damsté, J. S.: Spatial heterogeneity of sources of branched tetraethers in
2688 shelf systems: The geochemistry of tetraethers in the Berau River delta
2689 (Kalimantan, Indonesia), Geochimica et Cosmochimica Acta, 186, 13-31,
2690 doi:10.1016/j.gca.2016.04.033, 2016.

2691 Sluijs, A., Bijl, P. K., Schouten, S., Röhl, U., Reichart, G.J., and Brinkhuis, H.: Southern
2692 Ocean warming and hydrological change during the Paleocene-Eocene Thermal
2693 Maximum, Climate of the Past, 7, 47-61, https://doi.org/10.5194/cp-7-47-2011,
2694 2011.

2695 Sluijs, A., and Brinkhuis, H.: A dynamic climate and ecosystem state during the
2696 Paleocene-Eocene Thermal Maximum: Inferences from dinoflagellate cyst
2697 assemblages on the New Jersey Shelf, Biogeosciences, 6(8), 1755-1781,
2698 https://doi.org/10.5194/bg-6-1755-2009, 2009.

2699 Sluijs, A., Brinkhuis, H., Stickley, C. E., Warnaar, J., Williams, G. L., and Fuller, M.:
2700 Dinoflagellate cysts from the Eocene - Oligocene transition in the Southern

Deleted: Sluijs, A., Schouten, S., Pagani, M., Woltering, M., Brinkhuis, H., Sinninghe Damsté, J. S., et al.: Subtropical Arctic Ocean temperatures during the Palaeocene/Eocene Thermal Maximum, Nature, 441, 610-613, 2006.¶

Formatted: English (US)

Formatted

Formatted: English (US)

Formatted

Ocean: Results from ODP Leg 189, In N. Exon, and J. P. Kennett (Eds.), Proceedings of the Ocean Drilling Program, scientific results, volume 189, College Station, Texas: U.S. Government Printing Office, 2003.

Sluijs, A., Frieling, J., Inglis, G. N., Nierop, K. G. J., Peterse, F., Sangiorgi, F., et al.: Late Paleocene – early Eocene Arctic Ocean sea surface temperatures; reassessing biomarker paleothermometry at lomonosov ridge, Clim. Past Discuss., doi:rg/10.5194/cp-2020-13, 2020.

Sluijs, A., Pross, J., and Brinkhuis, H.: From greenhouse to icehouse; organic walled dinoflagellate cysts as paleoenvironmental indicators in the Paleogene, Earth-Science Reviews, 68, 281-315, DOI: 10.1016/j.earscirev.2004.06.001, 2005.

Sluijs, A., van Roij, L., Harrington, G. J., Schouten, S., Sessa, J. A., LeVay, L. J., et al.: Warming, euxinia and sea level rise during the Paleocene–Eocene Thermal Maximum on the Gulf Coastal plain: Implications for ocean oxygenation and nutrient cycling, Climate of the Past, 10(4), 1421-1439, doi:10.5194/cp-10-1421-2014, 2014.

Somme, T. O., Helland-Hansen, W., and Granjeon, D., Impact of eustatic amplitude variations on shelf morphology, sediment dispersal, and sequence stratigraphic interpretation: Icehouse versus greenhouse systems, Geology, 37(7), 587-590, DOI: 10.1130/g25511a.1, 2009.

Staub, J.R., Cohen, A.D.: Kaolinite-enrichment Beneath Coals; A Modern Analog, Snuggedy Swamp, South Carolina, SEPM J Sediment Res Vol. 48(1):203–210, 1978.

Formatted: Indent: Left: 0 cm, Hanging: 0.75 cm

Formatted: English (US)

Formatted

Formatted: Indent: Left: 0 cm, Hanging: 0.75 cm

Formatted: English (US)

Formatted: English (US)

Formatted

Stickley, C. E., Brinkhuis, H., McGonigal, K. L., Chapronière, G. C. H., Fuller, M., Kelly, D. C., et al.: Late Cretaceous - Quaternary biomagnetostratigraphy of ODP Site 1168, 1170, 1171 and 1172, Tasmanian Gateway, In N. F. Exon, J. P. Kennett and M. J. Malone (Eds.), Proceedings of the Ocean Drilling Program, scientific results, volume 189, DOI:10.1029/GM151, 2004a.

Stickley, C. E., Brinkhuis, H., Schellenberg, S. A., Sluijs, A., Röhl, U., Fuller, M., et al.: Timing and nature of the deepening of the Tasmanian Gateway, Paleoceanography, 19, 4027, DOI: 10.1029/2004PA001022, 2004b.

Tang, X., Naafs, B. D., Pancost, R. D., Liu, Z., Fan, T., & Zheng, Y.: Exploring the influences of temperature on "H-shaped" glycerol dialkyl glycerol tetraethers in a stratigraphic context: Evidence from two peat cores across the late Quaternary, Frontiers in Earth Science, 8, 477, 2021.

Taylor, K. W. R., Huber, M., Hollis, C. J., Hernandez-Sanchez, M. T., and Pancost, R. D.: Re-evaluating modern and Palaeogene GDGT distributions: Implications for SST reconstructions, Global and Planetary Change, 108, 158-174, 10.1016/j.gloplacha.2013.06.011, 2013.

Thomas, D. J., Bralower, T. J., and Jones, C. E.: Neodymium isotopic reconstruction of the late Paleocene - early Eocene thermohaline circulation, Earth and Planetary Science Letters, 209(3-4), 309-322, DOI: 10.1016/S0012-821X(03)00096-7, 2003.

Thomas, D. J., Korty, R., Huber, M., Schubert, J. A., and Haines, B.: Nd isotopic structure of the Pacific Ocean 70–30 Ma and numerical evidence for vigorous ocean

Formatted: English (US)

Formatted: Indent: Left: 0 cm, Hanging: 0.75 cm

Formatted

Deleted: ¶

Formatted: English (US)

Deleted: ¶

Formatted

Formatted: English (US)

Formatted

circulation and ocean heat transport in a greenhouse world, Paleoceanography, PA2535, DOI: 10.1002/2013PA002535, 2014.

Tierney, J. E., and Russell, J. M.: Distributions of branched GDGTs in a tropical lake system: Implications for lacustrine application of the MBT/CBT paleoproxy, doi:10.1016/j.orggeochem.2009.04.014, 2009.

Tierney, J.E., Russell, J.M., Eggermont, H., Hopmans, E.C., Verschuren, D., Sinninghe Damsté, J.S.: Environmental controls on branched tetraether lipid distributions in tropical East African lake sediments, Geochimica et Cosmochimica Acta, 74 (17): pp. 4902-4918, DOI: 10.1016/j.gca.2010.06.002, 2010.

Tierney, J. E., Sinninghe Damsté, J. S., Pancost, R. D., Sluijs, A., and Zachos, J. C.: Eocene temperature gradients, Nature Geoscience, 10(8), 538-539, doi:10.1038/ngeo2997, 2017.

Tierney, J. E., and Tingley, M. P.: A TEX_{86} surface sediment database and extended bayesian calibration, Scientific Data, 2 doi:10.1038/sdata.2015.29, 2015.

Tierney, J. E., & Tingley, M. P.: BAYSPLINE: A new calibration for the alkenone paleothermometer, Paleoceanography and Paleoclimatology, 33(3), 281-301, doi:10.1002/2017PA003201, 2018.

Torsvik, T. H., Van der Voo, R., Preeden, U., Niocaill, C. M., Steinberger, B., Doubrovine, P. V., et al.: Phanerozoic polar wander, palaeogeography and dynamics, Earth-Science Reviews, 114(3-4), 325-368, doi:10.1016/j.earscirev.2012.06.007, 2012.

Formatted: English (US)
Formatted
Formatted: Not Highlight
Formatted: English (US), Not Highlight
Formatted: Not Highlight
Formatted: English (US), Not Highlight
Formatted: Not Highlight
Formatted: English (US), Not Highlight
Formatted: Not Highlight
Formatted: English (US), Not Highlight
Formatted: Not Highlight
Deleted: ¶
Formatted: English (UK)

2773 Truswell, E. M.: Palynomorph assemblages from marine Eocene sediments on the
2774 west Tasmanian continental margin and the South Tasman Rise. Australian
2775 Journal of Earth Sciences, 44, 633-654, 1997.

2776 Van Dijk, J., Fernandez, A., Bernasconi, S.M., Caves Rugenstein, J.K., Passey, S.R., White,
2777 T.: Spatial pattern of super-greenhouse warmth controlled by elevated specific
2778 humidity, Nature Geoscience, 13 (11), pp. 739-744, DOI: 10.1038/s41561-020-
2779 00648-2, 2020.

2780 Van Hinsbergen, D. J. J., De Groot, L. V., Van Schaik, S. J., Spakman, W., Bijl, P. K., Sluijs,
2781 A., et al.: A paleolatitude calculator for paleoclimate studies, PLoS ONE, 10(6),
2782 https://doi.org/10.1371/journal.pone.0126946, 2015.

2783 Warden, L., Kim, J. -., Zell, C., Vis, G. -., De Stigter, H., Bonnin, J., et al.: Examining the
2784 provenance of branched GDGTs in the tagus river drainage basin and its outflow
2785 into the Atlantic Ocean over the holocene to determine their usefulness for
2786 paleoclimate applications, Biogeosciences, 13(20), 5719-5738, doi:10.5194/bg-
2787 13-5719-2016, 2016.

2788 Warden, L., Moros, M., Weber, Y., and Sinninghe Damsté, J. S.: Change in provenance of
2789 branched glycerol dialkyl glycerol tetraethers over the Holocene in the Baltic Sea
2790 and its impact on continental climate reconstruction, Organic Geochemistry, 121,
2791 138-154, doi:10.1016/j.orggeochem.2018.03.007, 2018.

2792 Warnaar, J., Bijl, P. K., Huber, M., Sloan, L. C., Brinkhuis, H., Röhl, U., et al.: Orbitally
2793 forced climate changes in the Tasman sector during the middle Eocene,

Formatted

Formatted

Palaeogeography, Palaeoclimatology, Palaeoecology, 280, 361-370, http://dx.doi.org/10.1016/j.palaeo.2009.06.023, 2009.

Weijers, J. W. H., Lim, K. L. H., Aquilina, A., Damsté, J. S. S., and Pancost, R. D.: Biogeochemical controls on glycerol dialkyl glycerol tetraether lipid distributions in sediments characterized by diffusive methane flux, Geochemistry, Geophysics, Geosystems, 12(10), doi:10.1029/2011GC003724, 2011.

Weijers, J. W. H., Schouten, S., Spaargaren, O. C., and Sinninghe Damste, J. S.: Occurrence and distribution of tetraether membrane lipids in soils: Implications for the use of the TEX_{86} proxy and the BIT index, Organic Geochemistry, 37, 1680-1693, doi:10.1016/j.orggeochem.2006.07.018, 2006.

Weijers, J. W. H., Schouten, S., van den Donker, J C, Hopmans, E. C., and Sinninghe Damsté, J. S.: Environmental controls on bacterial tetraether membrane lipid distribution in soils, Geochimica Et Cosmochimica Acta, 71, 703-713, 2007a.

Weijers, J.W.H., Schefuß, E., Schouten, S., Damsté, J.S.S., Coupled thermal and hydrological evolution of tropical Africa over the last deglaciation, Science, 315 (5819), pp. 1701-1704, 2007b.

Westerhold, T., Marwan, N., Drury, A. J., Liebrand, D., Agnini, C., Anagnostou, E., et al.: An astronomically dated record of earth's climate and its predictability over the last 66 million years. Science, 369(6509), 1383-1387, doi:10.1126/science.aba6853, 2020.

Formatted: Not Highlight

Formatted: Not Highlight

Formatted: English (US), Not Highlight

Formatted: Not Highlight

Formatted: English (US), Not Highlight

Formatted: Not Highlight

Formatted: English (US), Not Highlight

Formatted: Not Highlight

Formatted: English (US), Not Highlight

Formatted: English (US), Not Highlight

Deleted: ¶

2815 Willard, D. A., Donders, T. H., Reichgelt, T., Greenwood, D. R., Sangiorgi, F., Peterse, F.,
2816 et al.: Arctic vegetation, temperature, and hydrology during early Eocene
2817 transient global warming events, Global and Planetary Change, 178, 139-152,
2818 doi:10.1016/j.gloplacha.2019.04.012, 2019.

2819 Williams, G. L., Fensome, R. A., and MacRae, R. A.: Dinoflaj3, American Association of
2820 Stratigraphic Palynologists, Data Series, 2, 2017.

2821 Williams, S. E., Whittaker, J. M., Halpin, J. A., and Müller, R. D.: Australian-Antarctic
2822 breakup and seafloor spreading: Balancing geological and geophysical
2823 constraints, Earth-Science Reviews, 188, 41-58,
2824 doi:10.1016/j.earscirev.2018.10.011, 2019

2825 Xie, S., Liu, X., Schubotz, F., Wakeham, S. G., & Hinrichs, K.: Distribution of glycerol
2826 ether lipids in the oxygen minimum zone of the eastern tropical north pacific
2827 ocean, Organic Geochemistry, 71, 60-71,
2828 doi:https://doi.org/10.1016/j.orggeochem.2014.04.006, 2014.

2829 Zeebe, R.E., Lourens, L.J.: Solar System chaos and the Paleocene–Eocene boundary age
2830 constrained by geology and astronomy, Science, 365 (6456), pp. 926-929, DOI:
2831 10.1126/science.aax0612, 2019.

2832 Zell, C., Kim, J. -., Hollander, D., Lorenzoni, L., Baker, P., Silva, C. G., et al.: Sources and
2833 distributions of branched and isoprenoid tetraether lipids on the Amazon shelf
2834 and fan: Implications for the use of GDGT-based proxies in marine sediments,
2835 Geochimica et Cosmochimica Acta, 139, 293-312, doi:10.1016/j.gca.2014.04.038,
2836 2014.

Deleted: Zachos, J. C., Schouten, S., Bohaty, S., Quattlebaum, T., Sluijs, A., Brinkhuis, H., et al.: Extreme warming of mid-latitude coastal ocean during the Paleocene-Eocene Thermal Maximum: Inferences from TEX and isotope data, Geology, 34(9), 737-740, 2006.¶

Formatted

Deleted: Zell, C., Kim, J. -., Dorhout, D., Baas, M., and Sinninghe Damsté, J. S.: Sources and distributions of branched tetraether lipids and crenarchaeol along the Portuguese continental margin: Implications for the BIT index, Continental Shelf Research, 96, 34-44, doi:10.1016/j.csr.2015.01.006, 2015.¶

Zell, C., Kim, J. -., Moreira-Turcq, P., Abril, G., Hopmans, E. C., Bonnet, M. -., et al.: Disentangling the origins of branched tetraether lipids and crenarchaeol in the lower Amazon River: Implications for GDGT-based proxies, Limnology and Oceanography, 58(1), 343-353, doi:10.4319/lo.2013.58.1.0343, 2013

Zhang, Y. G., Pagani, M., and Wang, Z.: Ring index: A new strategy to evaluate the integrity of TEX_{86} paleothermometry, Paleoceanography, 31(2), 220-232, doi:10.1002/2015PA002848, 2016.

Zhang, Y. G., Zhang, C. L., Liu, X. -., Li, L., Hinrichs, K. -., and Noakes, J. E.: Methane index: A tetraether archaeal lipid biomarker indicator for detecting the instability of marine gas hydrates, Earth and Planetary Science Letters, 307(3-4), 525-534, doi:10.1016/j.epsl.2011.05.031, 2011.

Deleted: ¶

Deleted: ¶

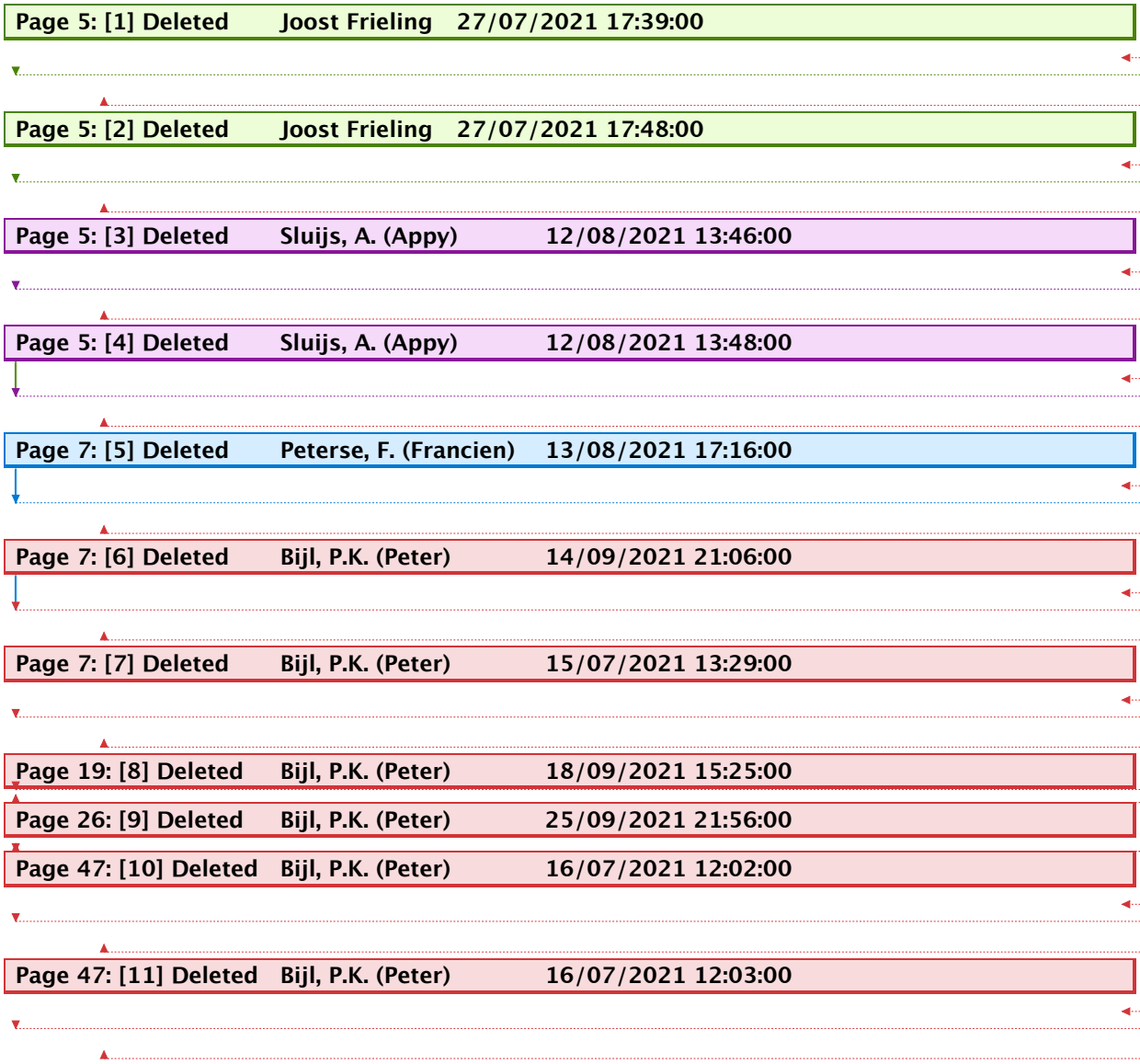
Page 5: [1] Deleted Joost Frieling 27/07/2021 17:39:00
Page 5: [2] Deleted Joost Frieling 27/07/2021 17:48:00
Page 5: [3] Deleted Sluijs, A. (Appy) 12/08/2021 13:46:00
Page 5: [4] Deleted Sluijs, A. (Appy) 12/08/2021 13:48:00
Page 7: [5] Deleted Peterse, F. (Francien) 13/08/2021 17:16:00
Page 7: [6] Deleted Bijl, P.K. (Peter) 14/09/2021 21:06:00
Page 7: [7] Deleted Bijl, P.K. (Peter) 15/07/2021 13:29:00
Page 19: [8] Deleted Bijl, P.K. (Peter) 18/09/2021 15:25:00
Page 26: [9] Deleted Bijl, P.K. (Peter) 25/09/2021 21:56:00
Page 47: [10] Deleted Bijl, P.K. (Peter) 16/07/2021 12:02:00
Page 47: [11] Deleted Bijl, P.K. (Peter) 16/07/2021 12:03:00